

INVESTIGATION OF PHASE INVERSION BEHAVIOR OF CELLULOSE-
IONIC LIQUID SOLUTIONS IN RELATIONSHIP WITH MEMBRANE
FORMATION

A THESIS SUBMITTED TO
THE GRADUATE SCHOOL OF NATURAL AND APPLIED SCIENCES
OF
MIDDLE EAST TECHNICAL UNIVERSITY

BY

ELİF NUR DURMAZ

IN PARTIAL FULLFILMENT OF REQUIREMENTS
FOR
THE DEGREE OF MASTER OF SCIENCE
IN
CHEMICAL ENGINEERING

MARCH 2017

Approval of the thesis:

**INVESTIGATION OF PHASE INVERSION BEHAVIOR OF CELLULOSE-
IONIC LIQUID SOLUTIONS IN RELATIONSHIP WITH MEMBRANE
FORMATION**

submitted by **ELİF NUR DURMAZ** in partial fulfillment of the requirements for the degree of **Master of Science in Chemical Engineering Department, MiddleEast Technical University** by,

Prof. Dr. Gülbin Dural Ünver
Dean, Graduate School of **Natural and Applied Sciences**

Prof. Dr. Halil Kalıpçılar
Head of Department, **Chemical Engineering**

Asst. Prof. Dr. Zeynep Çulfaz Emecen
Supervisor, **Chemical Engineering Dept., METU**

Examining Committee Members:

Prof. Dr. Levent Yılmaz
Chemical Engineering Dept., METU

Asst. Prof. Dr. Zeynep Çulfaz Emecen
Chemical Engineering Dept., METU

Asst. Prof. Dr. Erhan BAT
Chemical Engineering Dept., METU

Assoc. Prof. Dr. Çerağ Dilek Hacıhabiboğlu
Chemical Engineering Dept., METU

Prof. Dr. Nihal Aydoğan
Chemical Engineering Dept., Hacettepe University

Date: 03.03.2017

I hereby declare that all information in this document has been obtained and presented in accordance with academic rules and ethical conduct. I also declare that, as required by these rules and conduct, I have fully cited and referenced all material and results that are not original to this work.

Name, Last name : Elif Nur Durmaz

Signature :

ABSTRACT

INVESTIGATION OF PHASE INVERSION BEHAVIOR OF CELLULOSE- IONIC LIQUID SOLUTIONS IN RELATIONSHIP WITH MEMBRANE FORMATION

Durmaz, Elif Nur

M.S., Department of Chemical Engineering

Supervisor: Asst. Prof. Dr. Zeynep Çulfaz Emecen

March 2017, 121 pages

Cellulose membranes were produced from ionic liquid solutions by phase inversion technique and thermodynamic and kinetic aspects of the process were investigated to relate these to membrane morphology and performance. In thermodynamics part, polymer-solvent, polymer-nonsolvent and polymer-solvent-nonsolvent interactions were examined experimentally, together with Hansen solubility parameter estimations. Kinetics part consisted of measuring phase inversion rate. Obtained membranes were characterized by their morphology, crystallinity and separation performances.

Performances and SEM images of cellulose, cellulose acetate and poly(ether sulfone), PES, membranes show that when amount of ionic liquid (1-ethyl-3-methylimidazolium acetate, EMIMAc) increased in the polymer solution and when the coagulation media is water rather than ethanol, membranes have denser selective layer. Bromothymol Blue retentions of non-dried cellulose membranes drop from 40% to 20% as dimethyl sulfoxide (DMSO) is added to the polymer solution in 1:1 ratio with ionic liquid and when it is added in 1:2 ratio retention reduced to approximately 10%. Rejections are not more than 7% for membranes obtained from coagulation in ethanol. Additionally when membranes were dried, Bromothymol Blue retentions increased to ca. 80% for all cellulose membranes while pure ethanol permeance drops to

approximately 1 L/m².h.bar from around 70 L/m².h.bar. XRD measurements of cellulose membranes indicate the highest crystallinity in membranes prepared from EMIMAc only and coagulated in water. Solubility parameters estimate that solvent quality of EMIMAc is higher for cellulose than EMIMAc-DMSO mixtures, while it is opposite for cellulose acetate and PES. The nonsolvent quality of water is found to be lower for cellulose solutions indicated by cloud point measurements and swelling tests. Cloud point and swelling test measurements and solubility parameter estimations agree that water is a stronger nonsolvent for cellulose acetate and PES.

Phase inversion rates from microscope observations are always lower when the nonsolvent is ethanol. However not seeing higher front rates in lower viscosity DMSO containing solutions, imply that phase inversion front rates do not only depend on viscosities for these solutions. Light transmission measurements, on the other hand, show more reliable results on membrane porosity rather than precipitation rate of polymer solution

Keywords: Phase Inversion, Membranes, Cellulose, Ionic Liquid

ÖZ

SELÜLOZ-İYONİK SIVI ÇÖZELTİLERİNİN FAZ DEĞİŞİM DAVRANIŞININ MEMBRAN OLUŞUMUNA YÖNELİK İNCELENMESİ

Durmaz, Elif Nur

Yüksek Lisans, Kimya Mühendisliği Bölümü

Tez Yöneticisi: Asst. Prof. Dr. Zeynep Çulfaz Emecen

Mart 2017, 121 sayfa

Bu Çalışmada faz değişim tekniği ile selüloz-iyonik sıvı sistemlerinden membran üretilmiş ve faz değişiminin termodinamik ve kinetik davranışlarını membran morfolojisi ve performansı ile ilişkilendirilmiştir. Termodinamik özellikleri incelemek için, polimer-çözücü, polimer-çözmeyen ve polimer-çözücü-çözmeyen etkileşimlerine bakılmıştır. Bunlarla birlikte bahsedilen etkileşimler için Hansen çözünürlük parametreleri de göz önünde bulundurulmuştur. Kinetik kısımda faz değişim hızı ölçülmüş elde edilen membranlar morfoloji, kristallik ve ayırma performanslarına bakılarak karakterize edilmişlerdir.

Selüloz, selüloz asetat ve polietilen sülfon (PES) membranların ayırma performansları ve SEM görüntülerine şunlar söylenebilir: çözücü sadece iyonik sıvı (1-etil-3-metilimidazolyum asetat, EMIMAc) olduğu durumlarda ve de çözmeyenin etanol yerine su olduğu durumlarda oluşan membranın seçici geçirgen tabakası daha sıkı olmaktadır. Selüloz çözeltisine iyonik sıvıyla 1:1 oranında katılan dimetil sülfoksit (DMSO), selüloz membranların Bromotimol Mavisi tutma oranı %40 civarından

%20'ye düşmüş 1:2 oranında eklenince ise tutma oranı yaklaşık %10'a inmiştir.. Tutma oranları etanolde çöktürülerek elde edilen selüloz membranlar için %7'yi geçememiştir. Ayrıca membranlar kurutulduğunda Bromotimol mavisi tutma oranları bütün selüloz membranlar için %80'e çıkmış saf etanol geçirgenlikleri ise yaklaşık 70 L/m².h.bar'dan 1 L/m².h.bar civarına düşmüştür. Bununla birlikte selüloz membranların XRD ölçümleri, membran çözücüsünün sadece EMIMAc olduğu ve çözmeyenin su olduğu şartlarda daha çok kristallenmeye işaret etmektedir.

Çözünürlük parametreleri selüloz için EMIMAc'ın EMIMAc-DMSO karışımından daha iyi bir çözücü olduğunu işaret etmektedir. Bu durum diğer polimerler için ise tam tersidir. Bulutlanma noktası ve şişme testleri selüloz içeren sistemler için suyun daha zayıf bir çözmeyen olduğunu göstermektedir. Bununla birlikte, bulutlanma noktası testleri, şişme testleri ve çözünürlük parametre hesaplamaları suyun selüloz asetat ve PES için daha güçlü bir çözmeyen olduğunu işaret etmektedir.

Mikroskop ile faz değişim gözlemleri sırasında etanolün çözmeyen olduğu her durumda faz değişim cephesinin sudan daha yavaş olduğu görülmüştür. Ancak beklenildiği gibi düşük vizkoziteli, DMSO içeren çözeltilerde daha yüksek faz değişim hızı gözlemlenmemiştir. Bu durum faz değişim cephesi hızlarında viskozitenin yanı sıra başka faktörlerin de rol oynadığını göstermektedir. Işık geçirgenliği ölçümleri ise polimer çözeltilisinin çökme hızından çok membran porozitesini göstermektedir.

Anahtar kelimeler: Faz Değişimi, Membranlar, Selüloz, İyonik Sıvı

To Family and Friends

ACKNOWLEDGEMENTS

Firstly, I am very grateful to be in ulfaz-Emecen group, where I spent amazing three years that I learned laughter is also a part of doing science. I would like to express my very great appreciation to Asst. Prof. Dr. Zeynep ulfaz-Emecen for making this environment possible for us. Also, I am very thankful to her for giving endless support and guidance to me in addition to her limitless patience. I would like to thank every member of the research group, Faqih, Kaan, Canan, Begüm, Kübra, Hazal, Zeynep and Esra for their support, suggestions and of course their friendship.

I would like to express my gratitude to my family for their endless support in any kind and for teaching me to dream. Additionally, I would like to thank all friends who turn out to be family for me. Without Canan, Irmak, Müge and Özge’s friendship life in Ankara would not be bearable and I am thankful to them for making *one and half* to have new meanings. I am also grateful to Tahaberk and Samet for their friendship and support. I wish to thank also Murphy for not letting me alone with his laws.

I would like to thank Prof. Dr. Nihal Aydoğan and her group for the contribution in DLS measurements. Additionally, I wish to acknowledge the help provided by Prof. Dr. Necati Özkan.

I would like also to acknowledge the financial support provided by the Scientific and Technological Research Council of Turkey (TUBITAK MAG115M520).

TABLE OF CONTENTS

ABSTRACT.....	v
ÖZ.....	vii
ACKNOWLEDGEMENTS.....	x
TABLE OF CONTENTS.....	xi
LIST OF TABLES.....	xiv
LIST OF FIGURES.....	xv
NOMENCLATURE.....	xix

CHAPTERS

INTRODUCTION	1
1.1. Phase Inversion.....	4
1.1.1. Nonsolvent Induced Phase Separation (NIPS).....	6
1.2. Cellulose as a Membrane Polymer	13
1.2.1. Cellulose.....	13
1.2.2. Cellulose Dissolution	14
1.2.3. Ionic Liquids	15
1.2.4. Regeneration of Cellulose from Ionic Liquids.....	17
1.2.5. Membranes from Ionic Liquid Solutions	20
Aim of this Study	22

EXPERIMENTAL METHODS	23
2.1. Materials	23
2.2. Solution Preparation	23
2.3. Solution Characterization	24
2.3.1. Solvent Viscosity.....	24
2.3.2. Solution Viscosity	25
2.4. Membrane Casting.....	25
2.5. Light Transmission Measurements.....	25
2.6. Phase Inversion Front Observations	27
2.7. Solubility Parameter Calculations	29
2.8. Swelling Tests.....	29
2.8.1. Preparation of Dense Films for Swelling Tests.....	29
2.8.2. Swelling Test Procedure.....	30
2.9. Cloud Point Measurement	30
2.10. Dynamic Light Scattering	31
2.11. Performance Tests.....	32
2.11.1. Pure Solvent Permeance	32
2.11.2. Retention Tests	32
2.12. Membrane Morphology	34
2.13. Crystallinity.....	34
RESULTS AND DISCUSSION	35
3.1. Membrane Characterization	35
3.1.1. Membrane Morphology.....	35
3.1.2. Membrane Crystallinity.....	44
3.1.3. Performance Tests	50

3.2.1.	Theoretical Approach: Hansen Solubility Parameters	56
3.2.2.	Polymer-Nonsolvent Interactions: Swelling Tests.....	57
3.2.3.	Polymer-Solvent Interactions: Dynamic Light Scattering	59
3.2.4.	Polymer-Solvent-Nonsolvent Interactions: Cloud Points	63
3.3.	Factors Affecting Kinetics of Phase Inversion	65
3.3.1.	Phase Inversion Kinetics Measurements	67
3.3.1.1.	Phase Inversion Front Observations (Instantaneous Phase Inversion Rates) 67	
3.3.1.2.	Light Transmission Measurements (Cumulative Phase Inversion Measurements).....	75
	CONCLUSIONS.....	83

APPENDICES

APPENDIX A	97
XRD Measurements	97
APPENDIX B	99
Solution Viscosities.....	99
APPENDIX C	101
Solubility Parameters	101
APPENDIX D	103
DLS Measurements	103

LIST OF TABLES

TABLES

Table 2-1 Dope Solutions and Ingredients	24
Table 2-2 List of Filtration Conditions of Retention Tests	33
Table 3-1 Thicknesses of Cellulose Membranes.....	38
Table 3-2 Morphological Properties of Prepared Membranes	42
Table 3-3 RED Values of Solvent and Nonsolvent Interactions with Polymer	56
Table 3-4 Water and Cloud Point Concentrations of Solutions at 23 °C in Mass and Molar Basis	63
Table 3-5 Solution Viscosity at Shear Rate 1 s ⁻¹	66
Table 3-6 Diffusivities of Nonsolvents in Solvents Calculated from Wilke-Chang Equation	73
Table C - 1 Solubility Parameters of Ternary System Components	101
Table C - 2 Ra and RED Values of Interactions between Two Species	102

LIST OF FIGURES

FIGURES

Figure 1-1 Classification of Membrane Applications by the Average Pore Size Retrieved from [2].....	2
Figure 1-2 Schematic Drawing of a Simple Membrane System.....	3
Figure 1-3 Typical ternary diagram of NIPS system	7
Figure 1-4 Schematic Drawings of Phase Separation Membrane Morphologies	9
Figure 1-5 SEM images of some phase inversion membranes (a) cellulose membrane, symmetric and dense, (b) PES membrane, symmetric and porous (spongy) [10], (c) PES hollow fiber membrane, asymmetric and porous [6], (d) PES membrane, asymmetric and porous (finger-like macrovoids)	10
Figure 1-6 Molecular Structure of Cellulose (Hydrogen Bonds Are Indicated), Retrieved from [16].....	13
Figure 1-7 Schematic Drawing of Dissolution of Cellulose with Imidazolium Based Ionic Liquid [21]	15
Figure 2-1 Schematic Drawing of Casting Bar	25
Figure 2-2 Schematic Drawing of Light Transmission Measurement Setup.....	26
Figure 2-3 Typical Normalized Output of Light Transmission Measurements.....	27
Figure 2-4 Schematic Drawing of Phase Inversion Front Observations.....	28
Figure 2-5 Ethanol Cloud Point Solutions of CA 1; from left to right 35%, 37.5%, 40%	31
Figure 2-6 Schematic Drawing of Filtration System	33
Figure 3-1 SEM Images of Cellulose Membranes Obtained by Coagulation in Water. Scale bars are 200 μm (600x) for cross-section images while 1 μm (100 000x) for side images.	36
Figure 3-2 SEM Images of Cellulose Membranes Obtained by Coagulation in Ethanol. Scale bars are 200 μm (600x) for cross-section images while 1 μm (100 000x) for side images.	37

Figure 3-3 SEM Images of Cellulose Acetate Membranes. Scale bars are 200 μm (600x) for cross-section images while 1 μm (100 000x) for side and surface images.	39
Figure 3-4 SEM Images of PES Membranes. Scale bars are 200 μm (600x) for cross-section images while 1 μm (100 000x) for side images.	41
Figure 3-5 XRD Pattern of Cellulose Powder.....	44
Figure 3-6 X-Ray Diffractograms of Nonsolvent and Support Side of C1-W (plots are shifted apart).....	45
Figure 3-7 XRD Patterns of Cellulose Membranes in the order of C1-W, C1-E, C2-W, C2-E, C3-W and C3-E (plots are shifted apart)	47
Figure 3-8 XRD Patterns of Cellulose Membranes (plots are shifted apart)	48
Figure 3-9 X Ray Diffractogram of Cellulose Acetate Powder	49
Figure 3-10 XRD Patterns of Cellulose Acetate Membranes Obtained from Coagulation in Water (plots are shifted apart)	50
Figure 3-11 Blue Dextran (20 kDa) Retention of Dried Membranes	51
Figure 3-12 Pure Water Permeances of Dried Membranes.....	52
Figure 3-13 Blue Dextran and Bromothymol Blue Retentions of Dried Cellulose Membranes	53
Figure 3-14 Bromothymol Blue Retentions of Dry and Non-dried Cellulose Membranes	54
Figure 3-15 Swelling Ratios of Films at Equilibrium	57
Figure 3-16 Swelling Ratios of (a) Cellulose, (b) Cellulose Acetate, (c) PES Films in Time	58
Figure 3-17 Representation of a Polymer Coil in Solvents of Different Quality.....	60
Figure 3-18 Multimodal Distribution of Particle Size	61
Figure 3-19 Hydrodynamic Radii of Polymers in Different Solvents	62
Figure 3-20 Viscosities of Solvent and Solvent Mixtures.....	65
Figure 3-21 Photographs Of Phase Inversion Front Observations at 0th 1st 5th 10th 60th Seconds of C1 Solution for Nonsolvent Water and Ethanol.....	68
Figure 3-22 Photographs of Phase Inversion Front Observations at 5th Seconds for C1 and C2 Solutions for Both Nonsolvents	69

Figure 3-23 Photographs of Phase Inversion Front Observations at 5th Seconds for C3 and C4 Solutions for Both Nonsolvents.....	70
Figure 3-24 Photographs of Phase Inversion Front Observations at 5th Seconds for Cellulose Acetate Solutions for Water as Nonsolvent.....	71
Figure 3-25 Photographs of Phase Inversion Front Observations at 5th Seconds for PES Solutions for Both Nonsolvents	71
Figure 3-26 x^2 vs. t Graphs of Cellulose Solutions for Both Nonsolvents.....	72
Figure 3-27 x^2 vs. t Graphs of Cellulose Acetates Solutions for Nonsolvent Water .	73
Figure 3-28 x^2 vs. t Graphs of PES solutions for Both Nonsolvents	73
Figure 3-29 Effective Diffusivities of Nonsolvents in Solvents	74
Figure 3-30 Light Transmission Measurement Results of C1 and C2 Solutions.....	75
Figure 3-31 Light Transmission Measurement Results of C3 and C4 Solutions.....	76
Figure 3-32 Light Transmission Measurement Results of Cellulose Acetate Solutions	76
Figure 3-33 Light Transmission Measurement Results of PES solutions	77
Figure 3-34 Cumulative Phase Inversion Rates of (a) Cellulose (b) Cellulose Acetate (c) PES Solutions Coagulated in Water and Ethanol.....	78
Figure 3-35 Cumulative Phase Inversion Rates of C1, CA1 and PES 1 Solutions Coagulated in Water.....	79
Figure 3-36 Membrane thickness over Final I/I_0 Values.....	80
Figure 3-37 Photographs of Phase Inversion Front Observations Taken at Times Final I/I_0 is reached.....	82
Figure A 1 - XRD Pattern of PES Powder and PES Membranes	97
Figure B 1 - Solution Viscosities at Different Shear Rates.....	99
Figure D 1 DLS Results of Cellulose-EMIMAc Solutions (Z-average).....	103
Figure D 2 DLS Results of Cellulose-EMIMAc Solutions (Z-average).....	104
Figure D 3 DLS Results of Cellulose-EMIMAc Solutions (Z-average).....	105
Figure D 4 DLS Results of Cellulose-SS1 Solutions (Z-average).....	106

Figure D 5 DLS Results of Cellulose-SS1 Solutions (Z-average).....	107
Figure D 6 DLS Results of Cellulose-SS2 Solutions (Z-average).....	108
Figure D 7 DLS Results of Cellulose-SS2 Solutions (Z-average).....	109
Figure D 8 Results of Cellulose Acetate – EMIMAc Solutions (Z-average).....	110
Figure D 9 Results of Cellulose Acetate – EMIMAc Solutions (Z-average).....	111
Figure D 10 Results of Cellulose Acetate – SS1 Solutions (Z-average).....	112
Figure D 11 Results of Cellulose Acetate – SS1 Solutions (Z-average).....	113
Figure D 12 DLS Results of Cellulose Acetate - DMSO Solutions (Z-Average)....	114
Figure D 13 DLS Results of Cellulose Acetate - DMSO Solutions (Z-Average)....	115
Figure D 14 Results of PES-EMIMAc Solutions (Z-Average).....	116
Figure D 15 Results of PES-EMIMAc Solutions (Z-Average).....	117
Figure D 16 Results of PES-SS1 Solutions (Z-Average).....	118
Figure D 17 Results of PES-SS1 Solutions (Z-Average).....	119
Figure D 18 Results of PES-DMSO Solutions (Z-Average).....	120
Figure D 19 Results of PES-DMSO Solutions (Z-Average).....	121

NOMENCLATURE

AMIMBr	—	1-allyl-3-methylimidazolium bromide
AMIMCl	—	1-allyl-3-methylimidazolium chloride
BMIMAc	—	1-butyl-3-methylimidazolium acetate
BMIMCl	—	1-butyl-3-methylimidazolium chloride
BSA	—	Bovine Serum Albumin
C	—	Cellulose
CA	—	Cellulose Acetate
DMAc	—	Dimethyl Acetamide
DMF	—	Dimethyl Formamide
DMSO	—	Dimethyl Sulfoxide
EMIMAc	—	1-ethyl-3-methylimidazolium acetate
EMIMCl	—	1-ethyl-3-methylimidazolium chloride
EMIMDEP	—	1-Ethyl-3-methylimidazolium diethyl phosphate
IL	—	Ionic Liquid
MCC	—	Micro-Crystalline Cellulose
MWCO	—	Molecular Weight Cut Off
NG	—	Nucleation and Growth
NIPS	—	Nonsolvent Induced Phase Separation
NMMO	—	N-methylmorpholine
NMP	—	N-methyl-2-pyrrolidone
NS	—	Nonsolvent
PES	—	Polyether Sulfone
PVA	—	Polyvinyl Alcohol
SD	—	Spinodal Decomposition

CHAPTER I

INTRODUCTION

A membrane is a selective barrier that separates species in a mixture by selectively permitting transport of certain species while restricting the others. Synthetic membranes are used in a wide range of areas including food and pharmaceutical industries, fuel-cells and water treatment applications. Although other materials (metal, ceramic, etc.) are also used for production of synthetic membranes, polymers take a large place in industrial applications and scientific research [1, 2]. Various production techniques for polymeric membranes are available. Track-etching, film expanding, interfacial polymerization, solution coating and phase inversion are one these techniques, and the resultant membranes are various in structure. For example, nonporous membranes may be produced with interfacial polymerization technique, while with track-etching and film-expanding porous membranes are produced. Polymer type and production technique is chosen based on the membrane application [2, 3].

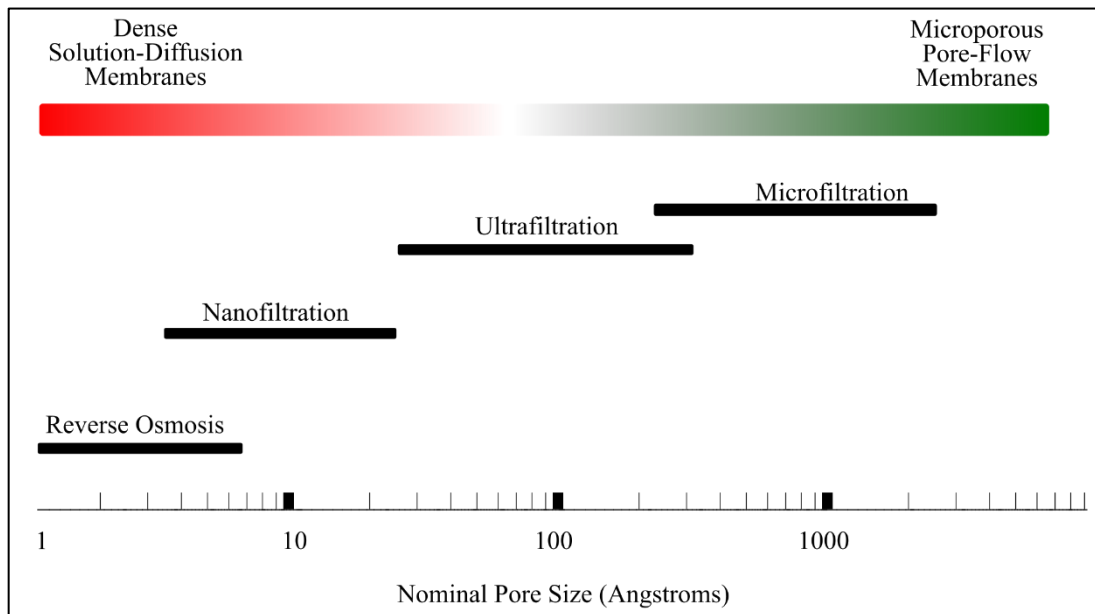


Figure 1-1 Classification of Membrane Applications by the Average Pore Size Retrieved from [2]

In Figure 1-1, a classification of pressure-driven membrane applications by membrane pore-size is given. Transport mechanisms through the pressure driven membranes are either by solution - diffusion or by pore flow. In the pore flow mechanism, species are transported by permeating through the pores and separation depends on the species size and membrane pore size. For solution-diffusion mechanism, on the other hand, species are transported by permeating through free-volume of the polymer. Permeability of a species across a polymer is the product of its solubility and its diffusivity in the polymer [2].

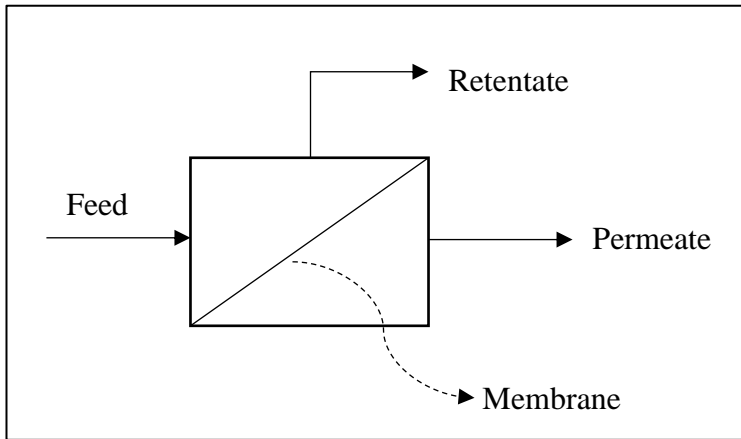


Figure 1-2 Schematic Drawing of a Simple Membrane System

In Figure 1-2 a simple representation of a membrane system, where feed stream is separated into permeate and retentate streams, is given. Performance of a membrane is defined by rate of separation and extent of separation. Flux of a membrane (J) is defined as permeate volume per unit membrane area and per time which is expressed generally in $L/m^2.h$ for liquid separation membranes. Since flux changes with driving force (transmembrane pressure difference for pressure-driven applications), permeance of a membrane is defined as flux over driving force, which is expressed in $L/m^2.h.bar$ usually. Permeability, on the other hand, is calculated by permeance multiplied by thickness of selective layer of the membrane. It is mostly expressed for nonporous membranes and is an intrinsic property of the polymer making up the membrane. These three parameters defines the rate of separation, while retention is a parameter that defines the extent of separation. Percent retention is expressed as given in Equation 1.1 [1,2].

$$\%R = 1 - \frac{C_P}{C_F} \quad (1.1)$$

where C_p and C_f concentration of permeate and retentate side, respectively.

1.1. Phase Inversion

Among the techniques of polymeric membrane production mentioned, phase inversion (phase separation) is the most common one. The simplicity of the technique and diversity of obtained membrane morphologies make the phase inversion technique appealing. In this technique, one-phase polymer solution separates into two phases as polymer-rich and polymer-lean phase by the precipitation of the polymer, which may be in several ways [2]. The polymer may be precipitated by lowering temperature (thermally induced phase separation), by evaporating the solvent (solvent evaporation) or introducing a nonsolvent to the solution (nonsolvent induced phase separation). For nonsolvent induced phase separation, the nonsolvent may be in vapor (vapor induced phase separation) or in liquid (liquid induced phase separation or immersion precipitation) state [2].

In either case of phase inversion, process starts with a homogenous polymer mixture, which means that for this solution free energy of mixing is negative. It is expressed as follows for closed systems at constant temperature and pressure

$$\Delta G_{mix} = \Delta H_{mix} - T\Delta S_{mix} \quad (1.2)$$

where ΔG_{mix} is the Gibbs free energy of mixing, ΔH_{mix} and ΔS_{mix} are enthalpy and entropy of mixing, respectively. Phase inversion is achieved by making this expression positive. Unlike low molecular weight solvents, polymers, due to their large molecular weight contribute less to the combinations of microscopic configurations of molecules in a mixture. This results in lower entropy of mixing relative to the low molecular weight species, which is explained well with Flory-Huggins theory using lattice model [1, 4]. Therefore, whether a polymer is compatible with another component or not mostly depends on enthalpy of mixing [1, 3].

To evaluate the enthalpy of mixing, solubility parameter approach is developed, firstly by Hildebrand. Hildebrand Solubility Parameters relates the enthalpy of mixing and solubility parameters.

$$\Delta H_{mix} = V^{mix} \phi_1 \phi_2 (\delta_1 - \delta_2)^2 \quad (1.3)$$

where V^{mix} is molar volume of mixture, ϕ_1 and ϕ_2 are volume fractions of components while δ_1 and δ_2 are the solubility parameters of the components. Since negative value of ΔG_{mix} is mostly depends on values of ΔH_{mix} approaching to zero, components with close values of solubility parameters are likely to mix.

Solubility parameter of a component is defined to be square root of cohesive energy density, which accounts for the strength of interactions between molecules per unit volume (eqn. 1.4).

$$\delta = \left[\frac{\Delta H_v - RT}{V} \right]^{1/2} \quad (1.4)$$

where ΔH_v is enthalpy of vaporization of the component and V is the molar volume. R is the ideal gas constant and T is temperature in Kelvin. By this definition, it is possible to find ΔH_v and δ , by vaporizing the substance. However, for polymers, δ is estimated commonly by swelling tests since polymers cannot be evaporated. The test consists of immersing the polymer into several solvents and the solubility parameter of the solvent that swells the polymer most is taken to be the closest value to solubility parameter of the polymer [4, 5].

In Hansen solubility parameter approach, a component has three solubility parameters referring to dispersion interactions, δ_D , permanent dipole – permanent dipole interactions, δ_p and hydrogen bonding, δ_H . These parameters have their roots in different sources of cohesive energy density, therefore sum of squares of these parameters gives the square of Hildebrand solubility parameter. To evaluate the compatibility of two components with Hansen Solubility Parameters, equation for *solubility parameter distance*, Ra , is developed (Eqn. 1.5)

$$Ra^2 = 4(\delta_{D2} - \delta_{D1})^2 + (\delta_{P2} - \delta_{P1})^2 + (\delta_{H2} - \delta_{H1})^2 \quad (1.5)$$

The factor 4 before the $(\delta_{D2} - \delta_{D1})^2$ term is determined from experimental data. Furthermore, another term R_o , which is called radius of solubility sphere, is also

evaluated experimentally for individual components. R_o defines a limit for solubility parameter distance, beyond which interactions between components are considered to be in low affinity. Relative energy difference, RED, is obtained by dividing the R_a value by R_o value of solute (Equation 1.6).

$$RED = \frac{R_a}{R_o} \quad (1.6)$$

While RED value lower than one indicates high affinity between components, increasing values of RED indicate the decreasing affinity. 1.0 is mentioned as boundary condition, near which the compatibility of substances is vague [5]. Solubility parameter approach may ease the application of phase inversion process in terms of choosing the proper solvent and the nonsolvent for the polymer.

1.1.1. Nonsolvent Induced Phase Separation (NIPS)

Nonsolvent induced phase separation is achieved by bringing a polymer solution into contact with a nonsolvent. Polymer solution in desired shape (flat sheet or hollow fiber for case of membranes) is either exposed to nonsolvent vapor or immersed in liquid nonsolvent bath (or first exposed to vapor and then immersed in liquid nonsolvent). This technique is very common since it basically requires three components: polymer, solvent and nonsolvent. Solvent should dissolve the polymer while the nonsolvent should not, and nonsolvent should be fully miscible with the solvent. As long as these requirements are fulfilled, it is possible to produce membranes with wide variety of morphologies.

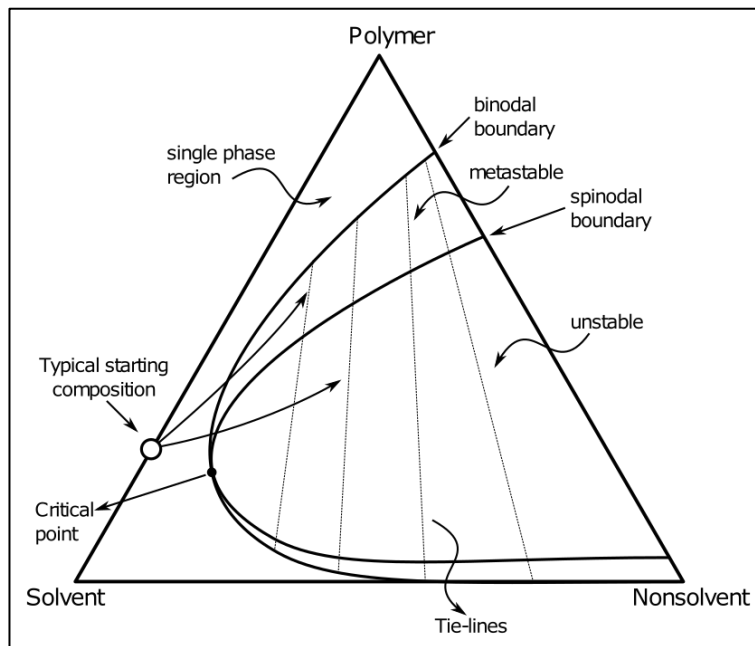


Figure 1-3 Typical ternary diagram of NIPS system

Three components of NIPS can be represented by ternary diagram as in Figure 1-3. The process starts with polymer solution which is usually at the polymer-solvent line and when nonsolvent is introduced to the system the composition proceeds towards inside of the triangle as nonsolvent diffuses in and solvent diffuses out of the polymer solution. Binodal boundary is the line that separates one-phase region and two-phase region of the diagram. Further from the boundary, the ternary system is not thermodynamically stable in one phase (i.e. $\Delta G_{mix} > 0$ for those compositions of components). Therefore, binodal boundary indicates the limit for miscibility of three components. However, for a certain region, components may not demix although they are beyond the binodal curve. Compositions in this region, which is called metastable region, can stand small composition disturbances without phase separation. Limit of metastable region is defined by spinodal curve. Beyond the spinodal curve, the second derivative of ΔG_{mix} with respect to composition is negative and the compositions in this region are unstable. The intercept of binodal and spinodal curve is defined as critical point. When phase inversion starts, one-phase polymer solution separates into

two phases as polymer-rich and polymer lean phase. These phases are represented by points on the binodal boundary and they are in equilibrium with each other; therefore, in ternary diagram the compositions of those phases are linked with tie-lines to each other. When a polymer solution enters the two-phase region, the upper end of tie-line represents the polymer-rich phase, while the lower end represents the polymer-lean phase. If phase separation starts from above critical point then the polymer-rich phase forms matrix and polymer-lean phase forms the pores. Otherwise, polymer-lean phase forms matrix and polymer-rich phase precipitates as dispersed polymer particles. The ratio of polymer-rich and polymer-lean phase at the end of the process is considered as porosity of the total membrane [1-3].

The point where the phase separation starts is an important factor that determines the final membrane morphology. If phase separation starts in metastable region, the demixing mechanism is called nucleation and growth (NG) and if it starts beyond the spinodal boundary, then the mechanism is referred to as spinodal decomposition (SD). These demixing mechanisms result in different structures in final membrane morphology. In NG mechanism, phase inversion starts as nucleation of polymer-lean phase (for composition path above critical point) and these nuclei grow as phase inversion proceeds. Common morphology for membranes obtained with this mechanism is spongy with open or closed cells depending on when polymer matrix solidifies. If polymer chains are fixed at earlier stages of NG, then closed-cell structure is observed. However, if solidification occurs after the nuclei grow so that they merge with each other, then the open-cell structure is observed, an example for this type structure is given in Figure 1-5 (b). With spinodal decomposition, bi-continuous structure is observed commonly, both polymer-rich and polymer-lean phases are formed in continuous structure. Nodular structures (Figure 1-5 (c)) observed in membrane morphology has been attributed to nucleation and growth mechanism, but lately it is shown that the structure is also observed for SD mechanism [1,7].

Diffusion of nonsolvent starts from solution-nonsolvent interface and proceeds through inside of the cross-section of the solution. Since diffusion rate throughout the cross-section is not uniform, nonsolvent concentration is also not uniform. This means different locations in the solution may be in different stages of phase separation

process. It is possible for a cast solution having totally precipitated and not precipitated locations at the same time. This non-uniformity is the reason for anisotropic structure of resultant membrane [2] as seen in (c) and (d) images of Figure 1-5. For a membrane, anisotropy or asymmetry is defined as having different structures throughout the cross-section in terms of porosity or polymer density. For phase inversion membranes, it is also possible to obtain an isotropic structure with this technique. In this case, phase separation is slow; which allows nonsolvent to spread more homogeneously, therefore different locations in the solution are at the similar stages of phase separation process [8]. Consequently, morphology of the membrane obtained by phase separation depends on both thermodynamics and kinetics of the phase separation process. Schematic drawing and SEM images of typical membrane structure obtained by phase inversion are given in Figure 1-4 and Figure 1-5, respectively.

For an asymmetric membrane, thin skin layer, which has the smallest pores (if any) throughout the cross-section, provides selectivity and since it is a thin layer, permeation rate is higher when compared to thicker membranes in same density. Typically, skin layer is dense for reverse osmosis and gas separation membranes. For nanofiltration the layer is mainly microporous (pore sizes not exceeding 2.0 nm, [9]) and for ultrafiltration skin has pores in between $\sim 1-100$ nm. The layer below the skin provides mechanical support. Therefore, it is possible to have high flux, highly selective separation and good mechanical strength with asymmetric membranes and having it with one polymer makes whole production much easier. [1,2].

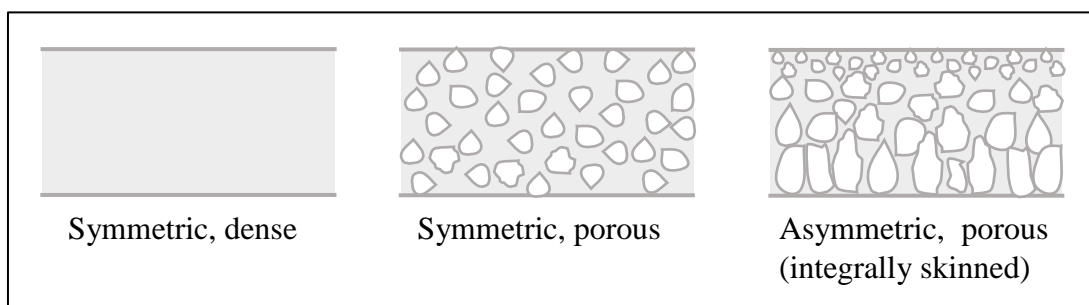


Figure 1-4 Schematic Drawings of Phase Separation Membrane Morphologies

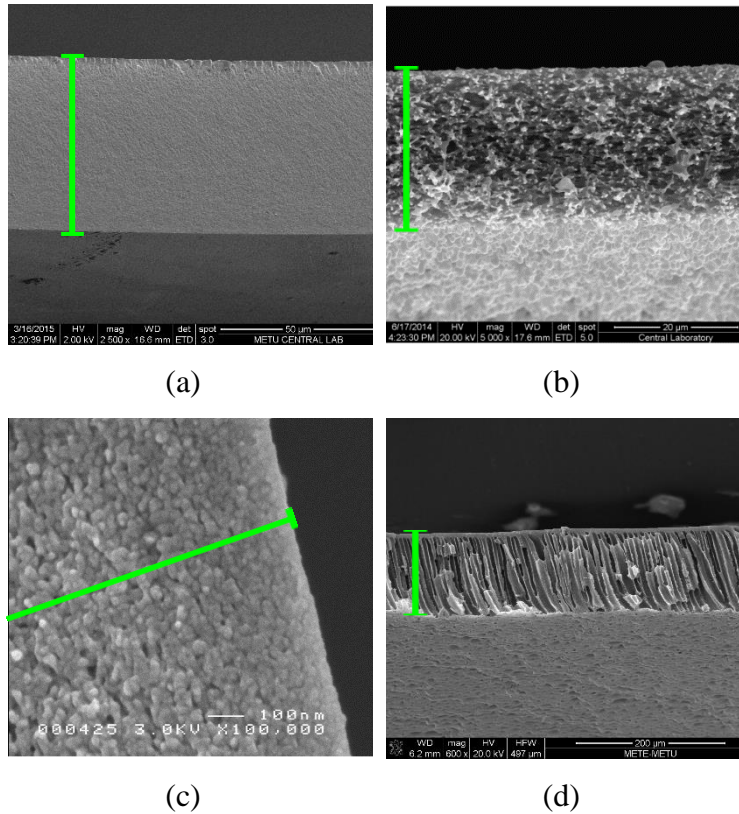


Figure 1-5 SEM images of some phase inversion membranes (a) cellulose membrane, symmetric and dense, (b) PES membrane, symmetric and porous (spongy) [10], (c) PES hollow fiber membrane, asymmetric and porous [6], (d) PES membrane, asymmetric and porous (finger-like macrovoids)

In Figure 1-5, scanning electron micrographs of membranes obtained with phase inversion technique are given. Figure 1-5 (a) is a cellulose membrane which is an example for symmetric and dense or microporous membrane. Figure 1-5(b) belongs to microfiltration membrane having symmetric and porous structure which is also an example for bi-continuous morphology. Figure 1-5 (c) is a hollow fiber PES membrane and increasing pore size from outer side to inner side shows the anisotropic structure and finally, Figure 1-5(d) exhibits an anisotropic structure with distinct skin layer. Large pores within the structure are called macrovoids and for the case of Figure 1-5 (d) the macrovoids are finger-like.

When, Loeb and Sourirajan discovered the immersion precipitation technique around 1960s, it became a breakthrough for membrane technology since it enabled to produce

integrally skinned asymmetric membranes, which provide higher flux when compared to membranes produced at that time. Since then, nonsolvent induced phase separations attract large research and industrial interest. How phase inversion proceeds and how membrane morphology is affected by thermodynamics and kinetics of the process is investigated both experimentally and by modeling.

Studies investigating the insight of the phase inversion process by experiments are mostly focusing on a certain ternary system. Developing a general model for nonsolvent induced phase separation process is a very complex task since it requires considering thermodynamic and mass transfer aspects of the system at the same time. Cohen et al. developed a model for production of porous membranes produced by nonsolvent induced phase separation [11]. They set a mass transfer model by dividing the flat-sheet formed polymer solution into two parts as diffusion layer and casting solution layer. And theoretical predictions were said to be similar with experimental observations. Later Smolders and coworkers [12] improved this model starting from excluding the quasi-steady state assumption that Cohen et al. did and considering the frictional forces between solvent and nonsolvent. They declared that their calculations were valid until diffusion gradients on bath-side or solution-side are disturbed (by demixing or convection). They confirmed the calculations of model with light transmission measurements. For mass transfer aspect of the nonsolvent induced phase separation, Yilmaz and McHugh developed a pseudo-binary model [13]. By neglecting macroscopic movement of the polymer chains, they were able to establish a set of equations on polymer-free basis (pseudo-binary), which is simpler than the actual diffusion equation. They mentioned this model was not valid only for specific cases and enabled to consider thermodynamic aspect and mass transfer aspect of the system, separately. They also stated that their calculations were restricted to a very short time and distance from the interface, which is decided by considering experimental observations. Their calculations were consistent with experimental data. In another paper [14], they showed how boundary conditions would affect the concentration profile. They set two types of boundary conditions by considering observations reported in literature and concluded that both of them is convenient to apply. They also concluded that change in nonsolvent bath conditions would change the membrane formation due to changing the flux ratio of solvent and nonsolvent. Finally,

thermodynamics of nonsolvent induced phase separation was modelled taking the Flurry-Huggins theorem as a basis in the all mentioned papers.

Investigation of phase inversion process experimentally is done for desired systems to understand the relation between kinetic and thermodynamic features of the system and resultant membrane morphology. Kinetic features of the system are commonly investigated by light transmission measurements and the microscopic observation of phase inversion front, which will be explained in experimental part. While thermodynamic features are generally modelled with Flory-Huggins theorem, there are experiments still needed to be done to implement the model, especially for determination of interactions between components of the system.

Gibbs free energy of mixing for a ternary system is given by the equation 1.7.

$$\Delta G_{mix} = RT(n_1 \ln \phi_1 + n_2 \ln \phi_2 + n_3 \ln \phi_3 + \chi_{12}n_1\phi_2 + \chi_{13}n_1\phi_3 + \chi_{23}n_2\phi_3) \quad (1.7)$$

where ϕ_i is the volume fraction and n_i is the number of moles of component i. χ_{ij} is the Flory-Huggins interaction parameter between components i and j. In the equation, numbers 1, 2 and 3, represent nonsolvent, solvent and polymer, respectively.

In order to estimate interaction parameters, there are some methods are suggested by Mulder [1]. For example, calorimetric measurements are suggested to find free energy of mixing to understand nonsolvent-solvent interactions. In addition to this, data from vapor-liquid equilibria and activity coefficient equations such as van Laar, Wilson or Margules are suggested to estimate the interaction parameter (χ_{1-2}). Moreover, swelling experiments and inverse gas chromatography are applied to calculate nonsolvent-polymer interaction parameter (χ_{1-3}). Lastly, for solvent-polymer interactions parameters (χ_{2-3}) membrane osmometry and vapor pressure osmometry are suggested.

Polymer choice for phase inversion is important since it determines the solvent and nonsolvent choice. Also it should be feasible for the application that the membrane is going to be used. For porous membranes aiming at aqueous filtrations, polymer should be chosen considering mainly ability to process for the aimed pore size and the fouling

behavior. On the other hand, for nonporous membranes permeability is an intrinsic feature of the polymer, therefore it directly affects the performance of the membrane [1].

Typical polymers used for phase inversion are cellulose esters, poly(acrylonitrile), poly(amide)s, poly(imide)s, poly(propylene), poly(sulfone), poly(ether sulfone), and poly(vinyl fluoride).

1.2. Cellulose as a Membrane Polymer

1.2.1. Cellulose

Cellulose is a renewable, biocompatible, biodegradable polymer, which is the most abundant polymer on earth [16]. It is found in plant cell wall together with lignin and hemicelluloses [15].

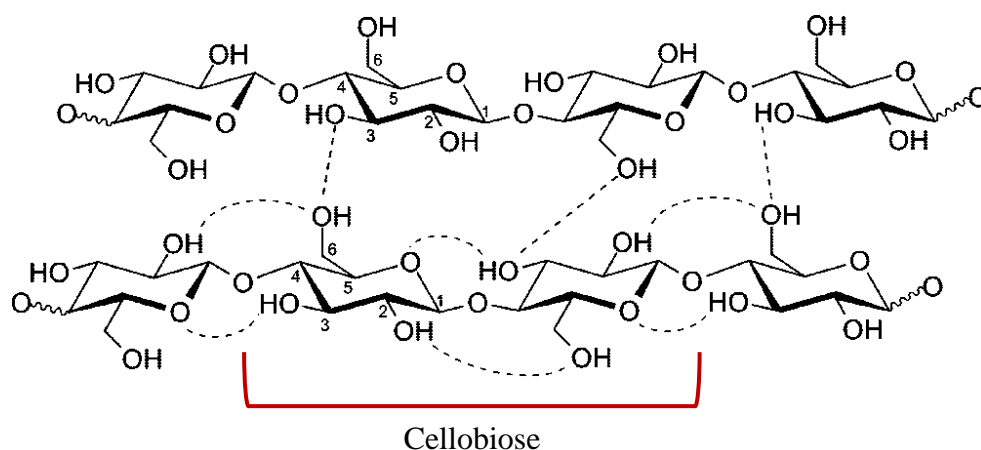


Figure 1-6 Molecular Structure of Cellulose (Hydrogen Bonds Are Indicated), Retrieved from [16]

In Figure 1-6 molecular structure of cellulose chains is given. As shown in this figure cellulose is a linear polymer, which consists of glucose units linked at C₁ and C₄ positions with glucosidic bonds. The repeating unit of cellulose, cellobiose, consists of two glucose molecules attached in reverse directions so that repeating units can be linked in mentioned locations continuously. The linear chain of cellulose makes many hydrogen bonds with itself and other cellulose chains. The strong glucosidic bonds and hydrogen bonds give cellulose chemical and mechanical strength. Additionally, while glucosidic bonds give hydrophobic property, large amount of hydrogen bonds results

in hydrophilic property. This amphiphilic feature of cellulose is important when solubility of cellulose is concerned [17,18].

Cellulose has different crystalline structures. They are named Cellulose – I to IV. Cellulose – I is the form found in native cellulose of plant and bacterial origin. After its discovery, it was figured out that Cellulose – I is a composite crystalline structure, which consists of two crystal forms, labeled as Cellulose – I α and Cellulose – I β . Cellulose – II is obtained by mercerization or regeneration of Cellulose – I and it is more thermodynamically stable than the former, therefore once cellulose is processed with these applications, it is not possible to obtain Cellulose – I again. Cellulose – III is obtained by treatment of I and II with ammonia and IV is transformed from III by annealing [19, 20].

1.2.2. Cellulose Dissolution

The crystalline structure and strong inter- and intra- molecular hydrogen bonds make cellulose hard to dissolve. Although, not being able to process this abundant and renewable polymer easily seems as an unfortunate feature, it makes cellulose a good candidate for applications with harsh conditions like organic solvent nanofiltration. Cellulose has been isolated nearly two centuries ago; however, the dissolving mechanism is still not totally understood [20].

Some of cellulose solvents (derivatizing solvents) dissolve cellulose by chemical reaction and changes the polymer into its derivatives, which causes cellulose to lose some of its desirable features. However, non-derivatizing solvents dissolve cellulose by physical dissolution, only. Although some debates are still going on about the dissolution mechanism of cellulose, in literature it is agreed that molecular dissolution of cellulose can be achieved by the solvent breaking the intra- and intermolecular hydrogen bonds and newly formed bonds between solvent and cellulose should be able to compete with initial bonds [16,17,21,22].

Traditionally, cellulose is dissolved by viscose process, which involves NaOH and CS₂ and an acidic solution. This process requires large amount of NaOH, CS₂, acidic solution and fresh water per amount of produced cellulose and it also produces large amount of waste. Other than being environmentally problematic, this process damages

the cellulose backbone, that is, it is a derivatizing solvent. N-methylmorpholine (NMMO) is also used for cellulose dissolution. Although it is a non-derivatizing solvent, lack of thermal stability and high cost make NMMO less favorable. Aprotic solvent-salt mixtures (e.g. N,N,-dimethylacetamide/lithium chloride, dimethyl sulfoxide/ tetrabutylammonium fluoride) and molten salt hydrates (e.g. $\text{LiClO}_4 \cdot 3\text{H}_2\text{O}$) are also used for cellulose dissolution; however, they suffer from limited dissolution efficiency and thermal stability [16,21].

1.2.3. Ionic Liquids

Since currently used cellulose solvents each have their own disadvantages, there is still a search for more preferable solvents. Ionic liquids (ILs) are one of these alternatives. Ionic liquids are defined as molten salts with melting point under $100\text{ }^\circ\text{C}$ [21]. ILs exhibit high polarity due to ionic nature, and they are able to break H-bond in the cellulose network.

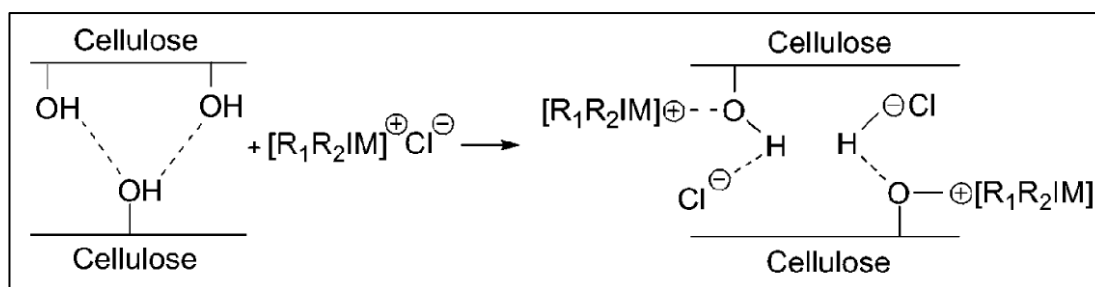


Figure 1-7 Schematic Drawing of Dissolution of Cellulose with Imidazolium Based Ionic Liquid [21]

Common opinion on dissolution mechanism of cellulose in ionic liquids is as follows: Ions of ionic liquids interact with oxygen and hydrogen atom of hydroxyl groups of polymer, making electron donor-electron acceptor complexes. By this way the H-bonds within the cellulose are broken which leads to cellulose dissolution as schematically represented by Figure 1-7 [17,21,23].

Dissolution efficiency of different ionic liquids are studied frequently [16,17, 24,-27]. Although it is agreed on the importance of the anion on solubility, there is a debate on

role of cation. It is discussed that hydrogen bond accepting ability of an anion is responsible for dissolution of cellulose [17, 18, 21].

Ionic liquids, even room temperature ionic liquids (those in liquid state at room temperature), have high viscosity due to strong molecular interactions within the solvent. Therefore, most of the time, dissolution process occurs slower than with common solvents. To accelerate the process, aprotic solvents like DMSO, DMAc and DMF can be added to solutions [28-32]. DMSO alone can only swell cellulose and dissolution of it even in very dilute solutions (0.1% cellulose) is not reported and not experienced in this study. Despite insolubility of cellulose in DMSO, addition of it increases the dissolution rate since it decreases the viscosity dramatically by diluting the ions in the solvent [17,33]. Similarly, to decrease the viscosity increasing the solution temperature is also an option. For systems that have negative heat of mixing values, dissolution of polymers at elevated temperatures is not thermodynamically favored. However, decrease in viscosity due to temperature increase becomes so dominant that thermodynamic effects are suppressed [34]. However, these kinetic improvements have limitations, for DMSO while it helps mass transfer up to a certain concentration, after that concentration, it reduces the dissolution capacity of the ionic liquid [32]. In a similar way, increasing temperature decreases the viscosity, but increasing it to too elevated temperatures degrades cellulose. Effect of cosolvent and temperature on dissolution of cellulose in ILs show that, the dissolution process is kinetically dominated [18,34].

In regeneration of cellulose from ionic liquid solutions, the effective factor is lowering dissolution capacity of ionic liquid. Therefore, as a nonsolvent, water interrupts the H-bond between ionic liquid and cellulose more than methanol and ethanol. Furthermore, it is suggested that if an ionic liquid at total cellulose dissolution capacity is required, the ionic liquid should be completely dry [26,29,35].

In this study, 1-Ethyl-3-methylimidazolium acetate (EMIMAc) is chosen as the ionic liquid to be used. When compared to others, EMIMAc has relatively low viscosity since it is in liquid state at room temperature. Additional to its dissolution capacity, low toxicity of this ionic liquid makes it preferable compared to others [16,17,48].

1.2.4. Regeneration of Cellulose from Ionic Liquids

Membranes can be obtained via phase inversion from any polymer as long as a proper solvent and a nonsolvent exists. Studies on regeneration of cellulose in terms of precipitating it by a nonsolvent from an ionic liquid solution are increasing every day since the discovery of dissolution of cellulose in ionic liquids. Although there are a lot of studies on cellulose products [36-67], literature on cellulose membranes obtained from ionic liquid is very limited [68-74].

In literature, there are many studies reporting cellulose products obtained from ionic liquid solutions by precipitating the polymer with a nonsolvent. Cellulose products including films, fibers, beads, gels and filaments are obtained from different kinds of cellulose. The cellulose type used in mentioned studies are mainly microcrystalline cellulose, cotton linter and pulp cellulose although other sources are also studied like newspaper waste or bacterial cellulose. In these studies the most common ionic liquids are BMIMCl [36-47, 67] and EMIMAc [36, 48-58], which are followed by AMIMCl [59-63], EMIMCl [36, 64], BMIMAc [36,65,66] and AMIMBr [43,67]. In choosing ionic liquids, solvation efficiency is an important factor. So far, EMIMAc is found to be the most efficient one due to relatively low viscosity and relatively high dissolution capacity due to the anion type [36]. Additionally, water is the most common nonsolvent among these studies, while ethanol, methanol, CO₂, acetacronitrile and solvent-nonsolvent mixtures are also studied.

Common conclusions of the mentioned studies are as follows:

- Transformation of crystalline structure from Cellulose-I to Cellulose-II with regeneration is observed [38,42,49,51,53,57,63,65,66]
- Smooth surface, dense and nodular morphology for cross-section was observed for cellulose products obtained from ionic liquid solutions [40,44,45,53,56,57,59,60,63,64].
- Blended polymers and cellulose show good miscibility [41,43,49,51,59,60,67].

Mu et.al produced gels from BMIMCl and cotton linter cellulose by applying different nonsolvents as CO₂, water, ethanol and acetonitrile. They find that the highest crystallinity was observed for products coagulated in water among all regenerated samples [65]. Zhang and coworkers studied cellulose films. Different kinds of cellulose were used, which are cotton linter, microcrystalline cellulose, pine and bamboo pulp. Ionic liquid was only EMIMAc and the nonsolvent was water for all cases. According to SEM images, all produced films have smooth surface and dense and nodular cross-section [53]. Similarly in Gatenholm and coworkers' study, different kinds of cellulose (microcrystalline cellulose, spruce and bacterial cellulose) were used in solutions with EMIMAc to produce films by coagulation in ethanol. While XRD analyses showed totally amorphous patterns, SEM images indicated the nodular and dense structure [56]. In the study of Markstedt et al. [55] different kinds of cellulose (microcrystalline cellulose, spruce and bacterial cellulose) were dissolved in EMIMAc and 3D printed on several surfaces. The nonsolvent water was sprayed onto the solution and the cross-section of resulted products were porous. Zhang et al spun cellulose fibers from different cellulose solution technologies (Lyocell, Newdal, Viscose and IL-Cellulose) and found that fibers from BMIMCl-Cellulose solutions (Nonsolvent: water) have highest crystallinity and strongest mechanical properties with respect to solutions from other technologies [45].

In some of these studies, instead of using cellulose solely, it was blended with other polymers like PVA [37,59] chitin [43,67], chitosan [66], keratin [51] and silk fibroin [41,46]. Blending was applied in order to combine features of blended polymer and cellulose. In most of these studies it was reported that polymer properties were improved. Moreover, similar to blending, in order to improve the properties of product, cellulose – ionic liquid solutions were fed with different fillers such as halloysites nanotubes [62], sepiolite [44], zeolite [64], carbon black and graphene nanoplatelets [58] and montmorillonite [57].

Regeneration of cellulose from ionic liquid solutions as a membrane has also been studied. Zhu and coworkers [68] prepared composite membranes by casting cellulose/AMIMCl solution on PET nonwoven. SEM images of cellulose layer of membranes showed dense and layered structure. Non-dried membranes were reported

to show high permeance ($\approx 25 \text{ L/m}^2 \cdot \text{h} \cdot \text{bar}$) and $\approx 700 \text{ Da}$ of molecular weight cut-off (MWCO). Moreover, it was reported that membranes had antifouling behavior. On the other hand, Chen and coworkers [69] prepared cellulose membranes from BMIMCl solutions (Nonsolvent is water), while obtaining cellulose from wheat straw. SEM micrographs showed asymmetric structure as one side is denser than the other one. Additionally, dry membranes showed high permeance ($\approx 80 \text{ L/m}^2 \cdot \text{h} \cdot \text{bar}$) and 97% rejection of Bovine Serum Albumin (66 kDa, BSA). Liang and coworkers [70] produced hollow fiber membranes by precipitating wood pulp/AMIMCl solutions in water. Membranes had porous structure and SEM images of inner and outer surfaces indicated the anisotropic morphology, which became denser with increasing polymer concentrations. Swelling ratios in water decreased with increasing initial polymer concentration. Additionally, dry membranes' pure water permeance was approximately $10 \text{ L/m}^2 \cdot \text{h} \cdot \text{bar}$ and nearly 90% retention of BSA, both changing with initial polymer concentration. He and colleagues [71] prepared hollow fiber membranes from Bamboo Pulp/ BMIMCl solutions using DMSO as cosolvent. While morphology of membranes were porous, membranes had approximately $80 \text{ L/m}^2 \cdot \text{h} \cdot \text{bar}$ of pure water permeance and more than 80% retention of BSA, which is consistent with study of Chen's group [69]; although whether membranes were dried or not was not reported. Chu and group members [72], studied composite membranes containing cellulose (microcrystalline cellulose) and chitin (from crab shells). They coated the solution on PAN scaffold and PET nonwoven and coagulated it in ethanol. They found that their composite membrane had similar retention and higher flux than commercial PAN membrane. Nunes et al. [73] prepared cellulose multilayered membranes with two different techniques. One technique is casting microcrystalline cellulose/EMIMAc solution on several porous supports. Those membranes have MWCO of approximately 3 kDa and pure water permeance of nearly $14 \text{ L/m}^2 \cdot \text{h} \cdot \text{bar}$. The other technique was coating the porous support with solution of silylated cellulose in tetrahydrofuran. After coating, cellulose was converted into original form (de-silylated) by treating with acid. Membranes obtained from this method had MWCO value of 5 kDa at lowest with pure water permeance of $8 \text{ L/m}^2 \cdot \text{h} \cdot \text{bar}$. Pihlajamaki and coworkers [74] prepared cellulose nanofiltration membranes with TiO_2 additive and investigated effects of it on morphology and membrane performance. They used EMIMAc as solvent and water as

nonsolvent and membranes obtained by immersion precipitation were tested without drying. Produced membranes, whether containing TiO₂ or not, had a morphology of layered structure without any macrovoids. Addition of titanium dioxide slightly increased pure water fluxes while very moderately decreased retentions. Furthermore, no significant difference was reported on membranes with different amounts of TiO₂. Additionally, these membranes had fouling resistive behavior. All papers on cellulose membranes mentioned here reported that cellulose crystalline structure transformed from Cellulose – I to Cellulose – II after coagulation.

Finally, within our group Sukma prepared cellulose membranes from EMIMAc for organic solvent nanofiltration applications [88]. Separation performances of membranes were measured with probe solutions of different molecular size and different charges in ethanol and water. Membrane performances were related to membrane-solute-solvent interactions using different solvents in feed solutions and probe molecules of different size and charge. It is mentioned that increase in concentration of polymer solution and drying membranes after coagulation increased the rejection and decreased the permeance.

1.2.5. Membranes from Ionic Liquid Solutions

Since ionic liquids are strong solvents and environmentally friendly, they are used in preparation of membranes from other polymers as well. For example, Chung and coworkers [75-77] prepared cellulose acetate membranes from BMIMSCN, EMIMSCN and EMIMAc solutions and reported the membrane morphology is different from the ones obtained from conventional solvents. Again Chung et al. fabricated ultrafiltration [78,79] and nanofiltration [80] membranes from polybenzimidazole-EMIMAc solutions. Polystyrene-b-poly(4-vinylpyridine) block copolymer P10900-S4VP membranes were prepared from THF/DMF solutions with water induced phase separation. Different ionic liquids are used as co-solvent in the solutions and the effect of these ILs are studied in [81]. While regular pore structure was not observed for membranes from solutions without ionic liquid, pores become more regular as certain amount of ionic liquid added to the polymer solution. Nunes

and coworkers [82], prepared hollow fiber membranes from different solutions including EMIMAc/DMSO mixture. Also from PES-EMIMDEP solutions, ultrafiltration membranes were prepared. It was reported that the morphology was very different from the ones obtained from conventional solvents (NMP, DMAc and DMF).

Most of these studies mentioned above reported that, obtained membrane morphology changes when ionic liquid used as solvent instead of conventional solvents. The reason behind the different morphologies was mostly attributed to high viscosity of ionic liquid and its effect on phase inversion rate. Nunes et al. observed that PES membranes morphology was spongy when the solvent is ionic liquid while finger-like macrovoids observed for membranes obtained from PES-NMP, PES-DMAc and PES-DMF solutions [84]. They discussed that change in morphology is a result of high viscosity of the ionic liquid. Since the inflow of nonsolvent in solvent should be slower than the outflow of solvent in nonsolvent (due to viscosities of these components), the nonsolvent enters a more concentrated polymer solution than the case of conventional solvents. Therefore, polymer chain movements are more restricted and the phase separation mechanism is more likely to be nucleation and growth, which results as spongy-structure as they observe. Chung et al. fabricated cellulose acetate membranes from solutions with BMIMSCN, NMP and acetone [75]. They observe that membranes obtained from solutions with ionic liquid was nodular and denser when compared to the ones obtained from acetone and NMP. While the ones obtained from NMP have macrovoids, membranes obtained from solutions with acetone and ionic liquid this was not observed. They also observed that solution with ionic liquid has binodal curve closer to polymer-nonsolvent line when compared to others. Together with this, high viscosity of ionic liquid causes low nonsolvent inflow rate. These two factors cause polymer solution stays in the metastable region as they discussed, which results in phase inversion with nucleation and growth mechanism and consequently the nodular morphology.

Aim of this Study

In this study, it is aimed to investigate the thermodynamic and the kinetic features of phase separation of cellulose – ionic liquid solutions in relationship to membrane formation. Although there are many studies related on cellulose products obtained by regeneration from ionic liquid solutions, there are a few studies found in literature relating that to membrane fabrication. Together with cellulose, cellulose acetate was investigated as a cellulose derivative and polyether sulfone was investigated as a common membrane material that has a different character when compared to cellulose and cellulose acetate such as much lower hydrophilicity and lack of crystallinity. Solvent and nonsolvent strengths were varied and binary interactions in the polymer-solvent-nonsolvent system were investigated. Phase inversion rates of the different ternary systems were measured. The effect of changing parameters were considered in terms of membrane morphology and performance.

CHAPTER II

EXPERIMENTAL METHODS

2.1. Materials

Cellulose (cotton linter from fibers, medium) and cellulose acetate ($M_n \sim 50\,000$ Da by GPC) was purchased from Sigma Aldrich, and polyether sulfone (PES) was provided by BASF. Ionic liquid 1-ethyl-3-methylimidazolium acetate (EMIMAc, purity $\geq 95\%$) was used as main solvent and purchased from Sigma Aldrich. Co-solvent dimethyl sulfoxide (DMSO) and non-solvent ethanol were provided from both Sigma Aldrich and Merck. Pure ethanol and ultra-pure water were used in solutions, while for coagulation media ethanol was in technical grade and coagulant water was reverse-osmosis water.

2.2. Solution Preparation

Polymers were dried at $80\text{ }^\circ\text{C}$ at least for 24 hours prior to use. Ionic liquid was heated at $90\text{ }^\circ\text{C}$ for one hour, then at $70\text{ }^\circ\text{C}$ for three hours in order to get rid of the volatile impurities. Solutions were stirred with magnetic stirrer. If the only solvent was EMIMAc then solutions were heated while stirring. In Table 2-1 ingredients of solutions are listed with preparation conditions.

Table 2-1 Dope Solutions and Ingredients

Solution Code	Polymer	Solvent	Co-Solvent	Solvent/Cosolvent Ratio	Stirring temperature
C 1	8 % Cellulose	92 % EMIMAc	-	-	70 °C
C 2	8 % Cellulose	46 % EMIMAc	46 % DMSO	1:1 (SS1)	Ambient Temperature
C 3	8 % Cellulose	30.7 % EMIMAc	61.3 % DMSO	2:1 (SS2)	Ambient Temperature
C 4	10.6 % Cellulose	29.8 % EMIMAc	59.6 % DMSO	2:1 (SS2)	Ambient Temperature
CA 1	8 % Cellulose Acetate	92 % EMIMAc	-		45 °C
CA 2	8 % Cellulose Acetate	46 % EMIMAc	46 % DMSO	1:1 (SS1)	Ambient Temperature
PES 1	8 % PES	92 % EMIMAc	-		50 °C
PES 2	8 % PES	46 % EMIMAc	46 % DMSO	1:1 (SS1)	Ambient Temperature

In addition to the solution codes, when labelling membranes, letter ‘W’ refers to nonsolvent water and ‘E’ refers to ethanol as nonsolvent. Solvent mixtures SS1 and SS2 represent the EMIMAc and DMSO mixture in the ratio of 1:1 and 1:2, respectively.

2.3. Solution Characterization

2.3.1. Solvent Viscosity

Viscosities of the solvent and solvent mixtures were measured with capillary viscometer (Ubbelohde type) at 24 ± 1 °C. All measurements other than that for EMIMAc were repeated three times. EMIMAc was measured for once because it takes very long time to measure and water content of EMIMAc might increase due to ambient humidity which may cause error, even if the water content increase may be very small [35]

2.3.2. Solution Viscosity

Solution viscosities were measured with rotational viscometer (TA Instruments ARES rheometer) at 21.5 ± 1 °C at METU Central Laboratory. The viscometer type was coaxial cylinders.

2.4. Membrane Casting

Clear, amber-colored dope solutions were poured on a glass plate and casted with 250 μm casting bar (Figure 2-1) at room temperature in flat sheet form. Cast solutions were directly immersed in nonsolvent bath.

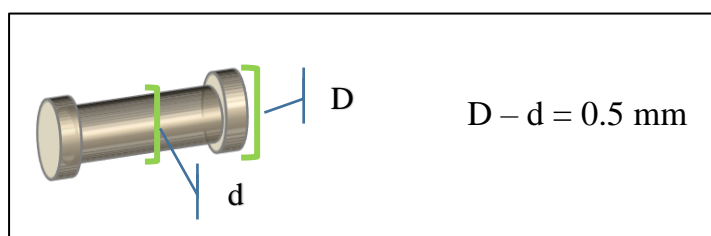


Figure 2-1 Schematic Drawing of Casting Bar

After coagulation, membranes were washed by immersing into reverse osmosis water twice for 1 hour and for a third time for 24 hours. Membranes other than cellulose acetate were stored in ethanol, and cellulose acetate membranes were stored in 0.25% sodium bisulfite solution (cellulose acetate membranes lose their integrity in ethanol). For membranes dried before characterization tests, the drying was done by applying convective flow of nitrogen gas above the membrane.

2.5. Light Transmission Measurements

During phase inversion, opaqueness in polymer solution increases and by making use of this decrease in light transmission, it is possible to measure phase inversion rate [1]. Experimental setup of light transmission measurements is given in Figure 2-2.

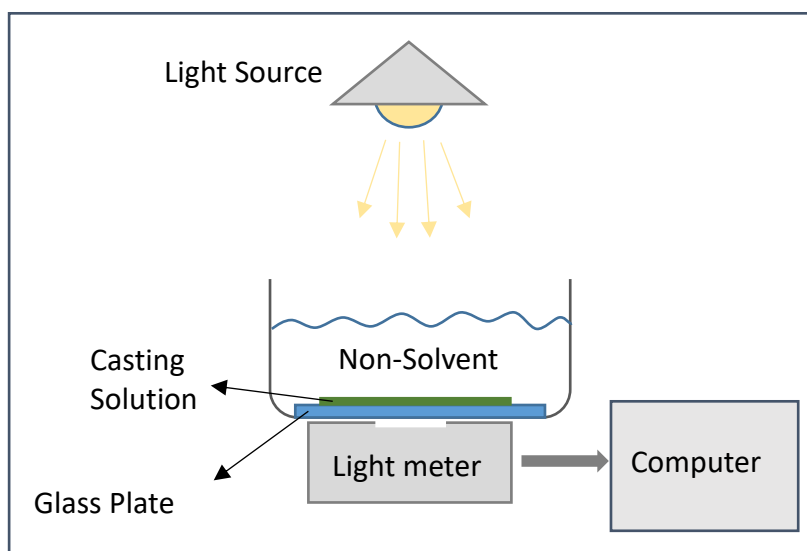


Figure 2-2 Schematic Drawing of Light Transmission Measurement Setup

Light meter placed below the nonsolvent bath measures the amount of light as a function of time. Light meter was in a cardboard box with a little hole above, ensuring that the measured light is only coming from light source after passing through nonsolvent bath and the polymer solution. After casting, polymer solution was immediately placed in nonsolvent bath and light that passes through the polymer solution was measured every second for about 17 minutes. Obtained data were normalized in the form of I/I_0 ; where I_0 is the value for amount of light before immersion and I is the value at any time after the immersion. Typical normalized output is given in Figure 2-3.

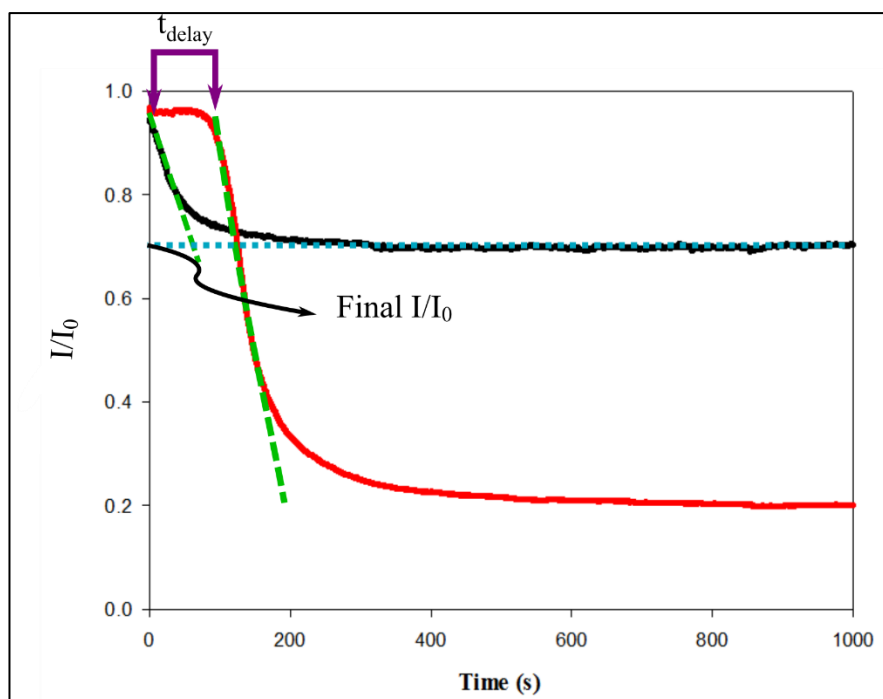


Figure 2-3 Typical Normalized Output of Light Transmission Measurements

Absolute values of initial slopes of light transmission graphs (green dashes in Figure 2-3) were considered as cumulative phase inversion rate. Since the measured light passes through the whole cross-section of polymer solution, the phase inversion rate was referred as cumulative. If phase inversion did not start immediately after the immersion, it was observed in the plot as a horizontal line at the beginning and the time interval between the immersion and starting point of phase inversion was called delay time (t_{delay}). Additionally, I/I_0 value after phase inversion is complete, which is observed as horizontal line at the end (blue dotted line in Figure 2-3), is determined and referred as “Final I/I_0 ”.

2.6. Phase Inversion Front Observations

A drop of polymer solution was placed in between microscope slide and a cover slip. While observing it with optical microscope, certain amount of nonsolvent (20 – 50 – 100 μL , depending on nonsolvent type and observations while precipitation front was

proceeding) was injected from one side of the solution. The progress of the phase inversion was traced as the movement rate of the precipitation front and this rate was considered as instantaneous phase inversion rate of the polymer solution. Zeroth second was taken as the instant the nonsolvent and solution totally contact each other. Thickness of the path that front passed through (from the nonsolvent-solution interface to last point of precipitated area, x) was measured every second. Square of this thickness (x^2) was plotted against time (t) in order to obtain information on diffusivity of nonsolvent in the solution. The slope of the x^2 vs. t plot is directly proportional to the diffusivity term as discussed by Strathmann and coworkers [8]. In Figure 2-4, a schematic drawing of what is seen at time t of phase inversion front observations is given, together with the terms of Equation 2.1.

$$x^2 = \frac{4 \cdot D_{eff} \cdot \varepsilon}{\tau} \cdot \frac{\rho_{NS} - \rho_{CP}}{\rho_{NS} + \rho_{CP}} \cdot t = \frac{4 \cdot D_{eff} \cdot \varepsilon}{\tau} \cdot \frac{1 - w_{CP}}{1 + w_{CP}} \cdot t \quad (2.1)$$

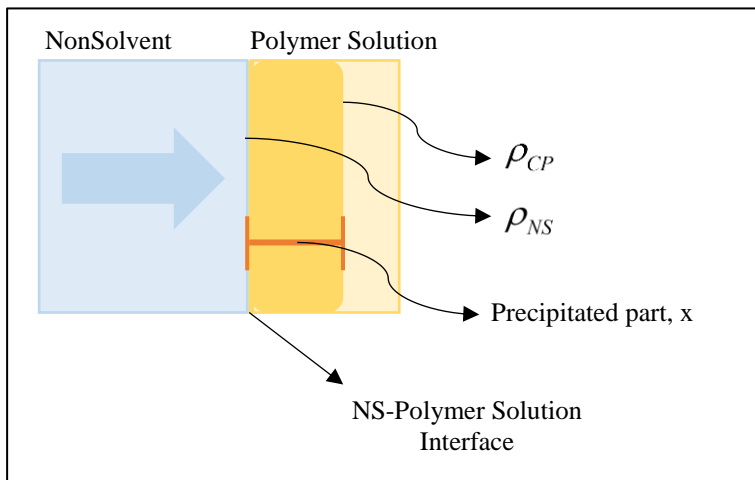


Figure 2-4 Schematic Drawing of Phase Inversion Front Observations

Where D_{eff} is diffusivity of nonsolvent in precipitating layer, ε and τ are porosity and tortuosity of the forming membrane, respectively. ρ_{NS} and ρ_{CP} are the concentration at the nonsolvent side and the concentration of nonsolvent at the precipitation point,

respectively. By dividing pure nonsolvent density these term simplifies into $\frac{1-w_{CP}}{1+w_{CP}}$

where w_{CP} is the weight fraction of nonsolvent at cloud point. The term $\frac{\rho_{NS} - \rho_{CP}}{\rho_{NS} + \rho_{CP}}$ is

not considered as dominant for the equation since it would be close to unity most of the time. Geometric terms ε and τ have certain empirical values, therefore $\frac{\varepsilon}{\tau}$ value

was considered as constant for membranes with similar structure as was done in most studies using this approach [85-87]. As a result, for similar membrane morphologies comparing slopes of x^2 vs. t plots is expected to be equivalent to comparing diffusivities.

2.7. Solubility Parameter Calculations

Hansen solubility parameters were used to have an idea about interactions within the ternary system, especially for solvent and nonsolvent quality. RED values were considered in order to be able to compare systems with each other with the same polymer. Parameter values were taken from [5] for the components other than ionic liquid, while the ones for EMIMAc was taken from [83], which were calculated by HSPiP software.

2.8. Swelling Tests

Swelling tests were applied to dense polymeric films in order to understand the polymer-nonsolvent interactions. Prepared membranes were transparent indicating that they are dense.

2.8.1. Preparation of Dense Films for Swelling Tests

For cellulose acetate dense films, 20% cellulose acetate – 80 % acetone solution was cast on glass plate and was put in an evaporation box. The box was flushed with nitrogen gas for 30 minutes at 0.6 L/min rate before putting the polymer solution and continued to flow at the same rate during the evaporation of acetone from the solution. After 1.5 hours of evaporation, film was peeled off from the glass plate and washed in 2 L tap water twice.

For PES films, 20% PES – 80% NMP (N-Methyl-2-pyrrolidone) solutions were prepared. Solution was cast on a glass plate and placed in vacuum oven at 80 °C. After 2 hours, vacuum was applied again and 7-8 hours after placing the polymer in oven, the film was peeled off from the plate and placed in vacuum oven again, for 24 hours. Finally, films were washed in 2L of tap water twice in order to ensure total solvent removal.

Since C1-W and C2-W membranes are found to be close to dense by SEM images and a solvent evaporation procedure was not possible for cellulose, dense films from this polymer were obtained by immersion precipitation method by coagulation of C 1 and C 2 solution in water.

2.8.2. Swelling Test Procedure

Obtained films were dried under vacuum for at least 2 days. Before immersing in nonsolvent, dry weights were measured. After immersion, films were wiped with paper towel and wet weights were measured on daily basis. After swelling reached the equilibrium (when wet weights are constant in time), tests were finalized. The swelling ratio was calculated as given in Equation 2.2

$$\% Swelling = \frac{m_{wet} - m_{dry}}{m_{dry} \cdot \rho_{NS}} \times 100\% \quad (2.2)$$

Where m_{wet} and m_{dry} are wet and dry weights of films, respectively and ρ_{NS} is the density of nonsolvent that dense films were immersed in. In calculations, density of water was taken as 1.00 g/cm³, while density of ethanol was taken as 0.79 g/cm³. The nonsolvent that swells a film more was considered as poorer nonsolvent for that polymer.

2.9. Cloud Point Measurement

Cloud point is the point on the binodal curve, where the solution is not stable in one phase any more. Therefore, it gives an idea about solution – nonsolvent relationship. Solutions were prepared with certain nonsolvent content, at once, instead of common titration method. Cloud point of the solution was decided to be in between clear

solution with highest nonsolvent content and turbid solution with lowest nonsolvent content. This is a faster way than titration method since solutions are very viscous and determining cloud point by titration takes a lot time. Also, it is possible to know the cloud point of solution with exact polymer concentration with the casting solutions. After solutions were prepared, they were stirred at 30-60 °C until homogenous mixture was reached, then solutions were cooled to 23 ± 2 °C, and turbid and clear solutions are determined by visual observations.

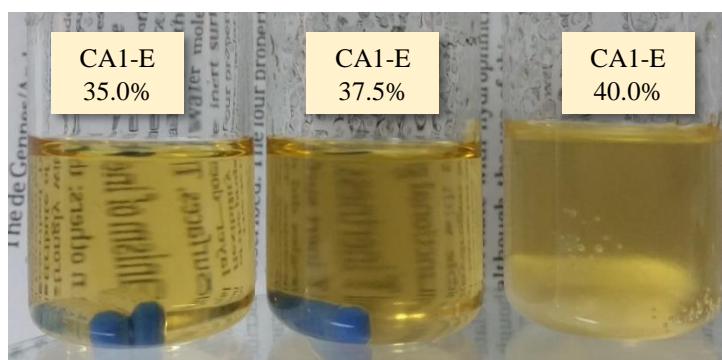


Figure 2-5 Ethanol Cloud Point Solutions of CA 1; from left to right 35%, 37.5%, 40%

In Figure 2-5 given image is belong to set of ethanol cloud point solutions of CA1 system at 35%, 37.5% and 40% ethanol from left to right. As seen in the picture, 35% ethanol solution is clear, while 37.5 % and 40% is turbid; therefore, it was concluded that ethanol cloud point of CA1 solution is in between 35% and 37.5%.

2.10. Dynamic Light Scattering

In order to understand the solvent quality, dynamic light scattering technique was used. Polymers were dissolved in various solvents and solvent systems in approximately 0.1% concentration. The measurements were carried out in both METU Central Laboratory and the Laboratory of Surface and Nanoscience Research Group from Hacettepe University. In both laboratories, the DLS equipment was Malvern CGS-3 ALV.

Hydrodynamic radius was measured for all systems. Since polymer coils get larger as the solvent quality increases (valid for total dissolution), it is concluded that the larger hydrodynamic radius of a polymer indicates the higher quality of a solvent for that polymer [83, 84].

2.11. Performance Tests

2.11.1. Pure Solvent Permeance

Pure water or pure ethanol permeance tests were applied to produced membranes prior to retention tests. Tests were applied with dead-end filtration system (Millipore, Amicon stirred cell). Pure solvent permeance was calculated as follows

$$PSP = \frac{J}{TMP} \quad (2.3)$$

where PSP stands for pure solvent permeance in L/m².h.bar, while J is solvent flux (L/m².h) and TMP is transmembrane pressure difference.

For dried membranes, pure solvent permeance tests were done at 4 bar only; while for non-dried membranes transmembrane pressure was applied at 2, 1.5 and 1 bar and slope of J vs. TMP graph was considered as PSP.

2.11.2. Retention Tests

Retention tests were done by filtering solutions of a number of probe molecules (Table 2-2). For dried membranes tests were done at 4 bar while for non-dried membranes tests were at 1 bar. Retention tests were done with stirred dead-end filtration cell (Figure 2-6). Solutions of probe molecules were fed to the system at 10 mL, and the system was pressurized with nitrogen gas. After 3 or 5 mL of permeate was taken (depending on filtration duration), the filtration was finalized and solution in the cell was taken as retentate. It is shown that during filtration probe molecules deposit on the membrane [88], which should be excluded from retention results in order to find membrane actual performance. Therefore, amount of deposition was calculated with mass balance and if it did not reach equilibrium, retention tests were continued for another set. During filtration, cell was stirred at 250 rpm in order to reduce concentration polarization. Properties of feed solutions are listed in Table 2-2

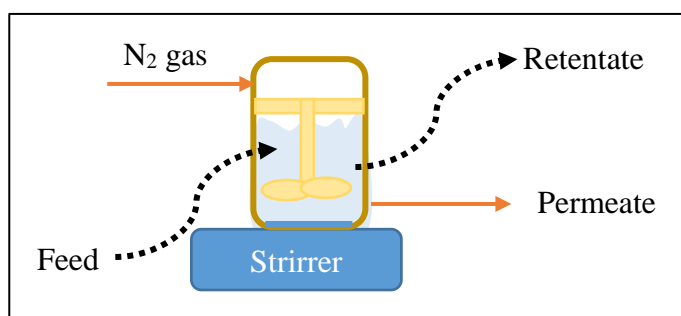


Figure 2-6 Schematic Drawing of Filtration System

Table 2-2 List of Filtration Conditions of Retention Tests

Probe Molecule	Molecular Weight	Solvent	Wavelength of UV/Vis Absorbance (nm)	Feed Solution Concen.	Membrane Drying after Coagulation	TMP (bar)
Bovine Serum Albumin	66 kDa	Water	278	1 g/L	YES	4
Blue Dextran	20 kDa	Water	623	0.04 mM	YES	4
Bromothymol Blue	624.4 Da	Ethanol	423	0.05 mM	YES	4
Bromothymol Blue	624.4 Da	Ethanol	423	0.05 mM	NO	1

% Retention is found as given in Equation 2.4.

$$\% \text{ Retention} = \left(1 - \frac{C_P}{\left(\frac{C_F + C_R}{2} \right)} \right) \times 100\% \quad (2.4)$$

Where C_P , C_F and C_R the concentrations of permeate, feed and retentate solutions, respectively. Concentrations of those solutions were determined by UV/Visible spectroscopy (Schimadzu UV-1601).

2.12. Membrane Morphology

The morphologies of the membranes were observed by scanning electron microscopy (SEM) analysis (FEI Nanosem 430) in METU Metallurgical and Materials Engineering Department. The SEM samples were prepared by breaking membranes in liquid nitrogen and dried under vacuum overnight, and then sputter-coated with gold particles.

Generally, there are three micrographs are available for a membrane, which are total cross-section, nonsolvent side and support side of the membrane. Nonsolvent side is the part of the membrane, which is on the nonsolvent-solution interface during coagulation, while support side is the one close to glass plate.

2.13. Crystallinity

Crystallinity of membranes and polymers were measured with Rigaku Ultima-IV X-Ray diffractometer in METU Central Lab. For polymer powders, samples were scanned between 5-40 degrees, while for membranes that interval is in between 3 – 40 degrees. Additionally, nonsolvent sides of cellulose and cellulose acetate membranes were analyzed with grazing incidence at 0.3, 0.5 and 0.7 degrees.

CHAPTER III

RESULTS AND DISCUSSION

3.1. Membrane Characterization

3.1.1. Membrane Morphology

Scanning electron micrographs of total cross-section (left column), nonsolvent side (middle column) and support side (right column) of cellulose membranes are given in Figure 3-1 and Figure 3-2.

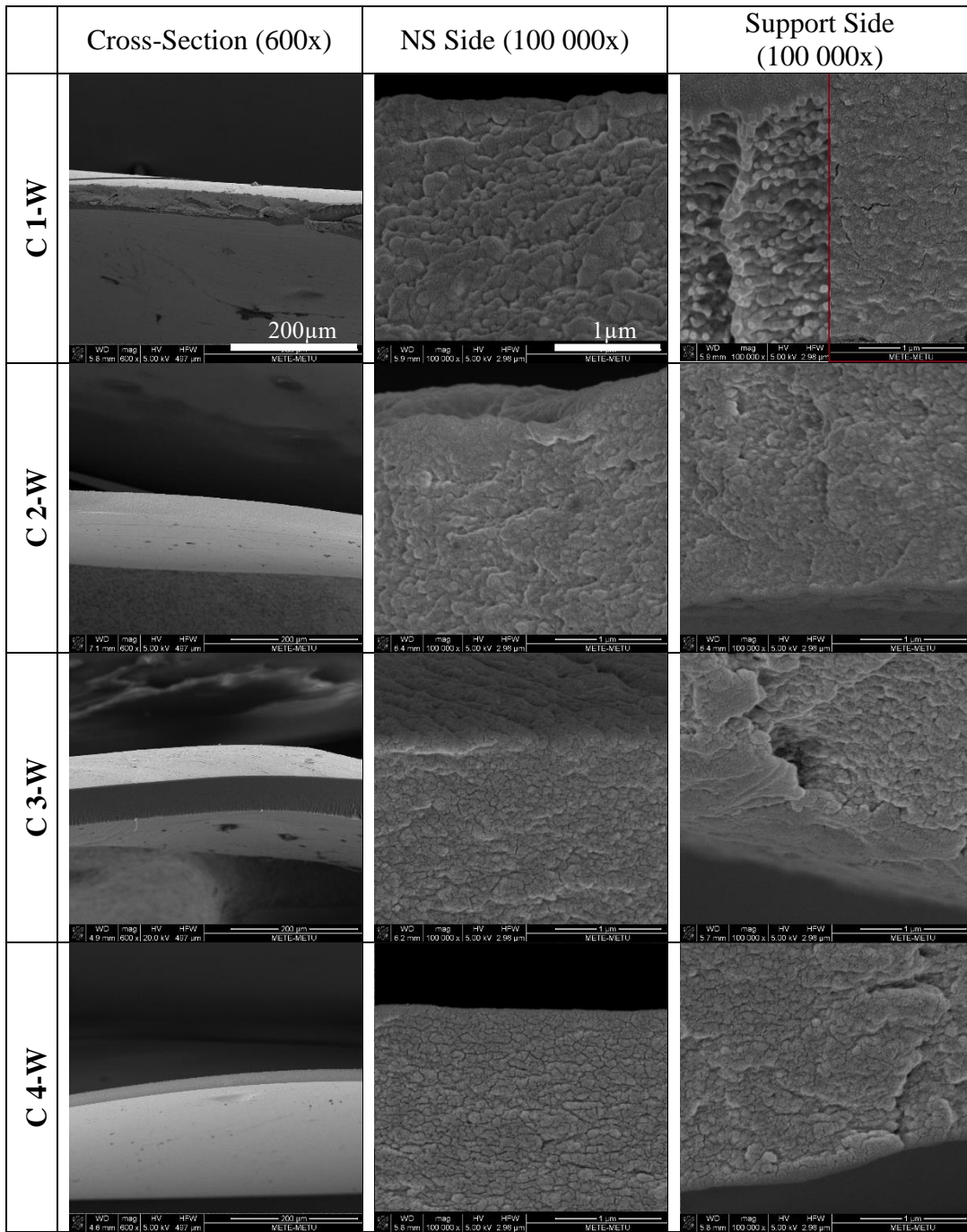


Figure 3-1 SEM Images of Cellulose Membranes Obtained by Coagulation in Water. Scale bars are 200 μm (600x) for cross-section images while 1 μm (100 000x) for side images.

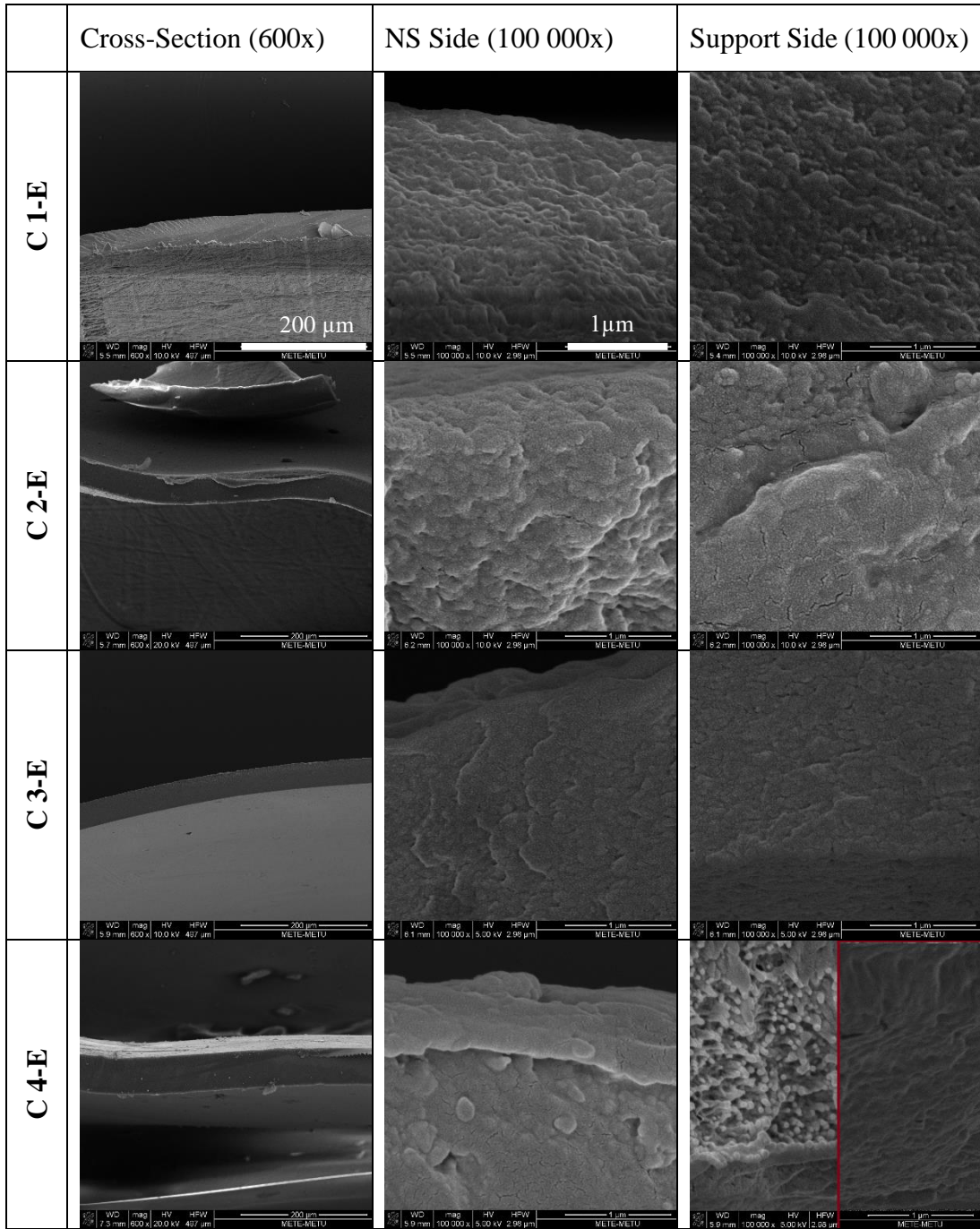


Figure 3-2 SEM Images of Cellulose Membranes Obtained by Coagulation in Ethanol. Scale bars are 200 μm (600x) for cross-section images while 1 μm (100 000x) for side images.

Morphologies of all cellulose membranes are very similar to each other, which may be classified as nodular, dense to microporous. The nodular morphology implies the presence of micropores since voids exist between nodules. IUPAC defines the micropore as pore size not exceeding 2.0 nm, and pores in that size are not possible to see with SEM. None of the cellulose membranes have macrovoids in their structure. All cellulose membranes are symmetric, which means that there is not a significant difference in structure throughout the cross section. Additionally, for membranes C1-W and C4-E two support side images are given, which belong to different SEM measurements. Two images were merged to show that porous-like structure seen once, was not observed for other sample. This may imply that slight asymmetry was present in some batches, meaning that the support side had somewhat larger (around 80 nm) pores. The absence of these in repeated membranes may be due to poor reproducibility, which was not reflected in performance tests. This is expected since it would be the nonsolvent side that determines the membrane performance whether or not the support side has larger pores. Thickness of cellulose membranes were given in Table 3-1, the values given with error margins belong to two (or more) measurements of different SEM analyses. Thickness of cellulose membranes are in the range of 10 to 60 μm ; and mostly lie around 40 μm . During drying step (after coagulation), membrane shrinking may not be always uniform which may cause large deviations in thicknesses (as in C4-E).

Table 3-1 Thicknesses of Cellulose Membranes

	Thickness (μm)
C 1-W	26 \pm 9
C 1-E	43.2
C 2-W	45 \pm 11
C 2-E	46
C 3-W	43 \pm 15
C 3-E	40
C 4-W	19
C 4-E	34 \pm 24

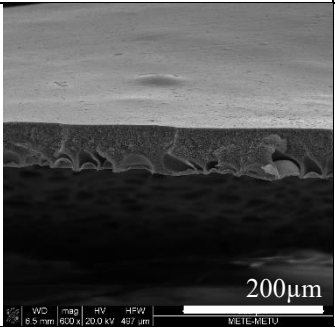
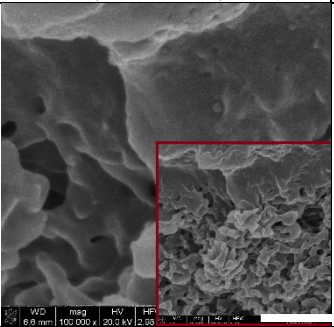
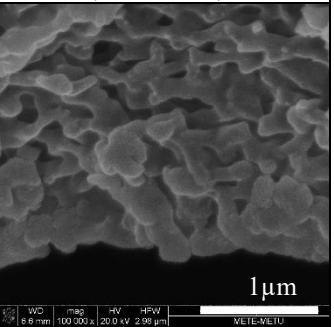
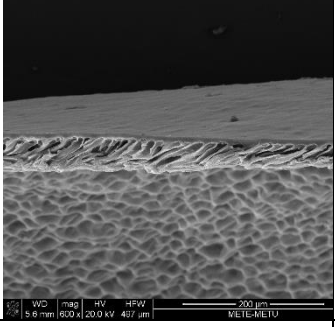
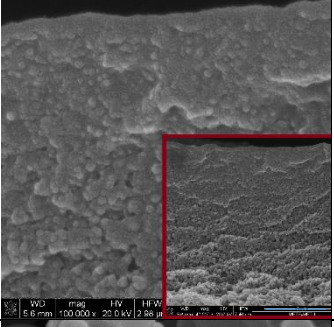
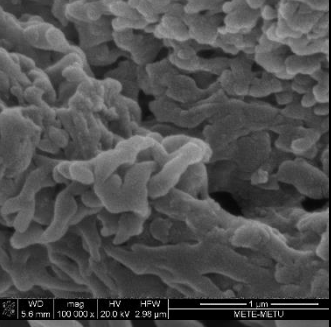
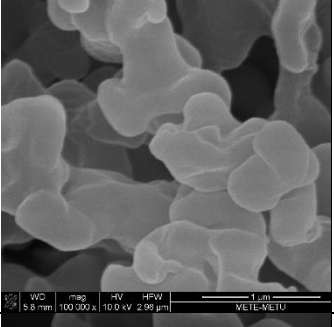
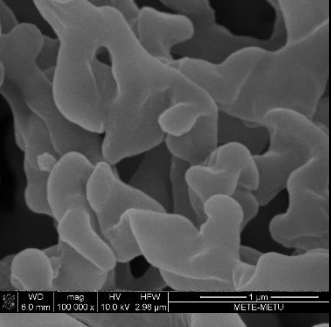
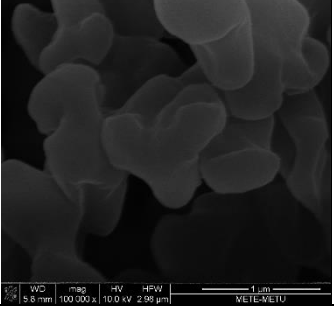
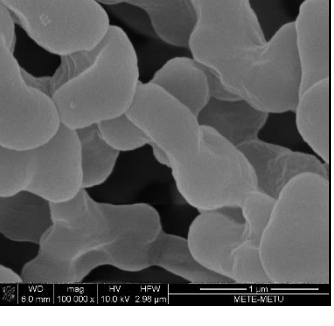
	Cross-Section (600x)	Nonsolvent Side (100 000x)	Support Side (100 000x)
CA 1-W			
CA 2-W			
CA 1-E	*Images are for top and bottom surfaces		
CA 2-E	*Images are for top and bottom surfaces		

Figure 3-3 SEM Images of Cellulose Acetate Membranes. Scale bars are 200 μm (600x) for cross-section images while 1 μm (100 000x) for side and surface images.

In Figure 3-3, SEM images of cellulose acetate membranes are given in the same magnification as in previous figures. Since cellulose acetate membranes obtained from coagulation in ethanol could not be broken with liquid nitrogen, images of those membranes are taken from surfaces. For membranes obtained from coagulation in water, two images are given for nonsolvent side. Image in smaller magnification (40000x) is given on the right bottom corner of larger magnification-images. For CA1-W and CA2-W inset scale bars are 3 μm .

Structure of cellulose acetate membranes are nodular, asymmetric and they all have macrovoids. CA 1-W membrane has a thickness of 67 μm and circular macrovoids exist at the support side. Distance between nonsolvent side surface and macrovoid initiation point is 38 μm . NS-side image of this membrane shows that it has a dense skin layer of approximately 1.3 μm thickness. Moreover, average pore sizes right under this skin layer and near support side are around 0.20 μm . CA 2-W membrane has again nodular and asymmetric structure and thickness of 45 μm . Macrovoids start 7 μm distance from the top (nonsolvent side) and have finger-like structure. Apparent skin layer (from the top surface until a measurable pore at the largest magnification) of this membrane is 1 μm thick, which is nodular unlike skin layer of CA1-W. This is an indication of that CA2-W apparent skin layer is looser when compared to skin layer of CA1-W. Additionally, while pore size beneath the apparent skin layer is approximately 39nm, pore size at the support side is two folds of the nonsolvent side.

Cross-section images are not available for CA membranes obtained from coagulation in ethanol. Surface images of these, show interconnected micron-sized pores for both membranes. They are extremely loose when compared to their water-coagulated counterparts.

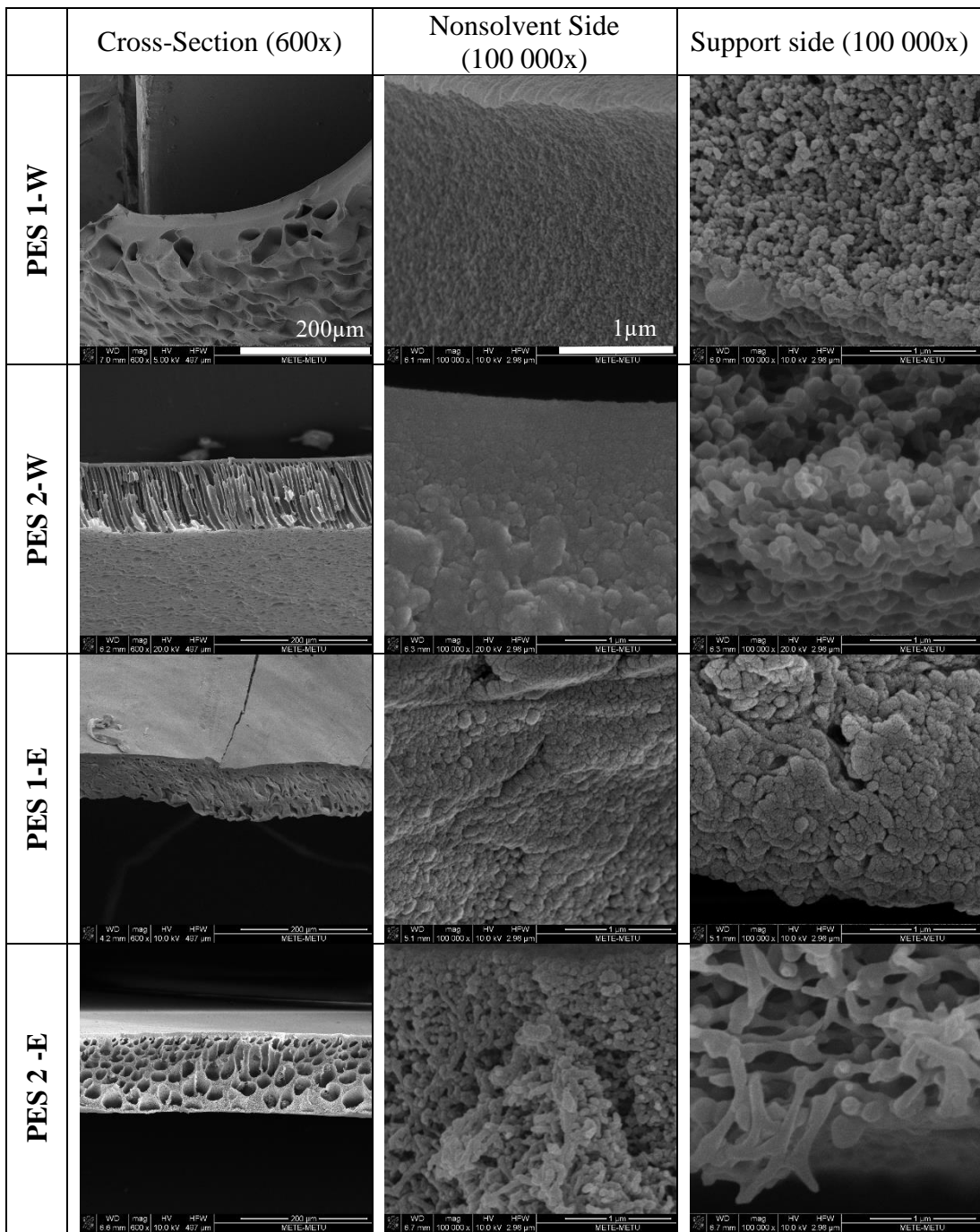


Figure 3-4 SEM Images of PES Membranes. Scale bars are 200 μm (600x) for cross-section images while 1 μm (100 000x) for side images.

SEM images for cross-section of PES membranes are given in Figure 3-4, again in same order and magnification. Asymmetric and nodular structure is observed for these membranes also. Similar to CA1-W, PES 1-W has circular macrovoids at the support side. The thickness of PES 1-W membrane is 76 μm and macrovoids start from 33 μm . While the smallest measurable pores beneath the nonsolvent side are ca. 20nm, support side has 60 nm pore size. 112 μm thick PES 2-W membrane has finger-like macrovoids initiating at 5 μm from the top (nonsolvent side). The measurable pores starts at 0.6 μm from NS side (apparent skin layer thickness) and they are 34 nm on average, while pore size at the support side has an average of 170 nm. Macrovoids start closer to the nonsolvent-side surface and their form changes from circular to finger-like when DMSO is added to solution. This is a common behavior for CA and PES membranes obtained from coagulation in water. According to Wang et al. this is an indication of that SS1 is better solvent than EMIMAc for these polymers [89].

Skin layers of PES membranes obtained by coagulation in ethanol are looser than membranes obtained by coagulation in water. For PES1-E, measurable pore size at nonsolvent side is around 34 nm and at support layer, this value is approximately 70 nm. For PES 2-E circular macrovoids get larger compared to the case PES 1-E. Pore size is about 49 nm beneath the apparent skin layer and 163 nm for support layer.

Table 3-2 Morphological Properties of Prepared Membranes

Membrane	Skin Layer Thickness	Pore size on NS side	Pore size on support side	Thickness (μm)	Macrovoids
C1-W	–	–	–	26 \pm 9	–
C1-E	–	–	–	43.2	–
C2-W	–	–	–	45 \pm 11	–
C2-E	–	–	–	46	–
C3-W	–	–	–	43 \pm 15	–
C3-E	–	–	–	40	–
C4-W	–	–	–	19	–
C4-E	–	–	–	34 \pm 24	–

Table 3-2 (continued)

CA1-W	Totally dense, 1.3 μm thick	0.25 μm under dense skin	0.16 μm	57 \pm 10 μm	Circular close to support side start at 38 μm .
CA2-W	Nodular, 1 μm thick	39 nm	78 nm	35 \pm 10 μm	Finger-like start at 7 μm
PES1-W	Nodular	20 nm	60 nm	91 \pm 16 μm	Circular close to support side start at 33 μm from top
PES1-E	Nodular, 7 μm	34 nm	70 nm	77 μm	Small macrovoids, all throughout the cross-section
PES2-W	Nodular, 0.6 μm	34 nm	170 nm	93 \pm 19 μm	Finger-like start at 5 μm
PES 2-E	10 μm	49 nm	163 nm	127 μm	Circular

In Table 3-2, observations on membrane morphologies are summarized. For cellulose membranes, structure and thickness of cross-sections are very similar to each other. Change in solvent and nonsolvent did not affect the cellulose membrane morphology. However, cellulose acetate membranes have asymmetric structure, unlike cellulose membranes. Additionally, both solvent and nonsolvent change the structure. For cellulose acetate membranes obtained from coagulation in water, circular macrovoids at the support side change to finger-like macrovoids extending whole throughout the cross-section upon addition of DMSO to starting solution. While CA1-W membrane shows a quite dense skin layer, CA2-W have nodular and porous skin layer. Ethanol as nonsolvent results in totally loose membrane structure with micron-size pores. Observations on PES membrane morphologies are more similar to cellulose acetate

ones than cellulose ones. For PES1-W circular macrovoids are also observed near the support side and again they change to finger-like macrovoids that start much closer to the nonsolvent side as DMSO is added to the initial polymer solution. Also, membranes from PES 2 solution have looser skin layer than the ones from PES 1 solution, indicating that for PES and cellulose acetate adding DMSO to the polymer solutions results in looser membrane morphology. In addition to that again for PES and CA, solutions coagulated in ethanol have looser structure than the ones coagulated in water.

3.1.2. Membrane Crystallinity

XRD measurements were done on polymer powders for 2θ between 5° and 40° . XRD pattern of cellulose powder is given in Figure 3-5. Gray dashed-lines at 15.4° , 22.7° and 34.7° are typical peaks seen for Cellulose-I structure [90]. Therefore, from the figure it is clear that cellulose powder used in polymer solutions to obtain membranes have Cellulose-I crystalline structure at the beginning.

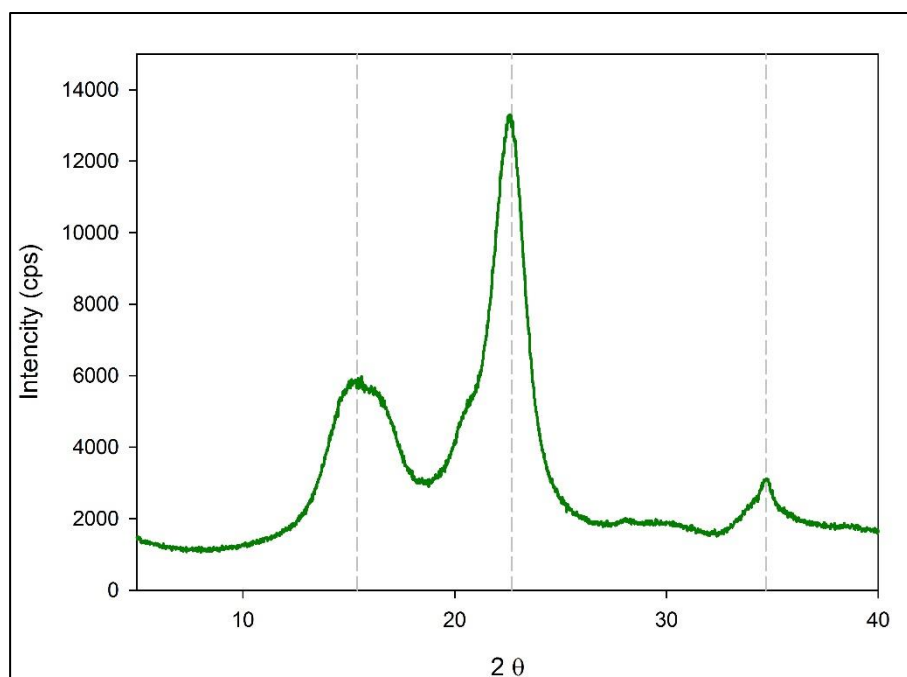


Figure 3-5 XRD Pattern of Cellulose Powder

XRD measurements were also done on membranes from C1, C2 and C3 solutions. Measurements were firstly done on both nonsolvent and support side of the C1-W membrane and it was seen that crystallinity is higher on the nonsolvent side (Figure 3-6). All measurements were taken from the nonsolvent side of the membranes.

Since the phase inversion rate may not be uniform along the cross-section of polymer solution, crystallinity at different parts of a membrane may be different also. These measurements were done with three different grazing incidence angles as 0.3° , 0.5° and 0.7° . With grazing angle, X-ray beam aims a part of membrane that is very close to nonsolvent-side surface, as the angle gets smaller the part of the membrane that the data is collected from, gets closer to the surface. Diffractograms of bulk and grazing incidence measurements applied to cellulose membranes are given in Figure 3-7, in which plots are shifted away on y-axis to make them more distinguishable and typical peaks for Cellulose-II structure are indicated with dashed lines.

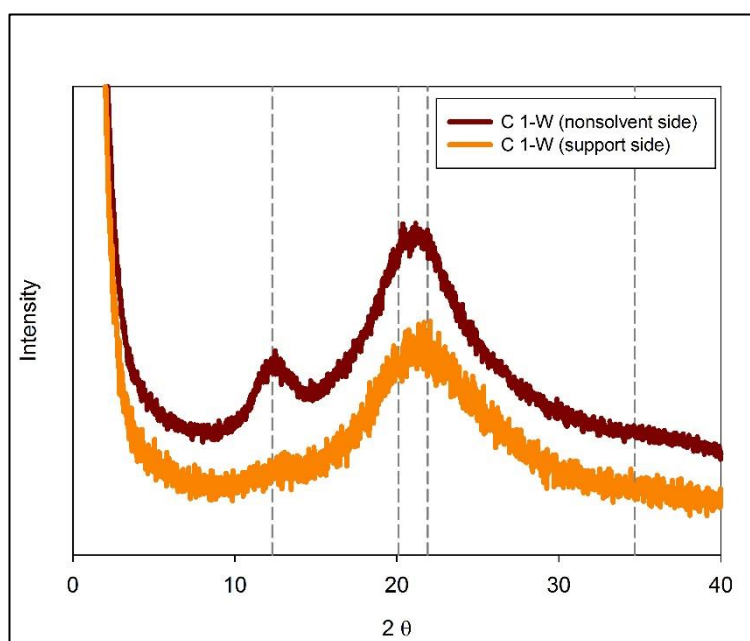


Figure 3-6 X-Ray Diffractograms of Nonsolvent and Support Side of C1-W (plots are shifted apart)

As seen in Figure 3-7, cellulose membranes have a peak between 20.1 and 21.9° in common and some membranes give peak at 12.3° . These peaks are typical for Cellulose – II structure [91]. Therefore, all cellulose membranes transformed from

Cellulose-I to Cellulose-II; even though, crystallinities vary from membrane to membrane. Since typical background hump for amorphous materials is seen around 20°, it may be confused with the peak at around 20° of Cellulose-II. Therefore, crystallinities of membranes were estimated by comparing the heights of the peak at 12.3° in Figure 3-8. Together with this peak, the heights of the peak around 20 degrees supports the crystallinity.

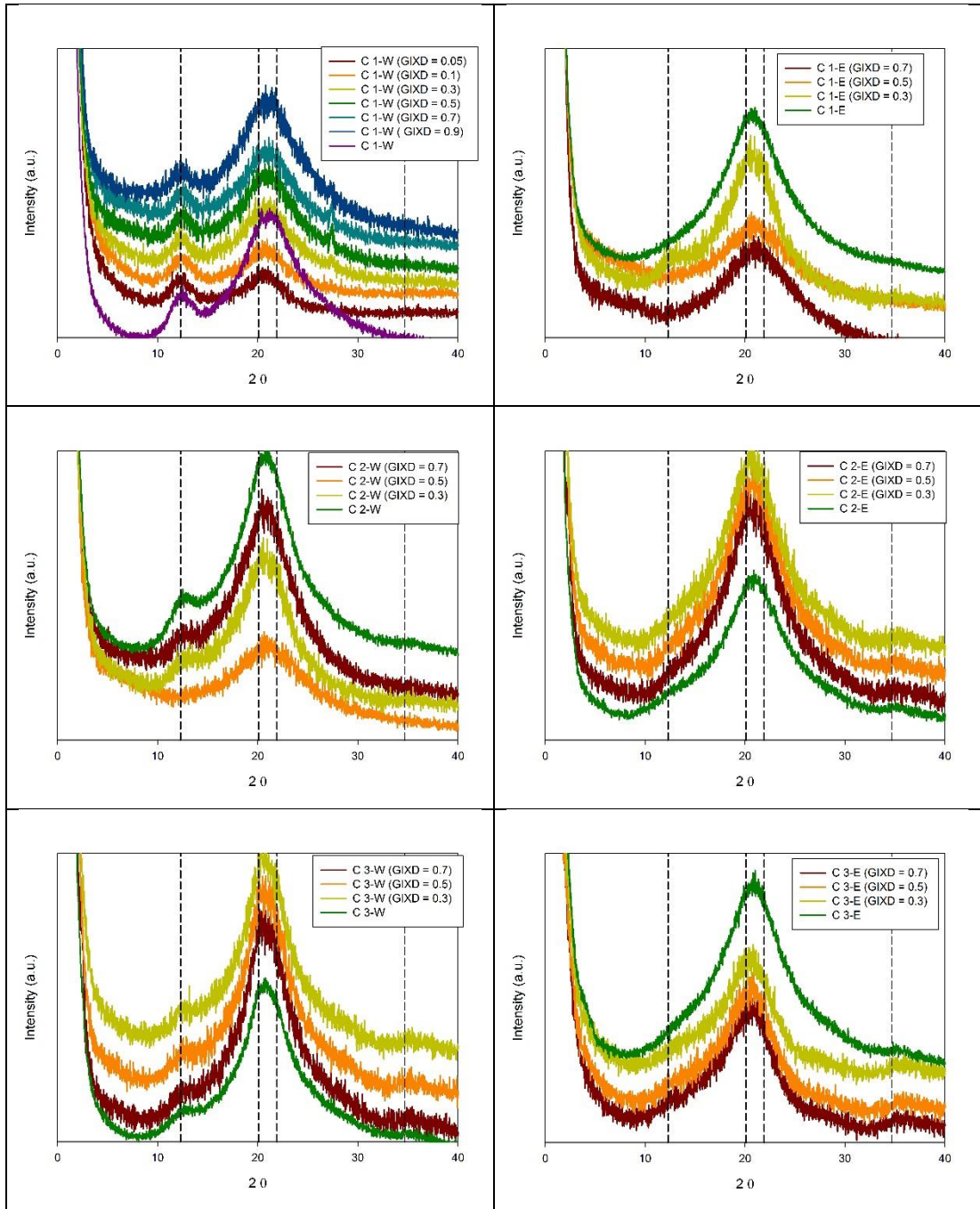


Figure 3-7 XRD Patterns of Cellulose Membranes in the order of C1-W, C1-E, C2-W, C2-E, C3-W and C3-E (plots are shifted apart)

In Figure 3-7, cellulose membranes have nearly the same pattern at different grazing angles and at the bulk measurement, which may imply that membranes have similar structure for the measured parts in terms of crystallinity. On the other hand, for C1-E membrane, peak at 12.3° is seen for grazing incidence angle 0.3° , while it is not seen

for other angles. This is an indication of that C1-E membrane has a limited region where cellulose is in crystalline form near the nonsolvent side.

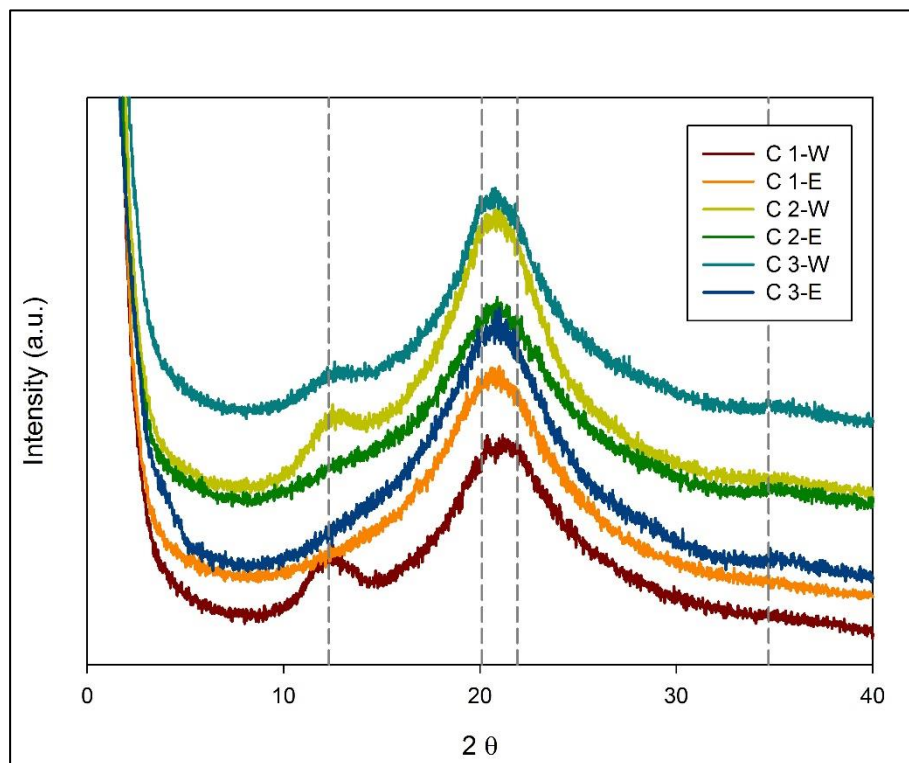


Figure 3-8 XRD Patterns of Cellulose Membranes (plots are shifted apart)

Decrease in crystallinity and change in crystalline structure from Cellulose I to Cellulose II are very common results of dissolution and regeneration of cellulose [19,20]. By comparing depths of peaks at 12.3° in Figure 3-8, crystallinities decrease in the order of C1-W > C2-W > C3-W. Crystallinity of membranes obtained from water are higher than the ones obtained from coagulation in ethanol as seen in [65]. In literature, regenerated products from ionic liquid solutions have higher crystallinity or ordered structure when compared to regenerated products obtained from conventional methods [45,65,81]. It is also discussed that cellulose in ionic liquid has sort of regular arrangement in molecular level [92]. When membranes obtained from coagulation in water are compared, as EMIMAc amount increases in the initial polymer solution, the

crystallinity of resultant membrane increases, which may be another indication of ordering effect of ionic liquid.

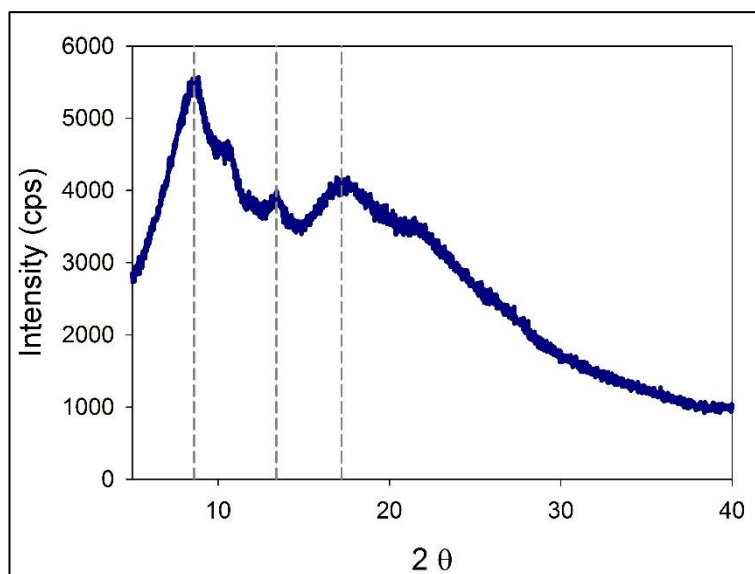


Figure 3-9 X Ray Diffractogram of Cellulose Acetate Powder

In Figure 3-9, XRD pattern of cellulose acetate powder is given, at 2θ is 8.6° , 13.4° and 17.2° , which are seen in literature also [93]. XRD measurements were done for cellulose acetate membranes obtained from coagulation in water including bulk and different grazing incidence angles. When patterns of powder (Figure 3-9) and the ones of membranes (Figure 3-10) are compared, it is observed that the peaks other than the one at 8.6° are disappeared.

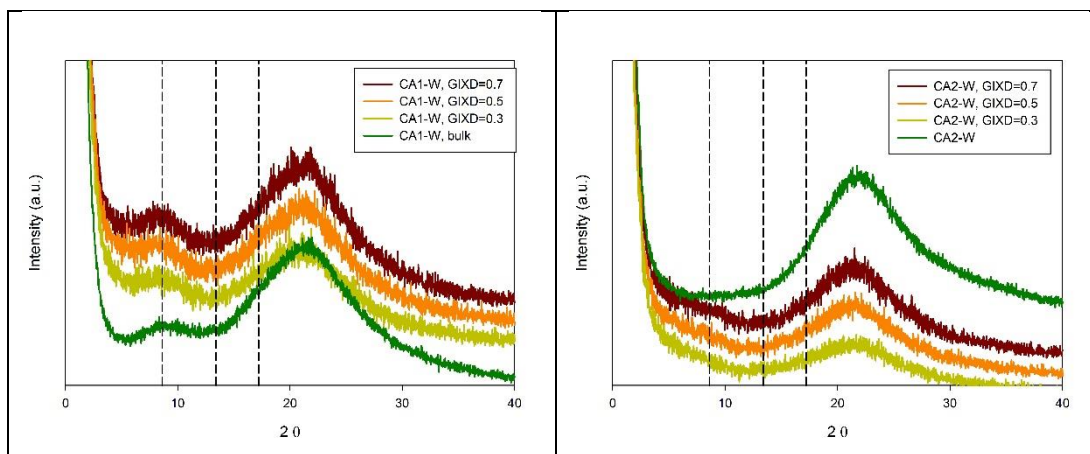


Figure 3-10 XRD Patterns of Cellulose Acetate Membranes Obtained from Coagulation in Water (plots are shifted apart)

The peak seen at 8.6° for CA1-W membrane in Figure 3-10 is absent in CA2-W membrane. Similar to the cellulose membranes, crystallinity of cellulose acetate membranes also decrease when DMSO is added to the polymer solution.

3.1.3. Performance Tests

Performance of obtained membranes were tested in terms of pure solvent permeance (pure water permeance and pure ethanol permeance) and retention tests. Performances of membranes, which were dried after coagulation, were tested firstly then for selected membranes, performance tests were applied without drying after coagulation (non-dried membranes).

In Figure 3-11, Blue Dextran (20 kDa, in water) retentions of dry membranes are given with pure water permeances in Figure 3-12.

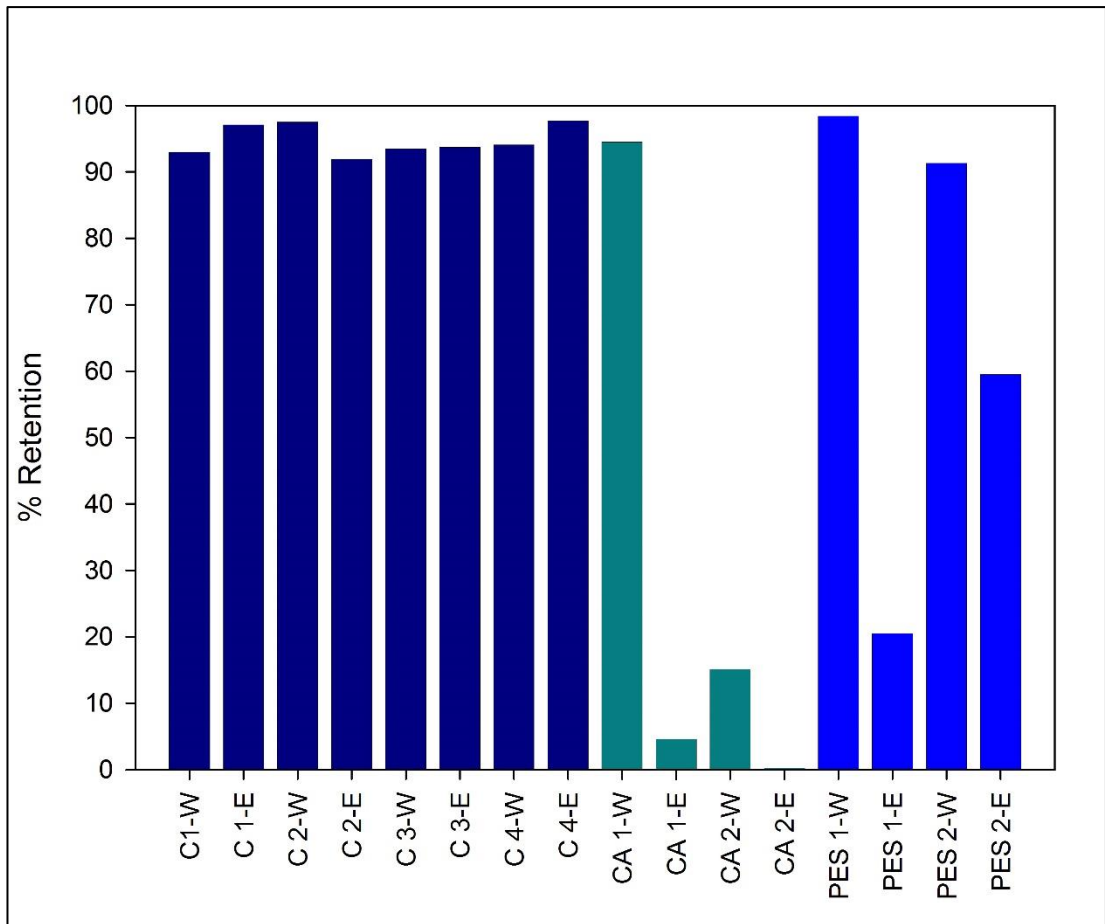


Figure 3-11 Blue Dextran (20 kDa) Retention of Dried Membranes

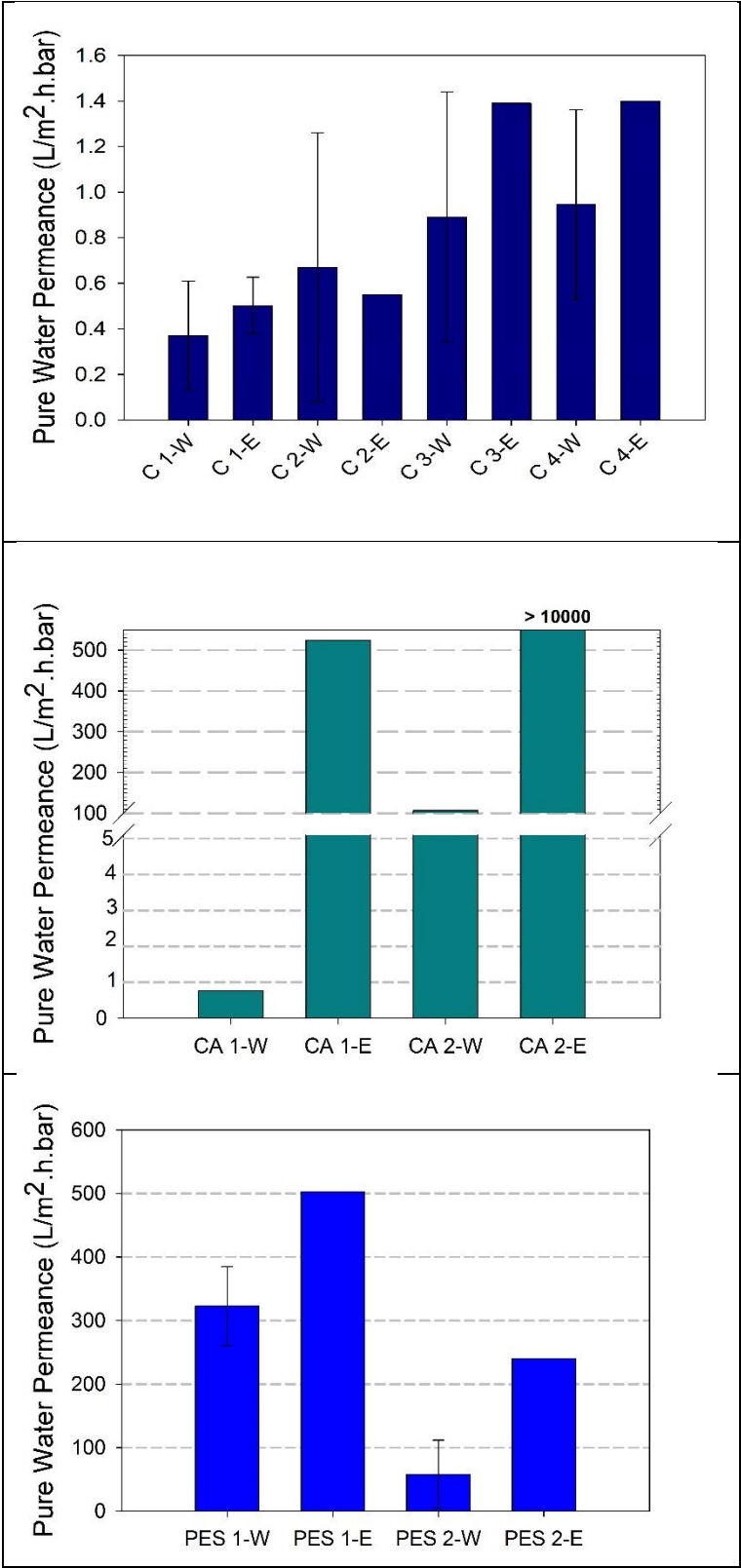


Figure 3-12 Pure Water Permeances of Dried Membranes

Rejection performances of membranes (dried) are in accordance with morphologies. Cellulose membranes perform similarly, in agreement with the observation that all eight cellulose membranes have very similar morphology with each other. For cellulose acetate membranes, Blue Dextran retention of CA 1-W has the highest performance since the skin layer of it is the densest. Retention of CA 2-W decreases to 15 %. CA 1-E and CA 2-E retentions are very low and pure water permeances are very high ($> 500 \text{ L/m}^2 \cdot \text{h} \cdot \text{bar}$ for CA1-E and > 10000 for CA2-E) as expected from extremely loose morphology. Since PES membranes obtained from coagulation in ethanol have looser skin than coagulation in water, rejection performances of those membranes are lower than PES-W membranes.

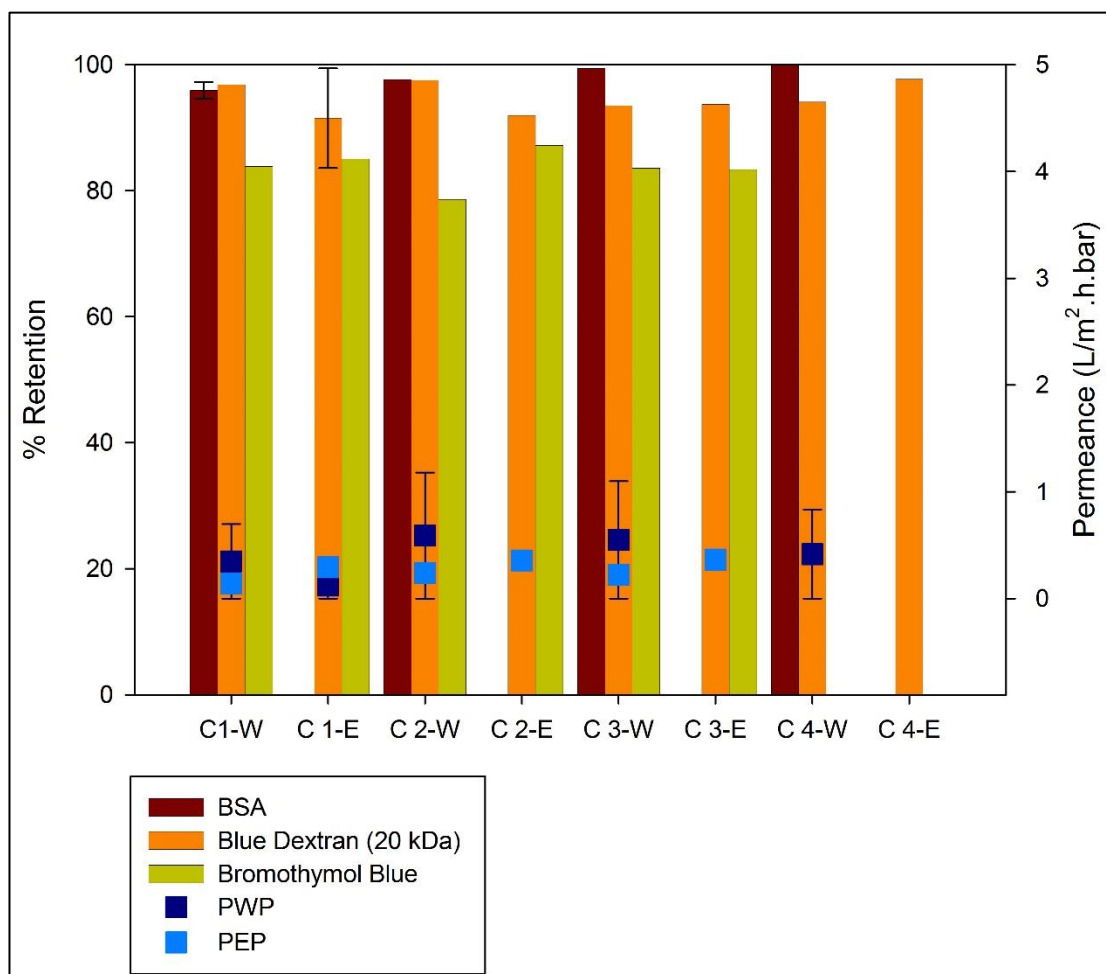


Figure 3-13 Blue Dextran and Bromothymol Blue Retentions of Dried Cellulose Membranes

To distinguish between cellulose membrane performances, dried membranes were tested with two other probe molecules, as well: BSA (66 kDa) and Bromothymol Blue (624.4 Da) (Figure 3-13). However, dried membranes performed similarly with all three probes. More than 90% retention for BSA and Blue dextran and around 80% retention of Bromothymol Blue was observed.

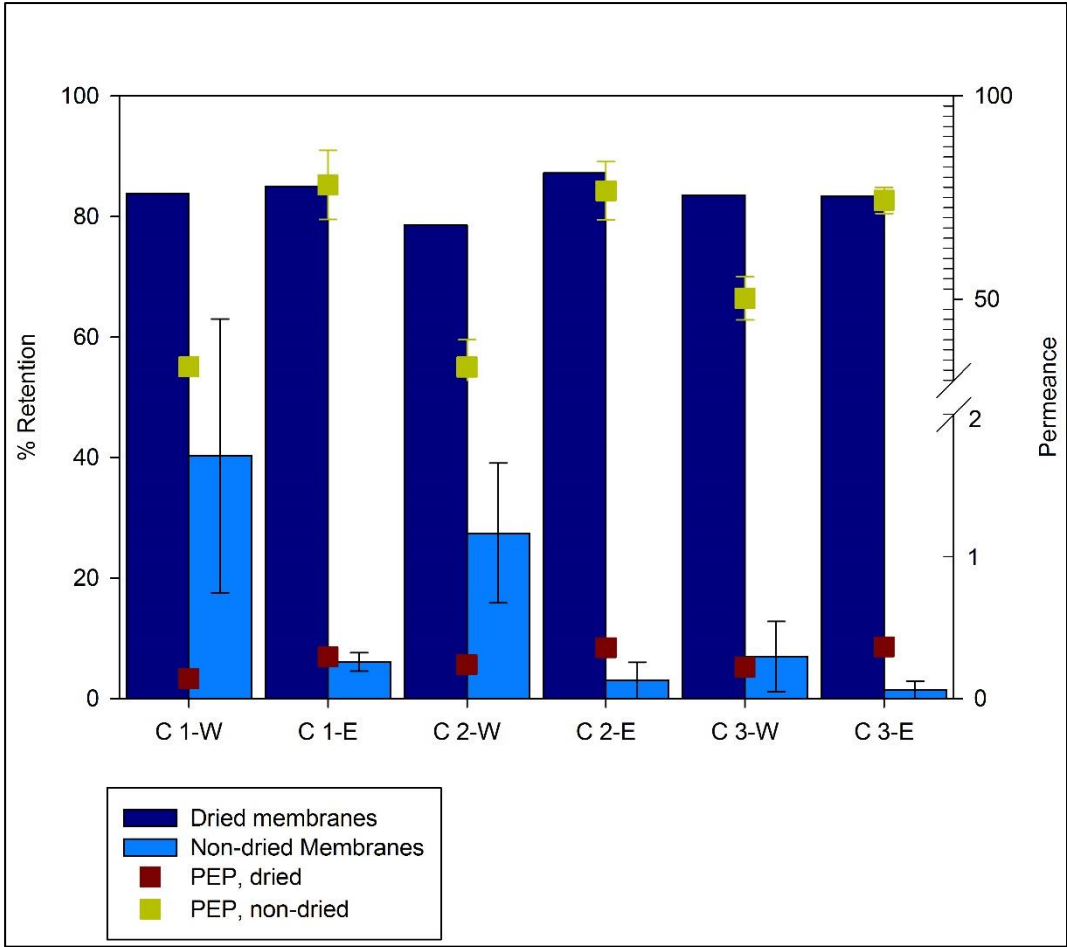


Figure 3-14 Bromothymol Blue Retentions of Dried and Non-dried Cellulose Membranes

Similar performances of cellulose membranes may be a result of drying step. If some porosity exist within structure of the membrane, it might collapse due to drying [94]. Once pores are collapsed with drying, the pores cannot regain their shape upon swelling with solvent of filtration tests. This is in accordance with the observation that

membrane could not reach initial size (right after coagulation) after drying followed by swelling. Performances of membranes that were not dried after coagulation (named non-dried membranes) are different from dry membrane performances. Drying step increased the retention while decreased the pure solvent permeance. While pure ethanol permeances of dried membranes could not exceed 1 L/m².h.bar, non-dried membranes have permeances of more than 50 L/m².h.bar, which implies that drying procedure caused some pores to collapse irreversibly. As opposed to ca. 80% Bromothymol Blue retentions of all dried membranes, non-dried membranes cannot reject Bromothymol Blue by more than 60%. While C1-W, C2-W and C3-W have Bromothymol blue retentions of about 40, 28 and 7%, respectively, their ethanol-coagulated counterparts have below 5% retention. These relatively low retentions and high permeances imply that these membranes are looser than the other ones. Therefore, membranes obtained from coagulation in ethanol are expected to be more porous than the ones obtained from coagulation in water. In addition, this supports the hypothesis that cellulose membranes are microporous, since pores are not obvious in SEM images but performances of those membranes are different. Not seeing porous structure in cellulose membranes with SEM may be due to drying procedure of SEM sample preparation.

3.2. Factors Affecting Thermodynamics of Polymer-Solvent-Nonsolvent Systems

Polymer-solvent and polymer-nonsolvent interactions within the ternary systems used for membrane fabrication via phase separation were evaluated both experimentally and theoretically. Dynamic light scattering (DLS) measurements were done for polymers in several solvents in order to find hydrodynamic radii. The size of polymer coil in a solvent indicates the solvent quality when compared to sizes in other solvents. In addition to the DLS measurements, Hansen solubility parameter approach was used to estimate the affinity between polymer and solvent. Similar to that, for investigation of polymer- nonsolvent interactions swelling tests were applied and solubility parameters were used.

3.2.1. Theoretical Approach: Hansen Solubility Parameters

RED values of polymer-nonsolvent and polymer-solvent interactions are given in Table 3-3. Solubility parameters and Ro values of components were taken from Hansen Solubility Parameters [5] except for EMIMAc, which is taken from Nunes et al. [83]. In that study, solubility parameter of ionic liquid is calculated by the software HSPiP. RED values for polymer-solvent and polymer-nonsolvent were calculated. If a solvent is a good solvent for a polymer, the RED value of the interaction should be less than unity and as it approaches zero the solvent quality improves. Similarly, RED value higher than 1 indicates the interactions between strong nonsolvent and polymer. As the value gets larger than 1 the interactions get worse indicating improved nonsolvent quality. Near the limit of 1, whether a solvent would dissolve the polymer or not, is uncertain [5].

Table 3-3 RED Values of Solvent and Nonsolvent Interactions with Polymer

Polymer-Solvent	RED P-S	Polymer-Nonsolvent	RED P-NS
Cellulose-EMIMAc	0.485	Cellulose-Water	1.224
Cellulose-SS1	0.701	Cellulose-Ethanol	1.024
Cellulose-SS2	0.778		
Cellulose Acetate-EMIMAc	1.119	Cellulose Acetate-Water	3.645
Cellulose Acetate-SS1	0.637	Cellulose Acetate-Ethanol	1.230
Cellulose Acetate-DMSO	0.614		
PES-EMIMAc	1.710	PES-Water	5.564
PES-SS1	1.150	PES-Ethanol	2.077
PES-DMSO	0.996		

SS1 and SS2 are the solvent mixtures of EMIMAc and DMSO in the ratio of 1:1 and 1:2, respectively. According to Table 3-3, EMIMAc as itself is better solvent for cellulose than solvent mixtures. Since only DMSO does not dissolve cellulose, it is reasonable to have larger RED values of solvent mixture – cellulose interactions than

ionic liquid-cellulose interactions. On the other hand, EMIMAc is near the solubility limit for cellulose acetate and PES; while, solvent mixtures of EMIMAc and DMSO have lower RED values indicating that SS1 is better solvent for those polymers.

Comparing nonsolvents, water seems to be the stronger nonsolvent for all polymers. The differences between water and ethanol get larger as the hydrophilicity of the polymer decreases ($C > CA > PES$). For cellulose, both nonsolvents are near the solubility limit (1.224 and 1.024 for water and ethanol, respectively) while for cellulose acetate only ethanol is at the limit (1.230). The poor nonsolvent quality of ethanol for cellulose acetate is apparent from the very loose morphology, supporting the RED value. Both nonsolvents are far from the limit for PES as 5.564 and 2.077 for water and ethanol, respectively.

3.2.2. Polymer-Nonsolvent Interactions: Swelling Tests

Swelling tests were applied as a measurement of polymer-nonsolvent interactions. Swelling ratios when equilibrium swelling is reached and swelling ratio in time are given in Figure 3-15 and Figure 3-16, respectively.

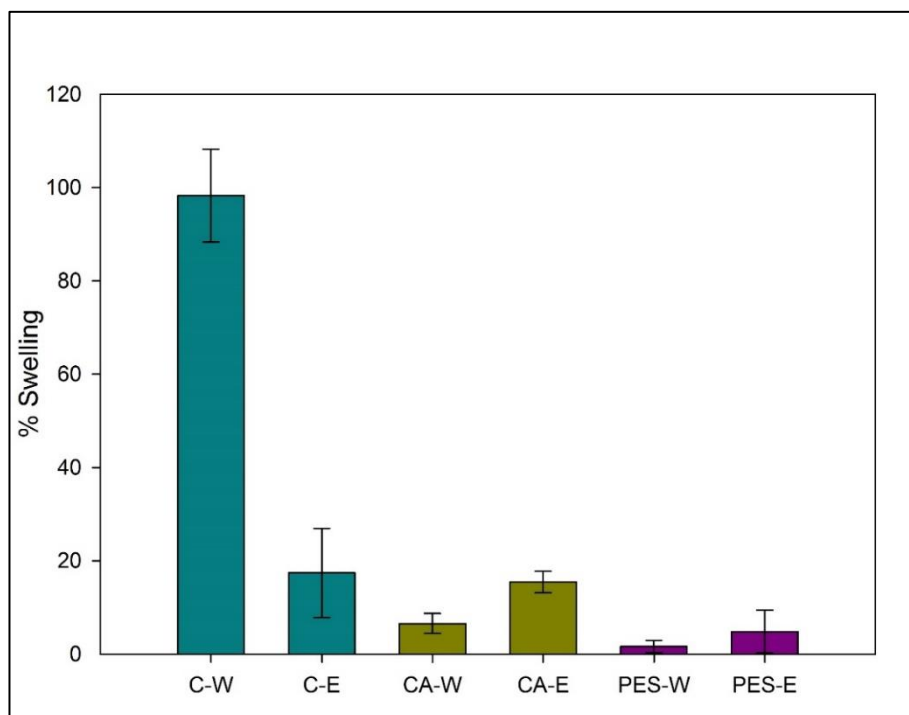


Figure 3-15 Swelling Ratios of Films at Equilibrium

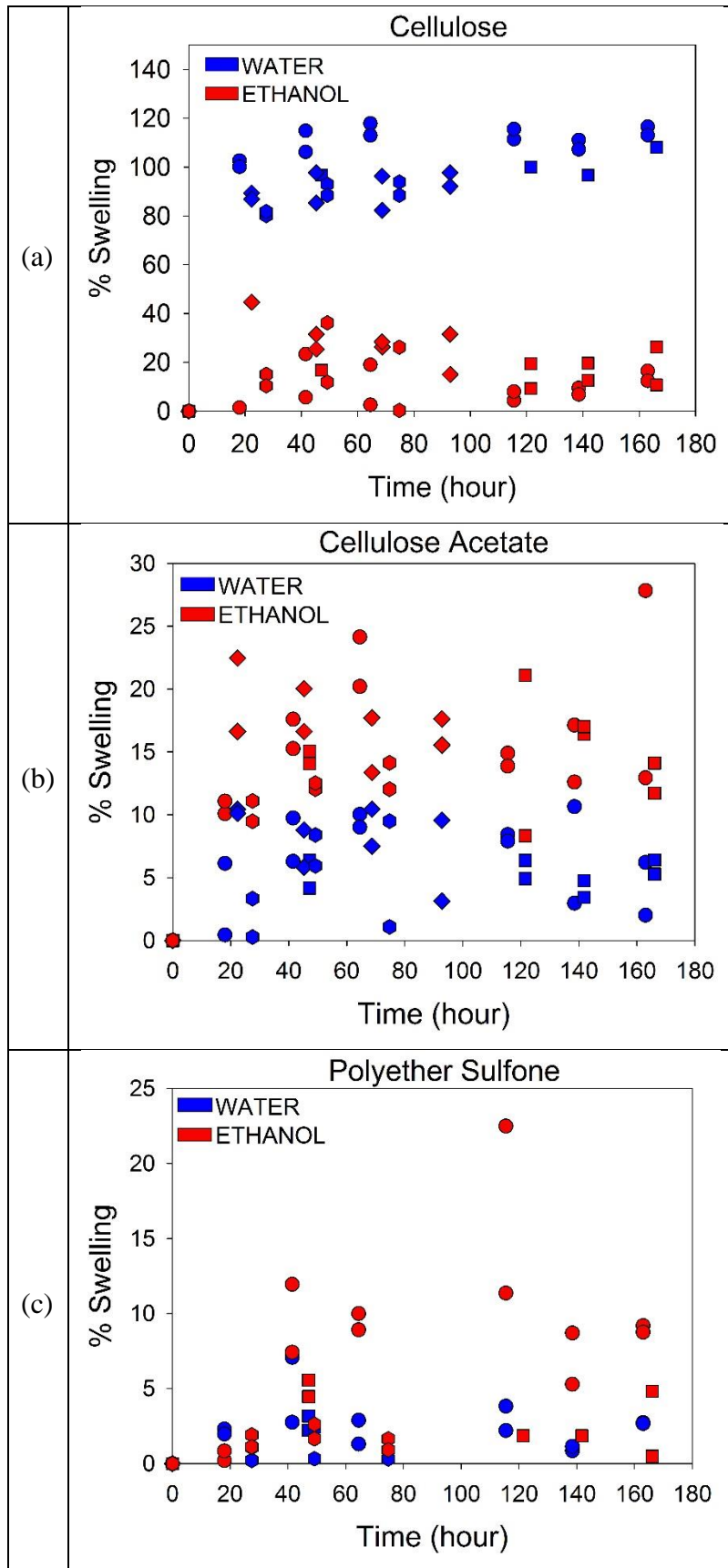


Figure 3-16 Swelling Ratios of (a) Cellulose, (b) Cellulose Acetate, (c) PES Films in Time

Water swells cellulose about five times more than ethanol indicating higher affinity between cellulose-water than cellulose-ethanol, while solubility parameters estimate similar nonsolvent quality. Water has much more H-bond capacity than ethanol, which explains the higher swelling ratio indicating poorer nonsolvent quality of water for cellulose. The difference in the swelling ratios of both nonsolvents fades for cellulose acetate and PES. For cellulose acetate and PES swelling ratios at equilibrium show that ethanol is slightly poorer nonsolvent than water. For cellulose acetate, ethanol being a poorer nonsolvent is also an expected behavior from solubility parameter calculations, since $RED_{CA-EtOH}$ is close to solubility limit. For PES, although both nonsolvents are expected to be strong nonsolvent from solubility parameter approach, RED value of PES-water interaction being larger than the one for PES-ethanol indicates that water is a stronger nonsolvent. Additionally, water uptake ratios are in accordance with hydrophilicities of polymer which is in the order of $C > CA > PES$, which is expected. Same trend seen in $RED_{polymer-water}$ values may indicate the accordance of the solubility parameter approach with experimental data.

3.2.3. Polymer-Solvent Interactions: Dynamic Light Scattering

Dynamic light scattering was used to assess the solvent quality. For dilute solutions polymer coils are more expanded in good solvent than theta solvent and coils are more compact in poor solvent as schematically drawn in Figure 3-17 [4]. Therefore, relative size of a polymer coil in different solvents can be considered as an indication of the relative quality of the solvent [83,84].

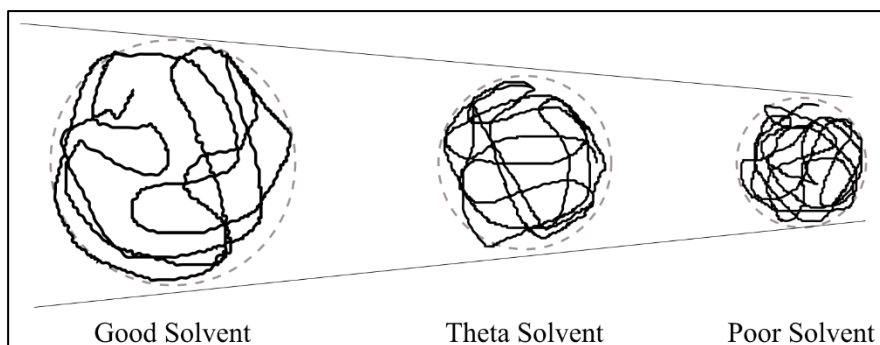


Figure 3-17 Representation of a Polymer Coil in Solvents of Different Quality

Cellulose, cellulose acetate and poly(ethersulfone) were dissolved in different solvents and solvent mixtures at polymer concentrations approaching infinite dilution (~ 0.1 wt.% polymer). In addition to solvents that were used in polymer solutions, DLS measurements were done in DMSO, which dissolves CA and PES. Approximately eight measurements were done for all solutions. For one sample of the solutions, three measurements were taken at different times within five months. Before the last, solutions were heated at 45°C for 29 hours. From a second sample from each of the solutions, one measurement was taken after dissolving the polymer and heating for 29 hours. No significant difference was observed in these different measurements, implying that the aggregates did not dissociate in time or with temperature. Measurements mostly result in multimodal distribution in Z-average hydrodynamic radius as in Figure 3-18, in which an example result of DLS measurement is given for cellulose acetate-DMSO solution. Peaks below 1 nm and above ca. 500 nm were considered irrelevant.

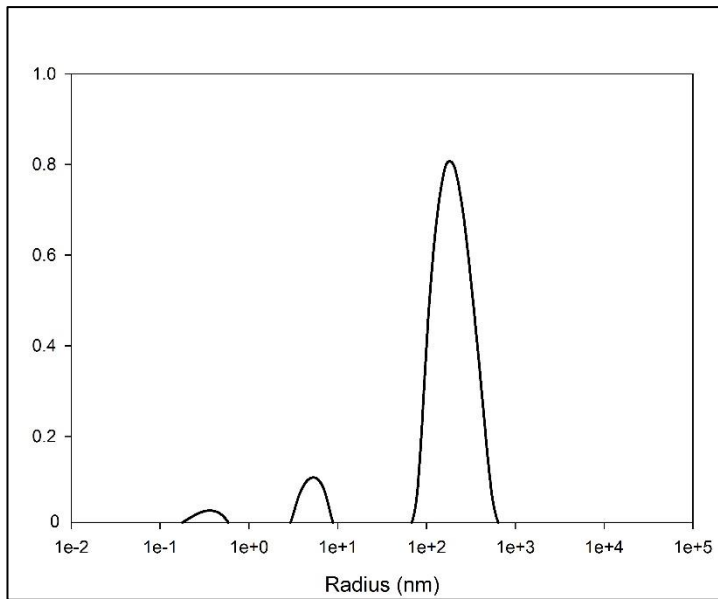


Figure 3-18 Multimodal Distribution of Particle Size

Peak points of distributions are considered as particle size. The size of large particles (more than hundred nanometers) indicate the existence of aggregates and the peaks at the values tens of nanometers were considered as the size of polymer coils, based on other data from literature [95].

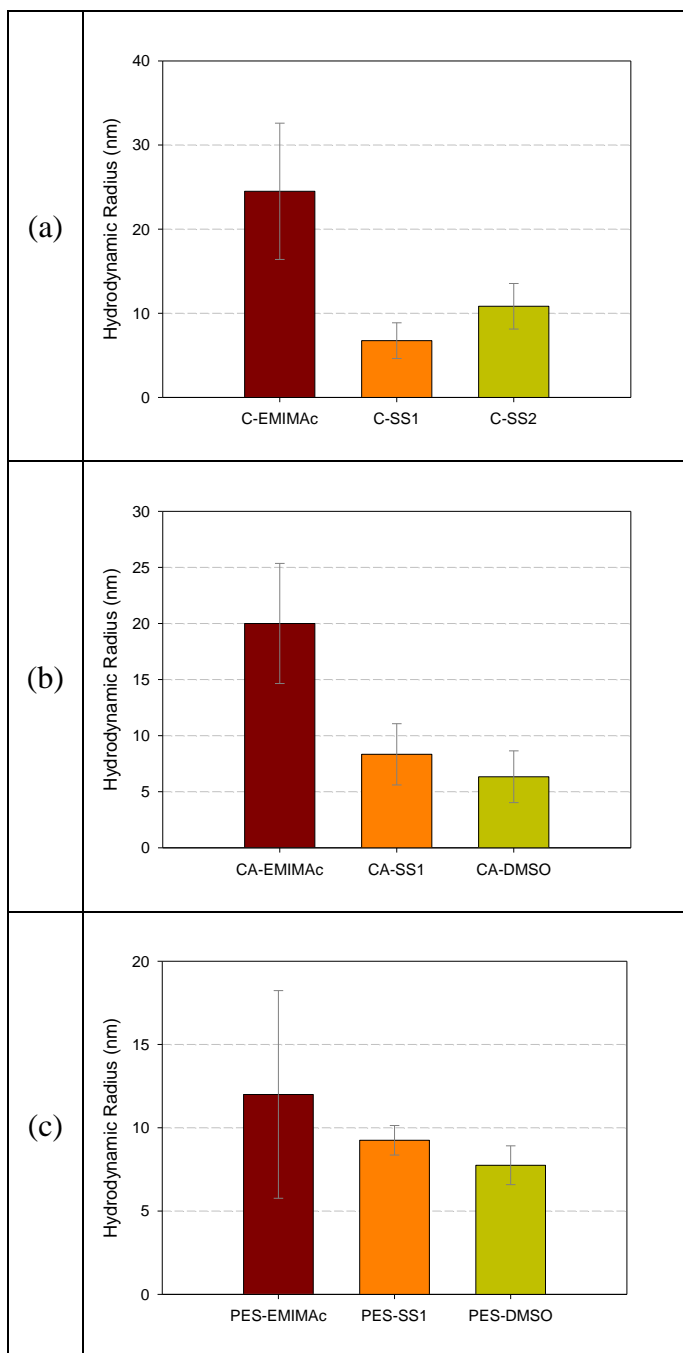


Figure 3-19 Hydrodynamic Radii of Polymers in Different Solvents

In Figure 3-19 (a), particle sizes imply solvent quality for cellulose is in the order of EMIMAc > SS2 > SS1. For cellulose acetate this is EMIMAc > SS1 ≈ SS2. For PES hydrodynamic radius values are close to each other within the error margin. While solubility parameter approach and results from these measurements are consistent for cellulose, they were not agree on solvent quality for cellulose acetate and PES.

This may result from difficulties in estimating interactions of ionic liquids with the polymers. It may also be implying that DLS analysis should be considered by taking into account the proportions and size of the aggregates or that it may lack the precision to be conclusive on solvent quality.

3.2.4. Polymer-Solvent-Nonsolvent Interactions: Cloud Points

Cloud points of solutions with water and ethanol as nonsolvents were determined in order to understand the solution-nonsolvent interactions. Cloud points of solutions were tabulated in Table 3-4 for both weight and molar basis. For molar basis cloud points, compositions are calculated as moles of nonsolvent per gram of polymer. This modification is done in order to understand how many nonsolvent molecules per same amount of polymer is needed to start phase separation.

Table 3-4 Water and Cloud Point Concentrations of Solutions at 23 °C in Mass and Molar Basis

Solution	Water (wt. %)	Water (mol NS/g polymer)	Ethanol (wt. %)	Ethanol (mol NS/g polymer)
C 1	9.15 ± 0.39	0.063	18.25 ± 0.15	0.050
C 2	6.05 ± 0.15	0.042	13.08 ± 0.95	0.035
C 3	4.15 ± 0.15	0.029	6.79 ± 0.24	0.018
C 4	2.65 ± 0.05	0.014	5.21 ± 0.22	0.014
CA 1	7.50 ± 0.50	0.052	36.35 ± 1.25	0.099
CA 2	8.40 ± 0.10	0.058	44.0 ± 1.0	0.119
PES 1	1.55 ± 0.55	0.011	21.65 ± 0.75	0.059
PES 2	1.95 ± 0.15	0.013	15.85 ± 0.65	0.051

In general, mass basis compositions of ethanol cloud points are higher than water cloud points for all solutions. In literature, for cellulose, this is explained with H-bond capacity. Since water is more capable to make H-bonds than ethanol, it decreases H-bond capacity of ionic liquid more than ethanol, therefore in a cellulose-ionic liquid-

water mixture cellulose tends to precipitate at lower nonsolvent concentrations than cellulose-ionic liquid-ethanol mixtures [29,96,97]. However, when molar-basis cloud point concentrations are considered, slightly more water molecules are needed to coagulate a polymer chain compared to ethanol. This may also be explained with the of high H-bond capacity of water. During coagulation like interactions of water and cellulose may dominate since both are capable of H-bonding, which is why swelling ratios of cellulose are very high for water compared to ethanol.

For cellulose, when cloud point compositions of solutions C 1, C 2 and C 3 (same polymer composition, increasing DMSO content) are compared, it is seen that as DMSO ratio is increased in the solution, cloud point compositions for both nonsolvent decreases. This is a result of DMSO itself not being a solvent for cellulose. Consequently, the solvent system, which is a mixture of solvent and a nonsolvent, is a weaker solvent and therefore coagulates at lower nonsolvent concentrations. For CA and PES solutions, ethanol cloud points are a lot higher than water cloud point compositions, indicating that ethanol is poorer nonsolvent for those polymer-ionic liquid systems. This is in agreement with solubility parameter estimations and swelling tests. Water cloud points of CA solutions with both solvent systems are close to each other as in PES solutions. While ethanol cloud point was increased for cellulose acetate solutions as DMSO was added (36% for CA1 and 44% for CA2), it decreased for PES solutions (22% for PES1 and 16% for PES2). This may be a result of different interactions of cellulose acetate and PES with the nonsolvent and solvent. Moreover, order of C 1, CA 1 and PES 1 solutions' water cloud point concentrations are in accordance with polymers' hydrophilicity order.

To summarize, water is found to be poorer nonsolvent for cellulose and cellulose – ionic liquid systems, when swelling tests and molar basis cloud point concentrations are considered. On the hand, in literature the opposite is implied taking the basis of water's H-bond capacity would make more polymer-nonsolvent H-bonds than ethanol. Solubility parameter approach for nonsolvent quality of water and ethanol for cellulose is not conclusive since RED values of both are close to unity. For CA and PES all criteria indicate clearly that ethanol is a poorer nonsolvent for the polymers and polymer-ionic liquid systems. Considering solvent quality, solubility parameter

approach and DLS measurements agree on EMIMAc being a better solvent for cellulose than solvent mixtures. In solubility parameter calculations, for cellulose acetate and PES RED_{S-P} values are higher than 1 for EMIMAc and it decreases as DMSO ratio in solvent increases, implying improving solvent quality with DMSO addition. On the other hand, solubility parameter estimations and DLS measurements do not agree when cellulose acetate and PES are considered.

3.3. Factors Affecting Kinetics of Phase Inversion

Viscosity of solution or solvent is important since it represents the media that nonsolvent diffuses in which is directly related to the phase inversion rate. Molar volume of nonsolvent represents how large the diffusing molecule is. Size of the molecule is important since movement of it is restricted as molecules gets larger. Both viscosity of solvent and the molar volume of nonsolvent is inversely proportional to the diffusivity of nonsolvent in solvent.

Solvent viscosity was measured with capillary viscometer, while solution viscosities were measured with rotational rheometer at different shear rates. Solvent and solution viscosities at shear rate 1 s^{-1} are given in Figure 3-20 and Table 3-5, respectively.

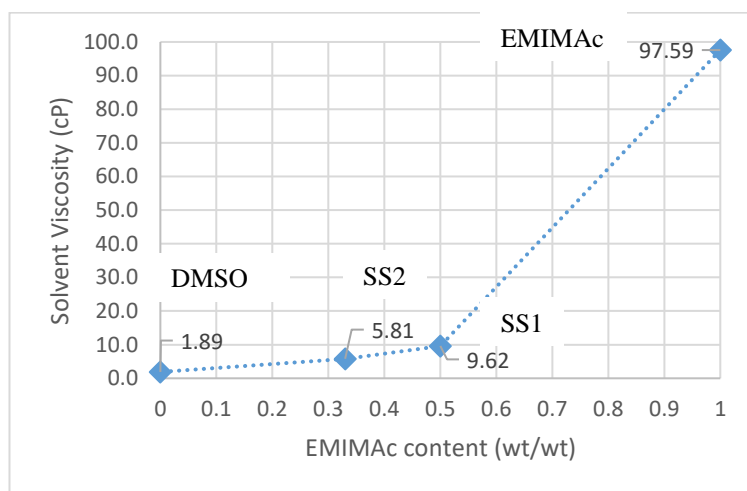


Figure 3-20 Viscosities of Solvent and Solvent Mixtures

Table 3-5 Solution Viscosity at Shear Rate 1 s⁻¹

Solution	Viscosity at shear rate 1 s⁻¹ (cP)
C 2	7.67
C 3	4.21
C 4	12.00
CA 1	11.18
CA 2	1.32
PES 1	5.35
PES 2	0.57

Viscosity of solution C 1 was above the equipment limit. Both solvent and solution viscosities decrease by an order of magnitude when DMSO added.

3.3.1. Phase Inversion Kinetics Measurements

3.3.1.1. Phase Inversion Front Observations (Instantaneous Phase Inversion Rates)

Instantaneous phase inversion rates of polymer solutions were investigated by analyzing the images taken during microscopic observations. How much distance phase inversion front moves in time and its relation with diffusivity of nonsolvent in solvent are considered. Strahmann and coworkers [8] analyzed this as considering diffusion of nonsolvent in solvent as in a tortuous, solid media, which is actually the precipitated polymer. Even though it is not totally solidified, the composition of a polymer solution that passed the cloud point may be considered as a tortuous solid-like media. Therefore, the diffusion may be considered as pseudo-binary diffusion of nonsolvent in solvent. The correlation between square of thickness of phase separated region (x^2) and time (t) is found by assuming the flux of nonsolvent should be proportional to the rate of phase inversion front (estimated by mass balance) as given in Equation 2.1 [8].

In Figure 3-21, images taken during phase inversion front proceeds are shown. These images are from the observations of the front of both nonsolvents in C1 solution at zeroth, first, fifth, tenth and sixtieth seconds.

One example image for each solution-nonsolvent couple at 5th second are given in Figure 3-22 to Figure 3-25 with average lengths of precipitated parts at the bottom of each image.

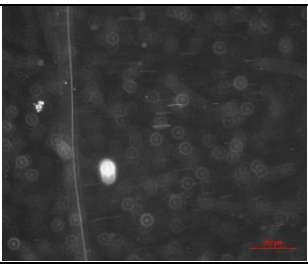
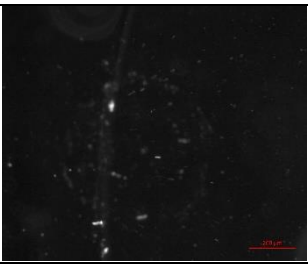
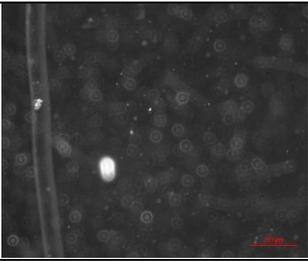
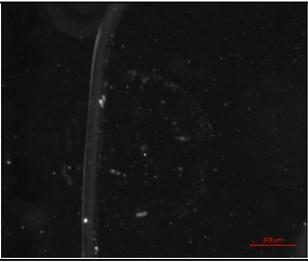
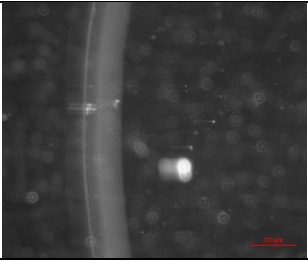
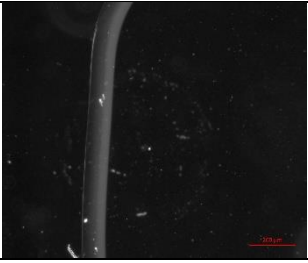
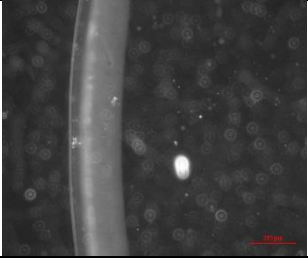
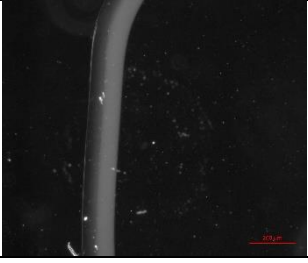
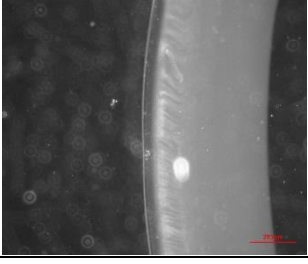
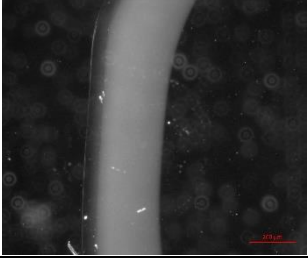
	C 1-W	C 1-E
t₀		
	$\sim 0 \mu\text{m}$	$\sim 0 \mu\text{m}$
t₁		
	$88 \pm 3 \mu\text{m}$	$72 \pm 4 \mu\text{m}$
t₅		
	$177 \pm 3 \mu\text{m}$	$109 \pm 2 \mu\text{m}$
t₁₀		
	$240 \pm 2 \mu\text{m}$	$148 \pm 2 \mu\text{m}$
t₆₀		
	$550 \pm 3 \mu\text{m}$	$342 \pm 9 \mu\text{m}$

Figure 3-21 Photographs Of Phase Inversion Front Observations at 0th 1st 5th 10th 60th Seconds of C1 Solution for Nonsolvent Water and Ethanol

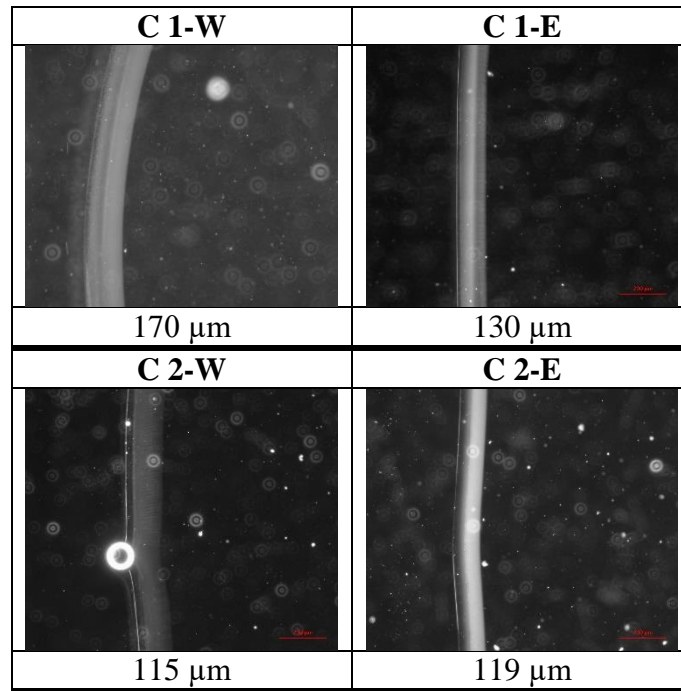


Figure 3-22 Photographs of Phase Inversion Front Observations at 5th Seconds for C1 and C2 Solutions for Both Nonsolvents

In Figure 3-22 and Figure 3-23, microscopic images of precipitated parts of cellulose solutions are very similar to each other in terms of structure and thickness when the nonsolvent is the same. Comparison of two nonsolvents, always shows slower front rates when the nonsolvent is ethanol. The structure of the precipitated parts for cellulose solutions are generally like a dense membrane similar to SEM images.

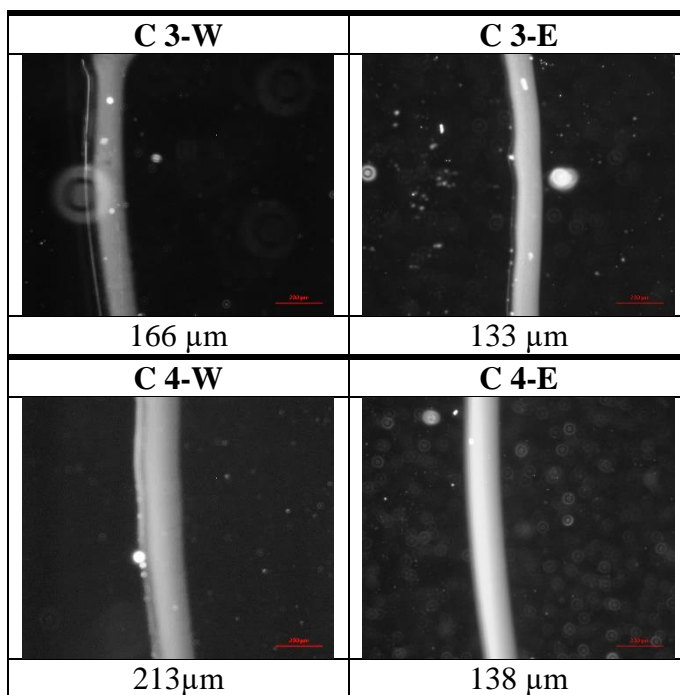


Figure 3-23 Photographs of Phase Inversion Front Observations at 5th Seconds for C3 and C4 Solutions for Both Nonsolvents

For cellulose acetate solutions, in Figure 3-24, images are given for only ternary systems with water as nonsolvent. When the nonsolvent is ethanol polymer does not precipitate as a continuous phase like others, instead its powder-like structure is dispersed. There is no difference between front rates of two cellulose acetates solutions, also no significant difference found between these and cellulose solutions. However, the structure of the precipitated part is looser for CA 2 solution than CA1 solution and also shows macrovoids appear earlier, as in SEM images.

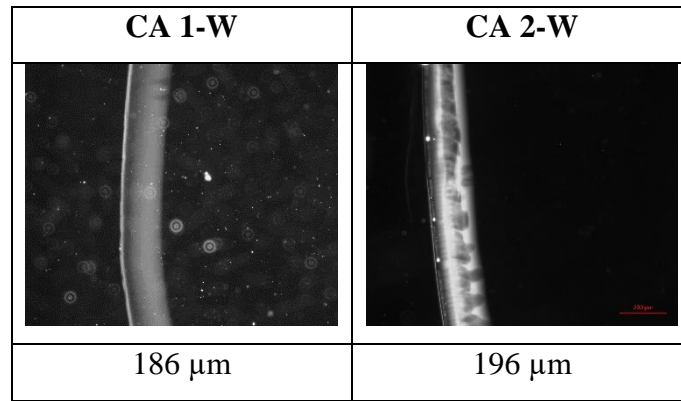


Figure 3-24 Photographs of Phase Inversion Front Observations at 5th Seconds for Cellulose Acetate Solutions for Water as Nonsolvent

Front rates of PES (Figure 3-25) solutions are a bit higher than solutions of other polymers. Especially for PES 2 solution, the front rates are clearly higher. Furthermore, when the nonsolvent is ethanol, rates are again lower than the case of water.

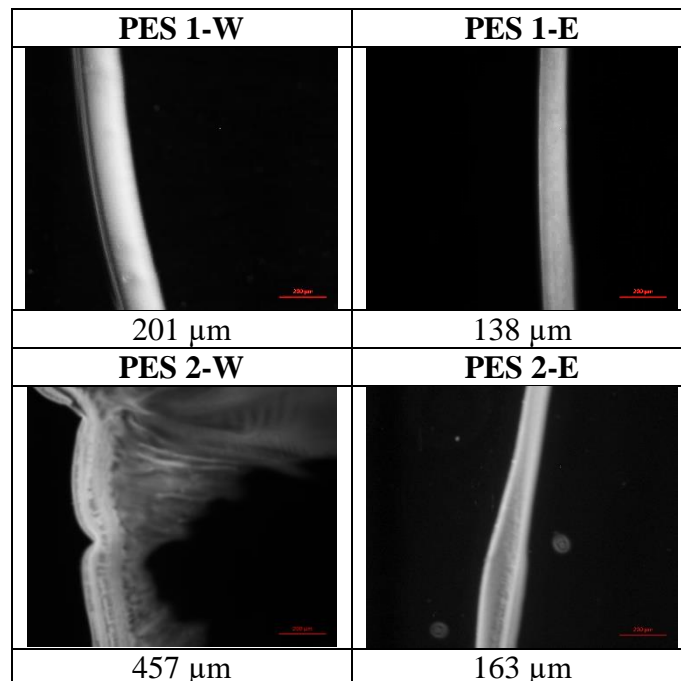


Figure 3-25 Photographs of Phase Inversion Front Observations at 5th Seconds for PES Solutions for Both Nonsolvents

Images of phase inversion front observations were also analyzed in terms of diffusivity of nonsolvent in the system, which is done by plotting x^2 vs. t (square of thickness of precipitated part by the time). These graphs are given in Figure 3-26, Figure 3-27 and Figure 3-28, for cellulose, cellulose acetate and PES solutions, respectively. The

average of slopes were divided by $\frac{\rho_{NS} - \rho_{CP}}{\rho_{NS} + \rho_{CP}}$ term in order to obtain a diffusivity value

(D'_{eff}) proportional to the D_{eff} (Figure 3-29). According to the model of Strathmann et

al. [8] the value $\frac{x^2 / t}{\frac{\rho_{NS} - \rho_{CP}}{\rho_{NS} + \rho_{CP}}}$ is equal to $\frac{D_{eff}}{4\tau / \varepsilon}$. Here D'_{eff} is compared for different

cases, roughly considering τ and ε to be similar. This actually may not be so, especially when comparing cellulose membranes with cellulose acetate and PES membranes. On the other hand, cellulose membranes obtained from different solvents and nonsolvents this may be a good assumption considering SEM and optical microscope images.

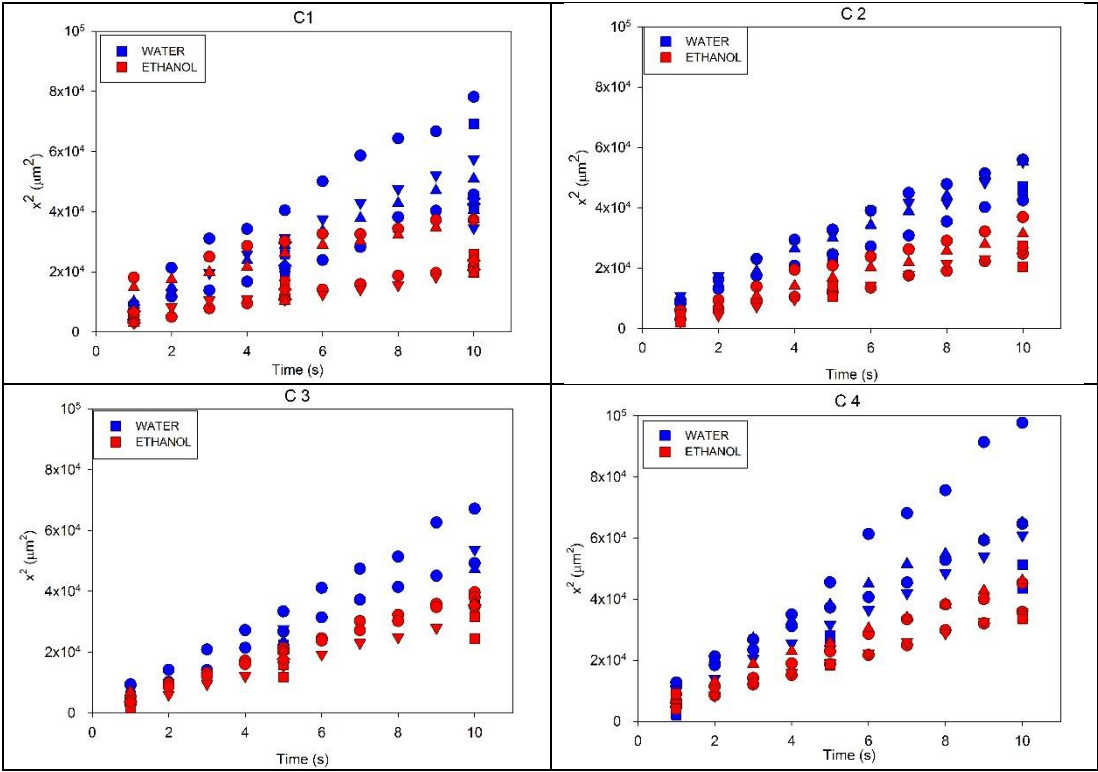


Figure 3-26 x^2 vs. t Graphs of Cellulose Solutions for Both Nonsolvents

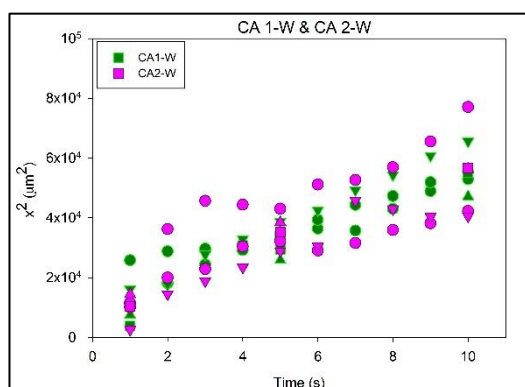


Figure 3-27 x^2 vs. t Graphs of Cellulose Acetates Solutions for Nonsolvent Water

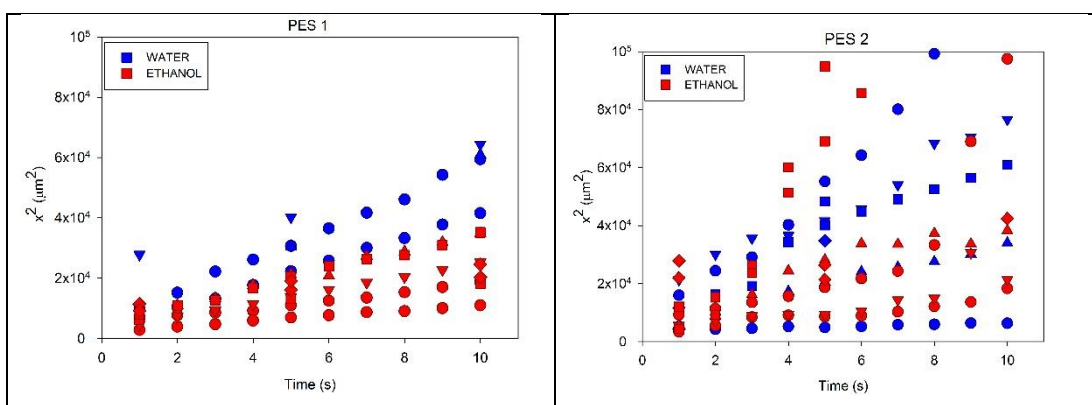


Figure 3-28 x^2 vs. t Graphs of PES solutions for Both Nonsolvents

In addition to experimental data, diffusivity of solvent in nonsolvent was estimated by Wilke-Chang equation, $D_{\text{Wilke-Chang}}$, which are given in Table 3-6.

Table 3-6 Diffusivities of Nonsolvents in Solvents Calculated from Wilke-Chang Equation

	$D_{\text{Wilke-Chang}}$ of Water (m^2/s)	$D_{\text{Wilke-Chang}}$ of Ethanol (m^2/s)
EMIMAc	5.05×10^{-11}	2.52×10^{-11}
SS1	4.06×10^{-10}	2.03×10^{-10}
SS2	6.35×10^{-10}	3.17×10^{-10}

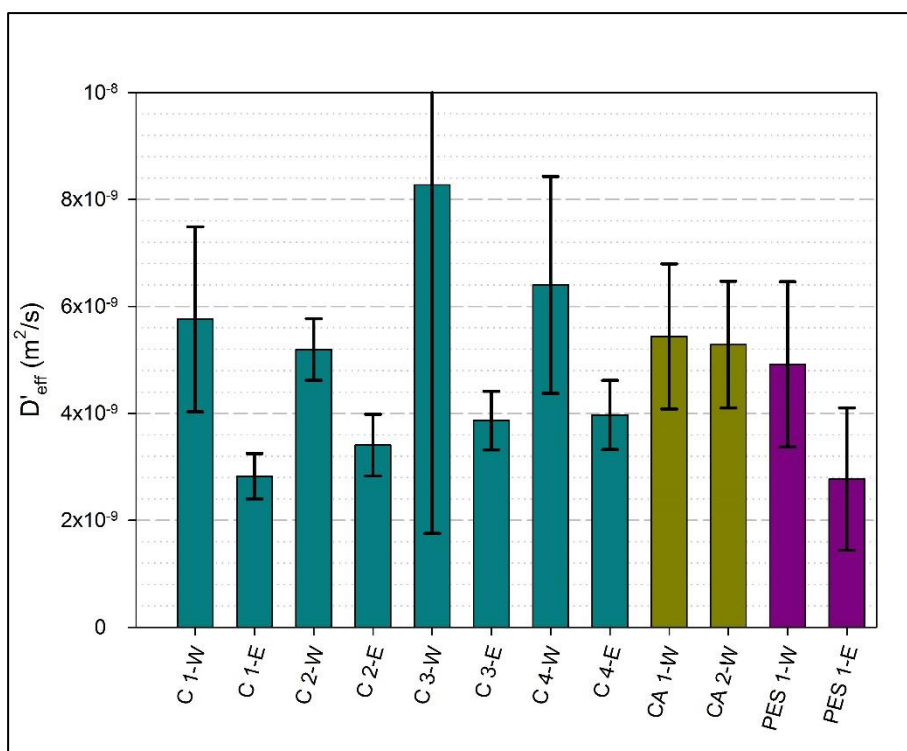


Figure 3-29 Effective Diffusivities of Nonsolvents in Solvents

Since, x values of images taken from observation of PES 2 solution were deviate a lot for same image, these values were not included in the Figure 3-29.

As seen in Figure 3-29 and images at 5th second also, rate of phase inversion front is always lower when the nonsolvent is ethanol than when nonsolvent is ethanol. Estimations of diffusivity from Wilke-Chang equation indicate that diffusivities of ethanol should be approximately half of diffusivities of water, which is the case in effective diffusivities. On the other hand, it was also expected from theoretical calculations that, when solvent viscosity decreases the diffusivity should increase. In Table 3-6 it is seen that there is one order of magnitude difference between diffusivities in EMIMAc and SS1 solvent mixture, which are not reflected in effective diffusivities in Figure 3-29. Therefore, it should be another factor that affects the phase inversion front rate, which decreases it as DMSO added to the system or increases it in the case of pure EMIMAc. This behavior may be due to H-bonding between the ionic liquid and the nonsolvents. Fadeeva et al., who measured diffusivities of water in

1-butyl-1-methylpyrrolidinium bis(trifluoromethylsulfonyl)amide and 1-butyl-1-methylpyrrolidinium trifluoromethylsulfonate ionic liquids, have found that water transport in these ionic liquids was faster than would be expected from hydrodynamic laws, which may support our observations [97].

3.3.1.2. Light Transmission Measurements (Cumulative Phase Inversion Measurements)

As a second measurement of phase inversion kinetics, light through the polymer solution during coagulation was measured. This technique uses the fact that the polymer solution becomes opaque during phase inversion. Since the amount of light that passes through all cross-section of the polymer solution in nonsolvent bath is measured, results of these measurements represents a cumulative value. In Figure 3-34, 'W' represents coagulation in water while 'E' represents coagulation in ethanol.

From Figure 3-30 to Figure 3-33, normalized graphs obtained during light transmission measurements are given individually for each measurement of cellulose, cellulose acetate and PES solutions.

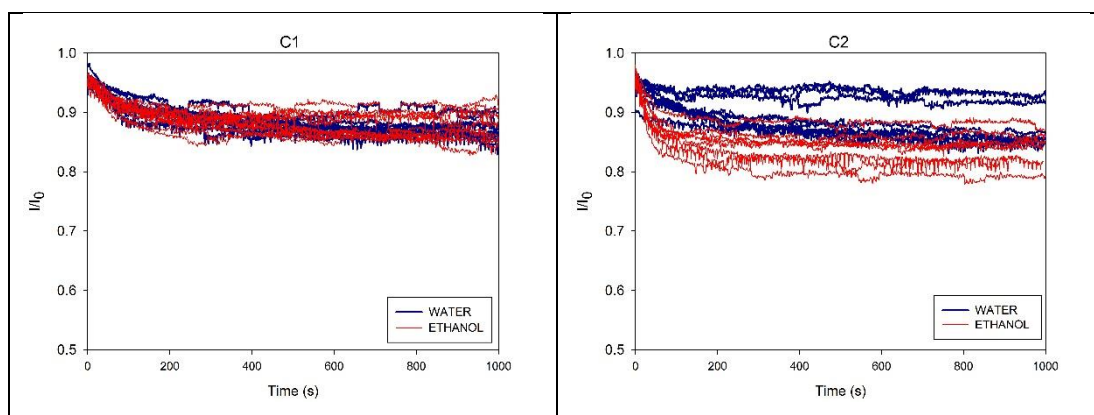


Figure 3-30 Light Transmission Measurement Results of C1 and C2 Solutions

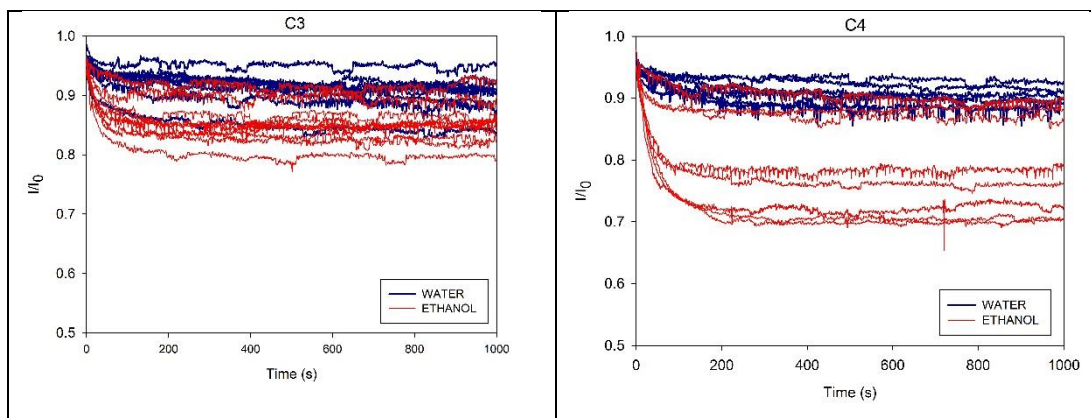


Figure 3-31 Light Transmission Measurement Results of C3 and C4 Solutions

Figure 3-30 and Figure 3-31 show the results of cellulose solutions. While no time delay is observed in any of cellulose membranes, the cumulative phase inversion rate is very slow when compared to other polymer solutions. Additionally, the difference between nonsolvents are not very significant, although it is more distinct for the solutions with DMSO. For solutions with DMSO, cumulative phase inversion rate is higher when nonsolvent is ethanol.

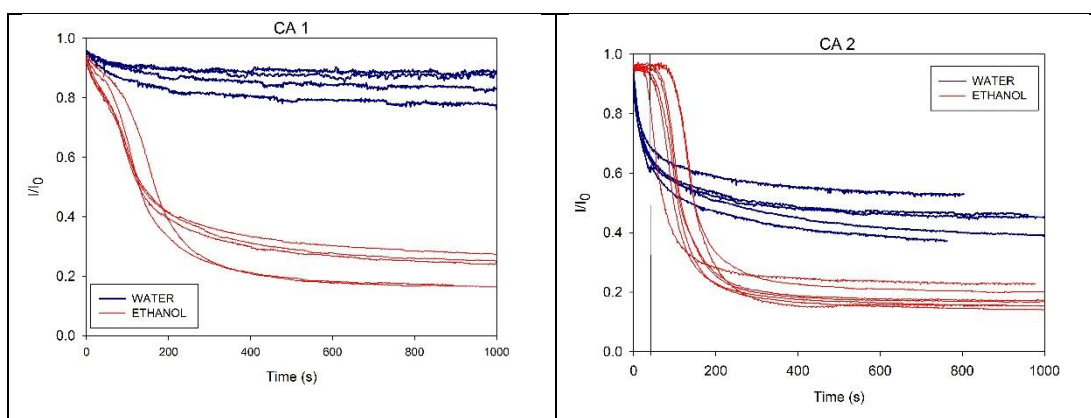


Figure 3-32 Light Transmission Measurement Results of Cellulose Acetate Solutions

In general, cellulose acetate solutions (Figure 3-32) have higher rate than cellulose solutions. Although, it seems like ethanol causes higher cumulative rates for CA1 solution, there are two different slopes on the ethanol plots of the CA1 graph. The time for first slope is considered as time delay, while the absolute value of second slope is considered as cumulative phase inversion rate. This behavior is unique for CA 1 solution, no behavior similar to that is observed for other solutions. Typical time delay occurs as in CA2 solution coagulated in ethanol, which is 55 seconds on average. The time delay indicates the poor nonsolvent quality for polymer solution.

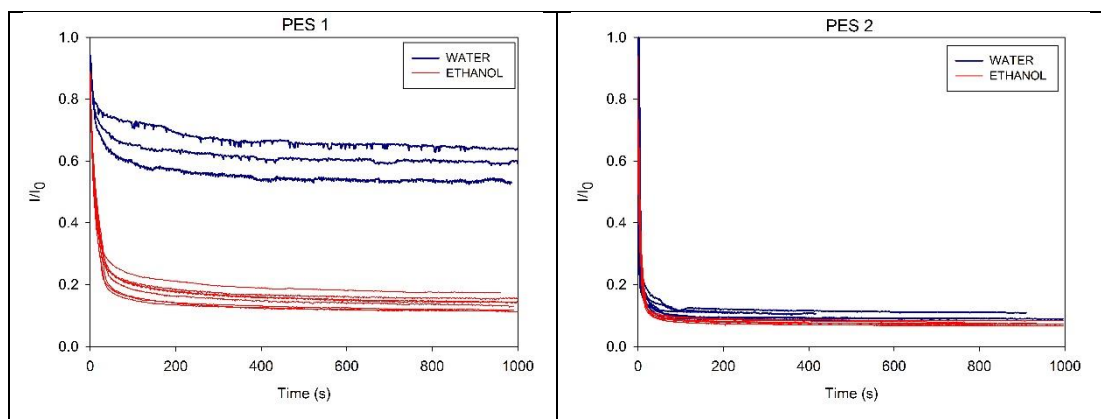


Figure 3-33 Light Transmission Measurement Results of PES solutions

For PES solutions (Figure 3-33), cumulative phase inversion rate is very fast when compared to cellulose and cellulose acetate solutions. Although the difference between nonsolvents is very clear for first solution, it is not for the case of second solution. However, the close results for different nonsolvents are most probably caused by very fast phase inversion rate of PES 2 solution, where differences cannot be distinguished by the data logging done every second.

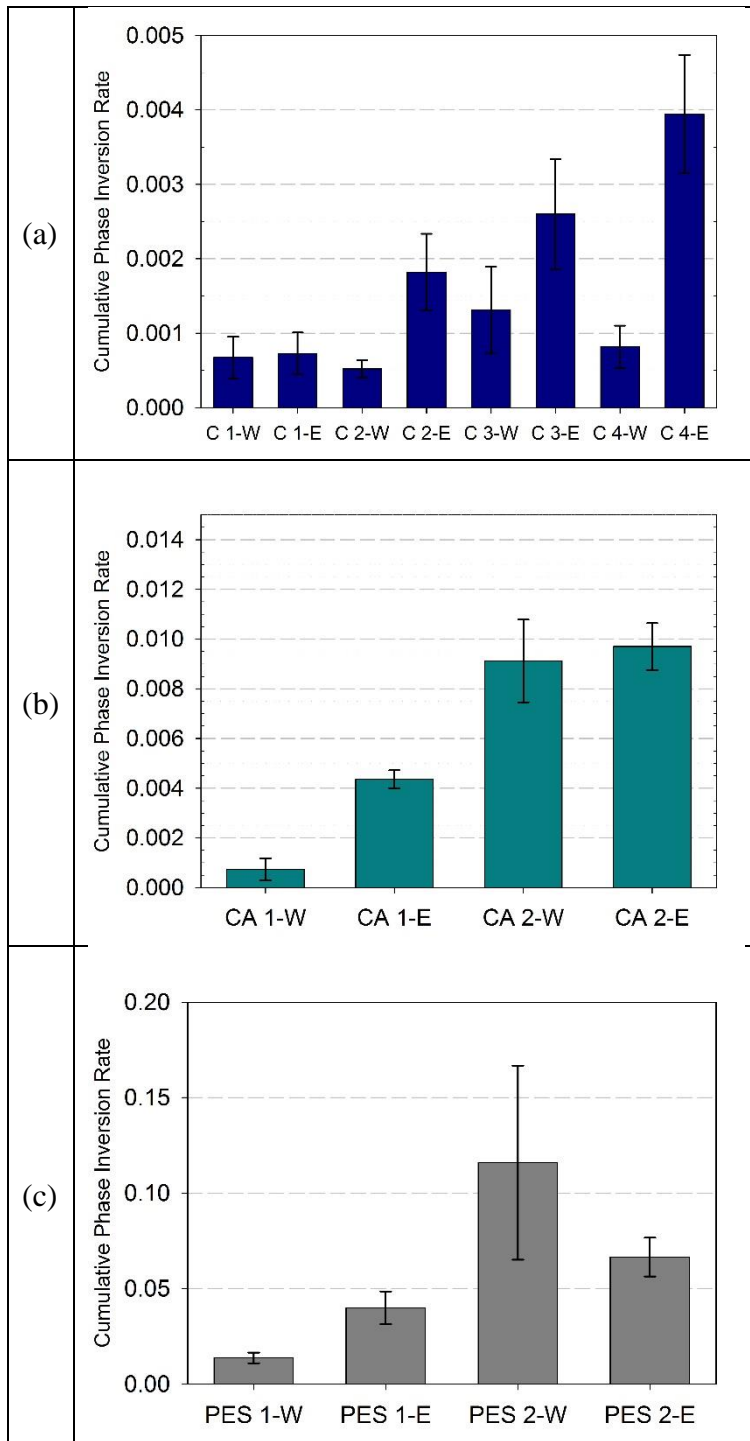


Figure 3-34 Cumulative Phase Inversion Rates of (a) Cellulose (b) Cellulose Acetate (c) PES Solutions Coagulated in Water and Ethanol

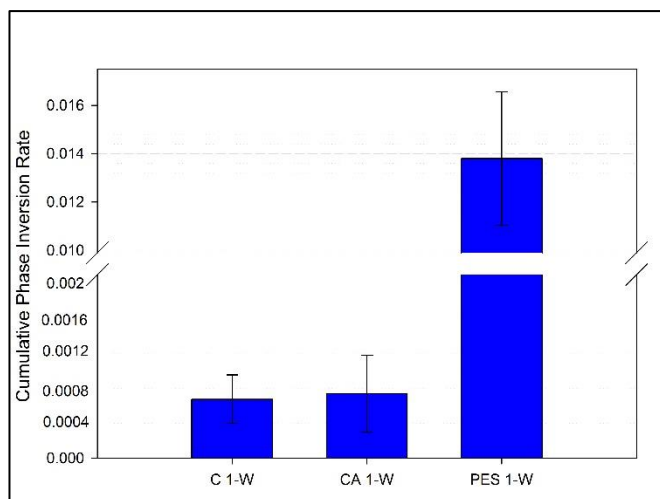


Figure 3-35 Cumulative Phase Inversion Rates of C1, CA1 and PES 1 Solutions Coagulated in Water

Averages of initial slopes of light transmission plots, which is referred to as cumulative phase inversion rate, are given in Figure 3-34 and in Figure 3-35 rates of C1, CA1 and PES1 solutions when coagulated in water are given. When cumulative phase inversion rates of three polymer solutions with DMSO were compared, there is a trend of $C < CA \ll PES$. However, for solutions without DMSO this trend is $C \approx CA \ll PES$ as seen in Figure 3-35.

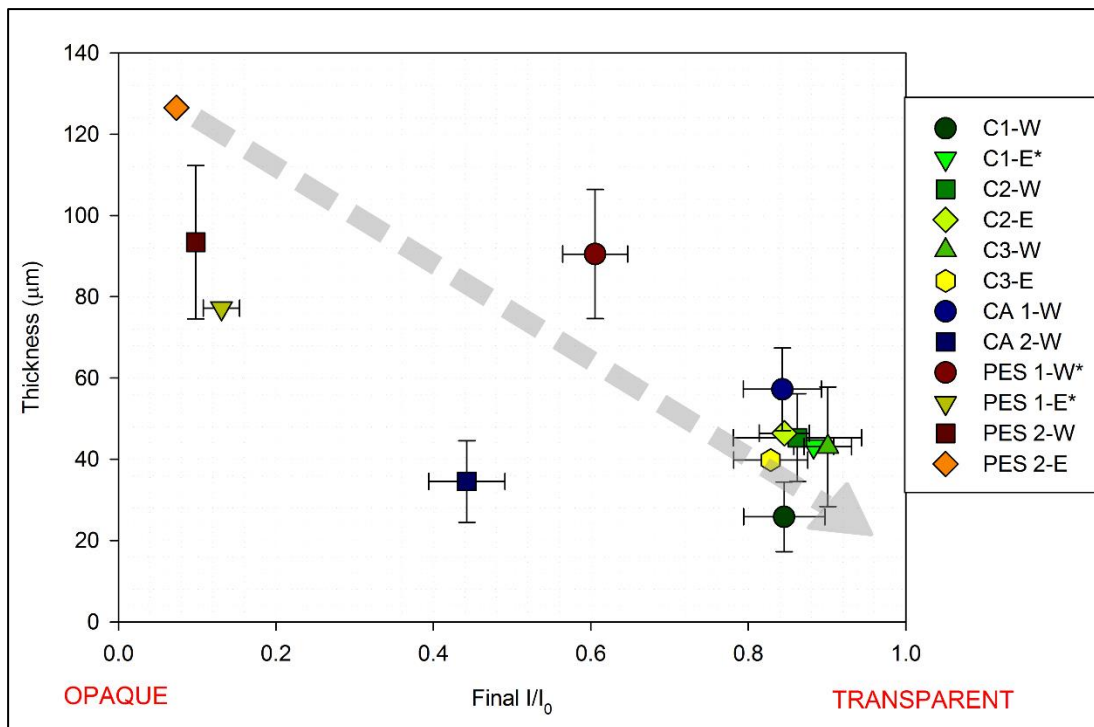


Figure 3-36 Membrane thickness over Final I/I₀ Values

For cellulose solutions, the cumulative rates are the lowest and they are very close to each other when solutions coagulated in water. However, when cellulose solutions are coagulated in ethanol, cumulative rates are increasing as DMSO added to the system. Additionally, for solutions with DMSO (C 2, C 3 and C 4) coagulation in ethanol causes higher cumulative phase inversion rates than coagulation in water.

Light transmission measurement uses the difference in light diffraction at the nonsolvent–polymer solution interface, the measurement is affected by porosity and pore size. Membrane thickness is plotted over Final I/I₀ values of membranes in Figure 3-36. Here, with the same casting thickness, a higher membrane thickness is considered to indicate higher porosity hence higher opaqueness. Thicknesses of membranes were measured from SEM images since it was the only available way. In these images some membranes were tilted which cause error in thickness measurement. These data points are marked with an asterisk in Figure 3-36. Final I/I₀ values of cellulose membranes are slightly lower for those three solutions (C2, C3 and C4) coagulated in ethanol than coagulated in water. This indicates that membranes

obtained from coagulation of solutions with DMSO in ethanol have slightly higher porosity than the ones coagulated in water, which is supported by lower Bromothymol Blue retentions of non-dried membranes that are coagulated in ethanol compared to those coagulated in water. That slightly higher porosity, creates extra turbidity, which is reflected as higher cumulative rates in the light transmission experiments.

Cumulative rates of CA 1 solution coagulated in different nonsolvents are very different; rate of CA1-W is less than half rate of CA1-E. When SEM images of these membranes considered, it is seen that while CA1-W have dense skin layer and small macrovoids, CA1-E has micron-size pores in its structure. This porosity of CA1-E causes large increase in opacity, which is reflected as higher cumulative phase inversion rate.

Cumulative rates of CA2 and PES2 solutions are significantly higher than the rates of cellulose, CA1 and PES1 solutions. This is considered to be due to opacity created by quickly occurring macrovoids seen in membranes obtained from CA2 and PES 2 solutions. SEM images also support that the ones with high cumulative rates have higher porosity. When time for phase inversion (time interval from immersion of the solution in NS until the Final I/I_0 is reached) is compared with the macrovoid-like structure initiation time in phase inversion front observations, it is found that macrovoids already exist for the time interval considered for the cumulative rate. For example, for CA 2 solution coagulated in water data from first twenty seconds are used to calculate cumulative phase inversion rate. It can be seen from Figure 3-24, macrovoids are already exist at fifth second. This implies that opacity results from macrovoids and large pores rather than precipitation kinetics alone. Therefore, most of the time, light transmission gives more reliable results on final membrane porosity than phase inversion rate. Images at the time interval considered for cumulative phase inversion rate for CA1-W, CA2-W, PES1-W, PES2-W, PES1-E and PES2-E are given in Figure 3-37 .

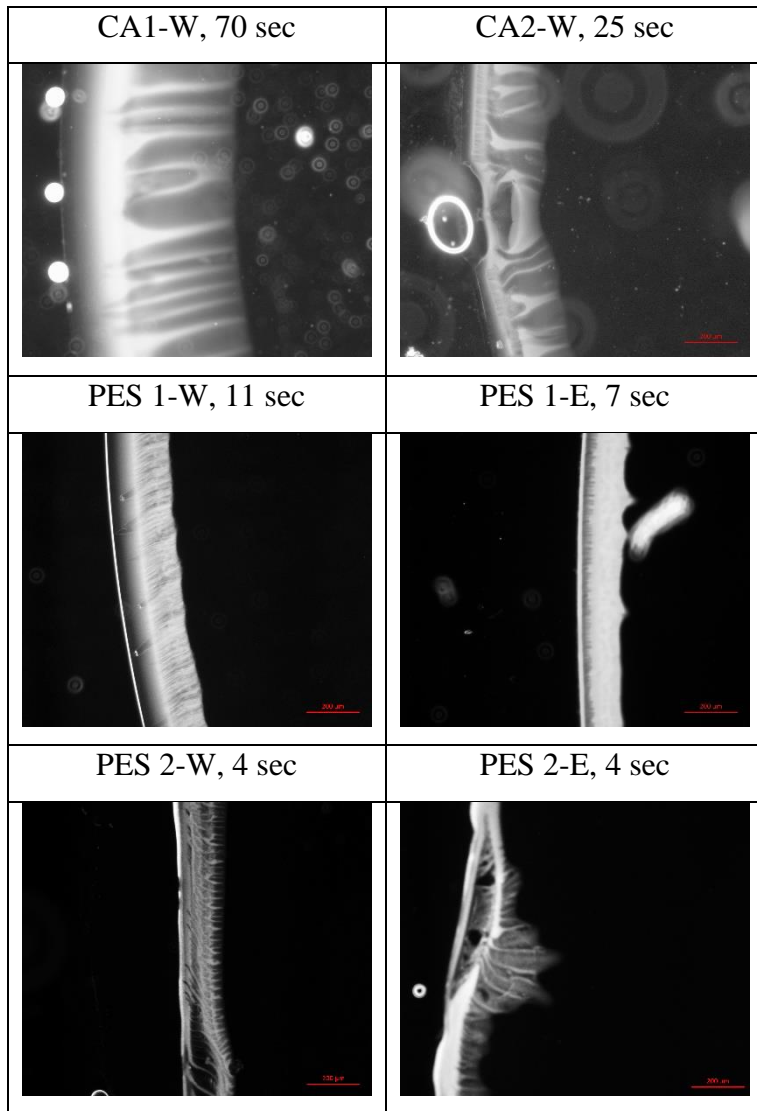


Figure 3-37 Photographs of Phase Inversion Front Observations Taken at Times Final I/I_0 is reached

CHAPTER IV

CONCLUSIONS

In this study, it is aimed to understand the relation between thermodynamic and kinetic aspects of the phase inversion process with resultant membrane morphology and performance. Cellulose, cellulose acetate and polyether sulfone solutions were prepared from EMIMAc and EMIMAc-DMSO mixtures. Solutions were cast as flat sheets and during formation of membranes, cumulative phase inversion rates of solution in nonsolvents water and ethanol measured. For instantaneous phase inversion rate, advancement of the phase inversion front was observed with optical microscopy. Meanwhile, to understand polymer-solvent-nonsolvent, polymer-solvent and polymer-nonsolvent interactions, cloud point measurements, dynamic light scattering and swelling tests were applied, respectively and these binary interactions were estimated by Hansen solubility parameters, as well. Performance of obtained membranes were tested with pure solvent permeance and retention tests. Scanning electron microscopy was used to investigate morphology of membranes and XRD analysis were done to assess crystallinity.

Cellulose membranes were prepared in eight different conditions and SEM images of these showed that they all have similar morphology as symmetric cross-section with nodular structure. None of these membranes had macrovoids in their morphology. This similarity of membranes was also seen in performance tests of dried membranes as around 90% retention for BSA and Blue Dextran (20 kDa) and around 80% retention of Bromothymol Blue. However, when cellulose membranes were tested without drying, their performance varied as Bromothymol Blue rejections were approximately 40% for the cellulose membrane obtained by coagulation in water of solution with only solvent as EMIMAc and below 5% for all cellulose membranes that obtained by coagulation in ethanol. Difference in non-dried membrane performances and existence of nodular structure in the membrane morphology implies the presence of micropores.

Cellulose acetate membranes, on the other hand, had asymmetric and nodular cross-section. Unlike cellulose membranes, they had macrovoids in their structure. These macrovoids were circular and at the support-side for the cellulose acetate membrane made from the solution that includes only EMIMAc as solvent, coagulated in water; while finger-like macrovoids expanding throughout the cross-section was observed for when DMSO was added to the solution. Moreover, skin layer of these membranes became looser as DMSO was added to the starting polymer solution. Surface images of cellulose acetate membranes obtained from coagulation in ethanol showed an extremely loose structure with micron-sized pores. Morphology of PES membranes had similar behavior with cellulose acetate ones. Circular macrovoids at the support-side became finger-like structure and skin layer got looser as DMSO was added to the polymer solution. In addition to that, skin layer of PES membranes obtained from coagulation in ethanol were looser than the ones of water-coagulated counterparts.

Performances of membranes were in accordance with their morphology as looser membranes (skin layer) had higher permeances and lower retentions than the denser ones.

Crystallinity of cellulose and cellulose acetate membranes were examined with XRD analysis. It was seen that membranes obtained from solutions that only have EMIMAc as solvent had higher crystallinity than the ones including DMSO, which was attributed to the ordering effect of ionic liquid reported in literature [45, 65, 81] Furthermore, diffractograms of cellulose membranes showed that water-coagulated membranes had higher crystallinity than ethanol-coagulated ones.

When membrane morphologies, crystallinity and separation performance are considered, it was observed that changing the nonsolvent from water to ethanol resulted in looser membranes (observed from SEM and/or retentions) that have lower crystallinity.

Considering the thermodynamics of phase inversion, ethanol is a stronger nonsolvent for cellulose and poorer for cellulose acetate and PES. On the other hand, at cloud point, ethanol concentrations in all solutions are higher than water concentrations, where the difference is much larger for cellulose acetate and PES. Considering the

phase inversion kinetics, instantaneous phase inversion rate with ethanol as nonsolvent was clearly slower for all solutions, which was attributed to the larger size of ethanol, decreasing its diffusivity. These findings imply that the slower phase inversion front rate in ethanol may have a dominant effect on membrane structure.

When DMSO is added to starting polymer solution, it was again observed that membranes became looser and of lower crystallinities. Considering thermodynamics, solvent quality of DMSO containing solvent mixtures decreases for cellulose as shown by solubility parameter estimations, DLS analysis and cloud point nonsolvent concentrations. For cellulose acetate and PES solubility parameters and cloud point concentrations indicate increasing solvent quality with DMSO addition. Instantaneous phase inversion rates do not reveal a difference between pure EMIMAc and EMIMAc-DMSO solvent mixtures, although the viscosity is significantly reduced with DMSO in the solvent system.

Therefore, the relationship of thermodynamics and phase inversion kinetics with membrane structure appears to require further investigation. The pitfalls in the analysis and predictions may be the following:

- Diffusivity in ionic liquids may not be only a simple function of viscosity and may be affected strongly by the ionic character and H-bonding. Hence, diffusivities of nonsolvent in ionic liquids may not be as low as expected.
- Solubility parameter estimations are prone to more uncertainty when ionic liquids are concerned compared to simple liquids.
- It may be necessary to consider DLS analysis by taking into account proportions and sizes of aggregates or this analysis may lack the precision to be conclusive on solvent quality.

Finally, cumulative phase inversion rate estimations from light transmission measurements correlated better with membrane porosity rather than phase inversion kinetics, since the technique relies on the change in opacity, which is significantly affected by the presence and size of pores and macrovoids.

REFERENCES

- [1] Mulder, M. (1991). *Basic Principles of Membrane Technology* (2nd ed.). Dordrecht: Kluwer Academic Publishers
- [2] Baker, R. (2012). *Membrane technology and applications* (3rd ed.). Chichester: J. Wiley
- [3] Strathmann, H. (2011). *Introduction to Membrane Science and Technology* (1st ed.). Weinheim, Germany: Wiley-VCH Verlag & Co
- [4] Young, R. & Lovell, P. (2011). *Introduction to polymers* (3rd ed.). Boca Raton: CRC.
- [5] Hansen, C. (2007). *Hansen solubility parameters* (2nd ed.). Boca Raton: CRC Press.
- [6] Çulfaz, P. (2010). *Microstructured Hollow Fibers and Microsieves: Fabrication, Characterization and Filtration Applications* (Ph.D.). University of Twente.
- [7] Nunes, S. & Inoue, T. (1996). Evidence for spinodal decomposition and nucleation and growth mechanisms during membrane formation. *Journal of Membrane Science*, 111(1), 93-103.
- [8] Strathmann, H., Kock, K., Amar, P., & Baker, R. (1975). The formation mechanism of asymmetric membranes. *Desalination*, 16(2), 179-203.
- [9] IUPAC Gold Book - micropore in catalysis. (2017). *Goldbook.iupac.org*. Retrieved 14 February 2017, from <https://goldbook.iupac.org/M03906.html>
- [10] GENÇAL, Y. (2014). *Fabrication and Characterization of Corrugated Microfiltration Membranes* (Master Thesis). Middle East Technical University.
- [11] Cohen, C., Tanny, G., & Prager, S. (1979). Diffusion-controlled formation of porous structures in ternary polymer systems. *Journal of Polymer Science: Polymer Physics Edition*, 17(3), 477-489.
- [12] Reuvers, A., van den Berg, J., & Smolders, C. (1987). Formation of membranes by means of immersion precipitation. *Journal of Membrane Science*, 34(1), 45-65.

- [13] Yilmaz, L., & Mchugh, A. (1986). Modelling of asymmetric membrane formation. I. Critique of evaporation models and development of a diffusion equation formalism for the quench period. *Journal of Membrane Science*, 28(3), 287-310.
- [14] Yilmaz, L., & Mchugh, A. J. (1988). Modeling of asymmetric membrane formation. II. The effects of surface boundary conditions. *Journal of Applied Polymer Science*, 35(7), 1967-1979.
- [15] Medronho, B. & Lindman, B. (2015). Brief overview on cellulose dissolution/regeneration interactions and mechanisms. *Advances in Colloid And Interface Science*, 222, 502-508.
- [16] Wang, H., Gurau, G., & Rogers, R. (2012). Ionic Liquid Processing of Cellulose. *Cheminform*, 43(19).
- [17] Pinkert, A., Marsh, K., Pang, S., & Staiger, M. (2009). Ionic Liquids and Their Interaction with Cellulose. *Chemical Reviews*, 109(12), 6712-6728.
- [18] Lindman, B., Karlström, G., & Stigsson, L. (2010). On the mechanism of dissolution of cellulose. *Journal of Molecular Liquids*, 156(1), 76-81.
- [19] Wertz, J., Mercier, J., & Bédoué, O. *Cellulose science and technology* (1st ed., pp. 87-146). Lausanne: CRC Press.
- [20] Lejeune, A. & Deprez, T. (2010). *Cellulose* (1st ed., pp. 1-38). Hauppauge, N.Y.: Nova Science Publishers.
- [21] Pinkert, A., Marsh, K., & Pang, S. (2010). Reflections on the Solubility of Cellulose. *Industrial & Engineering Chemistry Research*, 49(22), 11121-11130.
- [22] Gupta, K., Hu, Z., & Jiang, J. (2011). Mechanistic understanding of interactions between cellulose and ionic liquids: A molecular simulation study. *Polymer*, 52(25), 5904-5911.
- [23] Feng, L. & Chen, Z. (2008). Research progress on dissolution and functional modification of cellulose in ionic liquids. *Journal of Molecular Liquids*, 142(1-3), 1-5.

- [24] Swatloski, R., Spear, S., Holbrey, J., & Rogers, R. (2002). Dissolution of Cellulose with Ionic Liquids. *Journal of the American Chemical Society*, 124(18), 4974-4975.
- [25] Ohno, H. & Fukaya, Y. (2009). Task Specific Ionic Liquids for Cellulose Technology. *Chemistry Letters*, 38(1), 2-7.
- [26] Vitz, J., Erdmenger, T., Haensch, C., & Schubert, U. (2009). Extended dissolution studies of cellulose in imidazolium based ionic liquids. *Green Chemistry*, 11(3), 417.
- [27] Isik, M., Sardon, H., & Mecerreyes, D. (2014). Ionic Liquids and Cellulose: Dissolution, Chemical Modification and Preparation of New Cellulosic Materials. *International Journal of Molecular Sciences*, 15(7), 11922-11940
- [28] Zhao, Y., Liu, X., Wang, J., & Zhang, S. (2013). Insight into the Cosolvent Effect of Cellulose Dissolution in Imidazolium-Based Ionic Liquid Systems. *The Journal of Physical Chemistry B*, 117(30), 9042-9049.
- [29] Minnick, D., Flores, R., DeStefano, M., & Scurto, A. (2016). Cellulose Solubility in Ionic Liquid Mixtures: Temperature, Cosolvent, and Antisolvent Effects. *The Journal of Physical Chemistry B*, 120(32), 7906-7919
- [30] Andanson, J., Bordes, E., Devémy, J., Leroux, F., Pádua, A., & Gomes, M. (2014). Understanding the role of co-solvents in the dissolution of cellulose in ionic liquids. *Green Chemistry*, 16(5), 2528.
- [31] Xu, A., Zhang, Y., Zhao, Y., & Wang, J. (2013). Cellulose dissolution at ambient temperature: Role of preferential solvation of cations of ionic liquids by a cosolvent. *Carbohydrate Polymers*, 92(1), 540-544. [81]
- [32] Zhang, C., Kang, H., Li, P., Liu, Z., Zhang, Y., & Liu, R. et al. (2016). Dual effects of dimethylsulfoxide on cellulose solvating ability of 1-allyl-3-methylimidazolium chloride. *Cellulose*, 23(2), 1165-1175.
- [33] Lv, Y., Wu, J., Zhang, J., Niu, Y., Liu, C., He, J., & Zhang, J. (2012). Rheological properties of cellulose/ionic liquid/dimethylsulfoxide (DMSO) solutions. *Polymer*, 53(12), 2524-2531.

- [34] Andanson, J., Pádua, A., & Costa Gomes, M. (2015). Thermodynamics of cellulose dissolution in an imidazolium acetate ionic liquid. *Chem. Commun.*, 51(21), 4485-4487.
- [35] Kuzmina, O., Sashina, E., Troshenkowa, S., & Wawro, D. (2010). Dissolved State of Cellulose in Ionic Liquids - the Impact of Water. *Fibres & Textiles in Eastern Europe*, 18(3), 32-37.
- [36] Kosan, B., Michels, C., & Meister, F. (2007). Dissolution and forming of cellulose with ionic liquids. *Cellulose*, 15(1), 59-66.
- [37] Hameed, N., Xiong, R., Salim, N., & Guo, Q. (2013). Fabrication and characterization of transparent and biodegradable cellulose/poly (vinyl alcohol) blend films using an ionic liquid. *Cellulose*, 20(5), 2517-2527.
- [38] Ma, X., Liu, C., Anderson, D., & Chang, P. (2016). Porous cellulose spheres: Preparation, modification and adsorption properties. *Chemosphere*, 165, 399-408.
- [39] Turner, M., Spear, S., Holbrey, J., & Rogers, R. (2004). Production of Bioactive Cellulose Films Reconstituted from Ionic Liquids. *Biomacromolecules*, 5(4), 1379-1384.
- [40] MAO, Z., JIE, X., CAO, Y., LIU, D., LIU, J., ZHOU, M., & YUAN, Q. (2011). Effect of Coagulation Bath Temperature on Structure and Gas Separation Properties of Cellulose Hollow Fiber Membranes. *Acta Polymerica Sinica*, 011(4), 395-401.
- [41] Zhou, L., Wang, Q., Wen, J., Chen, X., & Shao, Z. (2013). Preparation and characterization of transparent silk fibroin/cellulose blend films. *Polymer*, 54(18), 5035-5042.
- [42] Sun, L., Chen, J. Y., Jiang, W., & Lynch, V. (2015). Crystalline characteristics of cellulose fiber and film regenerated from ionic liquid solution. *Carbohydrate Polymers*, 118, 150-155.
- [43] Kadokawa, J., Hirohama, K., Mine, S., Kato, T., & Yamamoto, K. (2011). Facile Preparation of Chitin/Cellulose Composite Films Using Ionic Liquids. *Journal of Polymers and the Environment*, 20(1), 37-42.

- [44] Soheilmoghaddam, M., Wahit, M. U., Yussuf, A. A., Al-Saleh, M. A., & Whye, W. T. (2014). Characterization of bio regenerated cellulose/sepiolite nanocomposite films prepared via ionic liquid. *Polymer Testing*,33, 121-130.
- [45] Jiang, G., Huang, W., Li, L., Wang, X., Pang, F., Zhang, Y., & Wang, H. (2012). Structure and properties of regenerated cellulose fibers from different technology processes. *Carbohydrate Polymers*,87(3), 2012-2018.
- [46] Yao, Y., Zhang, E., Xia, X., Yu, J., Wu, K., Zhang, Y., & Wang, H. (2014). Morphology and properties of cellulose/silk fibroin blend fiber prepared with 1-butyl-3-methylimidazolium chloride as solvent. *Cellulose*,22(1), 625-635.
- [47] Liu, X., Chang, P. R., Zheng, P., Anderson, D. P., & Ma, X. (2014). Porous cellulose facilitated by ionic liquid [BMIM]Cl: fabrication, characterization, and modification. *Cellulose*,22(1), 709-715.
- [48] Ding, Z., Chi, Z., Gu, W., Gu, S., Liu, J., & Wang, H. (2012). Theoretical and experimental investigation on dissolution and regeneration of cellulose in ionic liquid. *Carbohydrate Polymers*,89(1), 7-16.
- [49] Liu, W., & Budtova, T. (2012). Ionic liquid: A powerful solvent for homogeneous starch–cellulose mixing and making films with tuned morphology. *Polymer*,53(25), 5779-5787.
- [50] K. (2015). Cellulose thin films from ionic liquid solutions. *Nordic Pulp and Paper Research Journal*,30(01), 006-013.
- [51] Kammiovirta, K., Jääskeläinen, A., Kuutti, L., Holopainen-Mantila, U., Paananen, A., Suurnäkki, A., & Orelma, H. (2016). Keratin-reinforced cellulose filaments from ionic liquid solutions. *RSC Adv.*,6(91), 88797-88806.
- [52] Zhang, M., Ding, C., Huang, L., Chen, L., & Yang, H. (2014). Interactions of collagen and cellulose in their blends with 1-ethyl-3-methylimidazolium acetate as solvent. *Cellulose*,21(5), 3311-3322.
- [53] Pang, J., Wu, M., Zhang, Q., Tan, X., Xu, F., Zhang, X., & Sun, R. (2015). Comparison of physical properties of regenerated cellulose films fabricated with different cellulose feedstocks in ionic liquid. *Carbohydrate Polymers*,121, 71-78.

- [54] Liebert, T., Wotschadlo, J., Gericke, M., Köhler, S., Laudeley, P., & Heinze, T. (2009). Modification of cellulose in ionic liquids towards biomedical applications. *Polysaccharide Materials: Performance by Design ACS Symposium Series*, 115-132.
- [55] Markstedt, K., Sundberg, J., & Gatenholm, P. (2014). 3D Bioprinting of Cellulose Structures from an Ionic Liquid. *3D Printing and Additive Manufacturing*, 1(3), 115-121.
- [56] Sundberg, J., Toriz, G., & Gatenholm, P. (2013). Moisture induced plasticity of amorphous cellulose films from ionic liquid. *Polymer*, 54(24), 6555-6560.
- [57] Mahmoudian, S., Wahit, M. U., Ismail, A. F., Balakrishnan, H., & Imran, M. (2014). Bionanocomposite fibers based on cellulose and montmorillonite using ionic liquid 1-ethyl-3-methylimidazolium acetate. *Journal of Materials Science*, 50(3), 1228-1236.
- [58] Härdelin, L., & Hagström, B. (2014). Wet spun fibers from solutions of cellulose in an ionic liquid with suspended carbon nanoparticles. *Journal of Applied Polymer Science*, 132(6).
- [59] Lu, Y., Liu, Y. X., Yu, H. P., & Sun, Q. F. (2011). Preparation, Characterization and Biocompatibility of Regenerated Cellulose/PVA Blend Membranes in 1-Allyl-3-Methylimidazolium Chloride. *Advanced Materials Research*, 179-180, 1108-1111.
- [60] Yu, Z., Jiang, Y., Zou, W., Duan, J., & Xiong, X. (2009). Preparation and characterization of cellulose and konjac glucomannan blend film from ionic liquid. *Journal of Polymer Science Part B: Polymer Physics*, 47(17), 1686-1694.
- [61] Xia, G., Wan, J., Zhang, J., Zhang, X., Xu, L., Wu, J., Zhang, J. (2016). Cellulose-based films prepared directly from waste newspapers via an ionic liquid. *Carbohydrate Polymers*, 151, 223-229.
- [62] Hanid, N. A., Wahit, M. U., Guo, Q., Mahmoodian, S., & Soheilmooghaddam, M. (2014). Development of regenerated cellulose/halloysites nanocomposites via ionic liquids. *Carbohydrate Polymers*, 99, 91-97.
- [63] Song, H., Niu, Y., Yu, J., Zhang, J., Wang, Z., & He, J. (2013). Preparation and morphology of different types of cellulose spherulites from concentrated cellulose ionic liquid solutions. *Soft Matter*, 9(11), 3013.

- [64] Soheilmoghaddam, M., Wahit, M. U., Whye, W. T., Akos, N. I., Pour, R. H., & Yussuf, A. A. (2014). Bionanocomposites of regenerated cellulose/zeolite prepared using environmentally benign ionic liquid solvent. *Carbohydrate Polymers*, 106, 326-334.
- [65] Liu, Z., Sun, X., Hao, M., Huang, C., Xue, Z., & Mu, T. (2015). Preparation and characterization of regenerated cellulose from ionic liquid using different methods. *Carbohydrate Polymers*, 117, 99-105.
- [66] Stefanescu, C., Daly, W. H., & Negulescu, I. I. (2012). Biocomposite films prepared from ionic liquid solutions of chitosan and cellulose. *Carbohydrate Polymers*, 87(1), 435-443.
- [67] Takegawa, A., Murakami, M., Kaneko, Y., & Kadokawa, J. (2010). Preparation of chitin/cellulose composite gels and films with ionic liquids. *Carbohydrate Polymers*, 79(1), 85-90.
- [68] Li, X., Zhu, L., Zhu, B., & Xu, Y. (2011). High-flux and anti-fouling cellulose nanofiltration membranes prepared via phase inversion with ionic liquid as solvent. *Separation and Purification Technology*, 83, 66-73.
- [69] Chen, H., Wang, N., & Liu, L. (2012). Regenerated cellulose membrane prepared with ionic liquid 1-butyl-3-methylimidazolium chloride as solvent using wheat straw. *Journal of Chemical Technology & Biotechnology*, 87(12), 1634-1640.
- [70] Liang, Y., Cheng, B. W., Song, J., Ji, X. J., Lu, F., & Guo, Z. G. (2011). Influence of Dope Concentration on Morphology And Properties of Cellulose Hollow Fiber Membranes Prepared from Cellulose/[Amim]Cl Dope Solution. *Advanced Materials Research*, 194-196, 2245-2248.
- [71] Ma, B., Qin, A., Li, X., & He, C. (2013). Preparation of Cellulose Hollow Fiber Membrane from Bamboo Pulp/1-Butyl-3-Methylimidazolium Chloride/Dimethylsulfoxide System. *Industrial & Engineering Chemistry Research*, 52(27), 9417-9421.
- [72] Ma, H., Hsiao, B. S., & Chu, B. (2011). Thin-film nanofibrous composite membranes containing cellulose or chitin barrier layers fabricated by ionic liquids. *Polymer*, 52(12), 2594-2599.

- [73] Livazovic, S., Li, Z., Behzad, A., Peinemann, K., & Nunes, S. (2015). Cellulose multilayer membranes manufacture with ionic liquid. *Journal of Membrane Science*, 490, 282-293.
- [74] Nevstrueva, D., Pihlajamäki, A., & Mänttari, M. (2015). Effect of a TiO₂ additive on the morphology and permeability of cellulose ultrafiltration membranes prepared via immersion precipitation with ionic liquid as a solvent. *Cellulose*, 22(6), 3865-3876.
- [75] Xing, D. Y., Peng, N., & Chung, T. (2010). Formation of Cellulose Acetate Membranes via Phase Inversion Using Ionic Liquid, [BMIM]SCN, As the Solvent. *Industrial & Engineering Chemistry Research*, 49(18), 8761-8769.
- [76] Xing, D. Y., Peng, N., & Chung, T. (2011). Investigation of unique interactions between cellulose acetate and ionic liquid [EMIM]SCN, and their influences on hollow fiber ultrafiltration membranes. *Journal of Membrane Science*, 380(1-2), 87-97.
- [77] Xing, D. Y., Dong, W. Y., & Chung, T. (2016). Effects of Different Ionic Liquids as Green Solvents on the Formation and Ultrafiltration Performance of CA Hollow Fiber Membranes. *Industrial & Engineering Chemistry Research*, 55(27), 7505-7513.
- [78] Xing, D., Chan, S., & Chung, T. (2012). Molecular interactions between polybenzimidazole and [EMIM]OAc, and derived ultrafiltration membranes for protein separation. *Green Chemistry*, 14(5), 1405..
- [79] Xing, D. Y., Chan, S. Y., & Chung, T. (2013). Fabrication of porous and interconnected PBI/P84 ultrafiltration membranes using [EMIM]OAc as the green solvent. *Chemical Engineering Science*, 87, 194-203.
- [80] Xing, D. Y., Chan, S. Y., & Chung, T. (2014). The ionic liquid [EMIM]OAc as a solvent to fabricate stable polybenzimidazole membranes for organic solvent nanofiltration. *Green Chem.*, 16(3), 1383-1392.
- [81] Madhavan, P., Sougrat, R., Behzad, A. R., Peinemann, K., & Nunes, S. P. (2015). Ionic liquids as self-assembly guide for the formation of nanostructured block copolymer membranes. *Journal of Membrane Science*, 492, 568-577.
- [82] Kim, D., Moreno, N., & Nunes, S. P. (2016). Fabrication of polyacrylonitrile hollow fiber membranes from ionic liquid solutions. *Polym. Chem.*, 7(1), 113-124.

- [83] Kim, D., Le, N. L., & Nunes, S. P. (2016). The effects of a co-solvent on fabrication of cellulose acetate membranes from solutions in 1-ethyl-3-methylimidazolium acetate. *Journal of Membrane Science*,520, 540-549.
- [84] Kim, D., Salazar, O. R., & Nunes, S. P. (2016). Membrane manufacture for peptide separation. *Green Chem.*,18(19), 5151-5159.
- [85] Kang, Y. S., Kim, H. J., Kim, Y. H., & Jo, W. H. (1988). The mechanism of asymmetric membrane formation via phase inversion process. *Polymer (korea)*,12(3), 279-287.
- [86] Fen'Ko, L. A., Semenkevich, N. G., & Bil'Dyukevich, A. V. (2011). The kinetics of membrane pore structure formation by phase inversion. *Petroleum Chemistry*,51(7), 527-535.
- [87] Kim, H. J., Tyagi, R. K., Fouda, A. E., & Jonasson, K. (1996). The kinetic study for asymmetric membrane formation via phase-inversion process. *Journal of Applied Polymer Science*,62(4), 621-629.
- [88] SUKMA, F.M. (2016). *Cellulose Membranes for Organic Solvent Nanofiltration* (Master Thesis). Middle East Technical University.
- [89] Hung, W., Wang, D., Lai, J., & Chou, S. (2016). On the initiation of macrovoids in polymeric membranes – effect of polymer chain entanglement. *Journal of Membrane Science*,505, 70-81.
- [90] Wang, S., Peng, X., Zhong, L., Jing, S., Cao, X., Lu, F., & Sun, R. (2015). Choline chloride/urea as an effective plasticizer for production of cellulose films. *Carbohydrate Polymers*,117, 133-139.
- [91] Forrd, E. J., Mendon, S. K., Thames, S. F., & Rawlins, J. W. (2010). X-ray Diffraction of Cotton Treated with Neutralized Vegetable Oil-based Macromolecular Crosslinkers. *Journal of Engineered Fibers and Fabrics*,5(1), 10-20.
- [92] Endo, T., Hosomi, S., Fujii, S., Ninomiya, K., & Takahashi, K. (2016). Anion Bridging-Induced Structural Transformation of Cellulose Dissolved in Ionic Liquid. *The Journal of Physical Chemistry Letters*,7(24), 5156-5161.

- [93] Gopiraman, M., Fujimori, K., Zeeshan, K., Kim, B. S., & Kim, I. S. (2013). Structural and mechanical properties of cellulose acetate/graphene hybrid nanofibers: Spectroscopic investigations. *Express Polymer Letters*,7(6), 554-563.
- [94] Burgal, J. D., Peeva, L., Marchetti, P., & Livingston, A. (2015). Controlling molecular weight cut-off of PEEK nanofiltration membranes using a drying method. *Journal of Membrane Science*,493, 524-538.
- [95] Rein, D. M., Khalfin, R., Szekely, N., & Cohen, Y. (2014). True molecular solutions of natural cellulose in the binary ionic liquid-containing solvent mixtures. *Carbohydrate Polymers*,112, 125-133.
- [96] Gupta, K. M., Hu, Z., & Jiang, J. (2013). Cellulose regeneration from a cellulose/ionic liquid mixture: the role of anti-solvents. *RSC Advances*,3(31), 12794.
- [97] Fadeeva, T. A., Husson, P., Devine, J. A., Gomes, M. F., Greenbaum, S. G., & Castner, E. W. (2015). Interactions between water and 1-butyl-1-methylpyrrolidinium ionic liquids. *The Journal of Chemical Physics*,143(6), 064503

APPENDICES

APPENDIX A

XRD Measurements

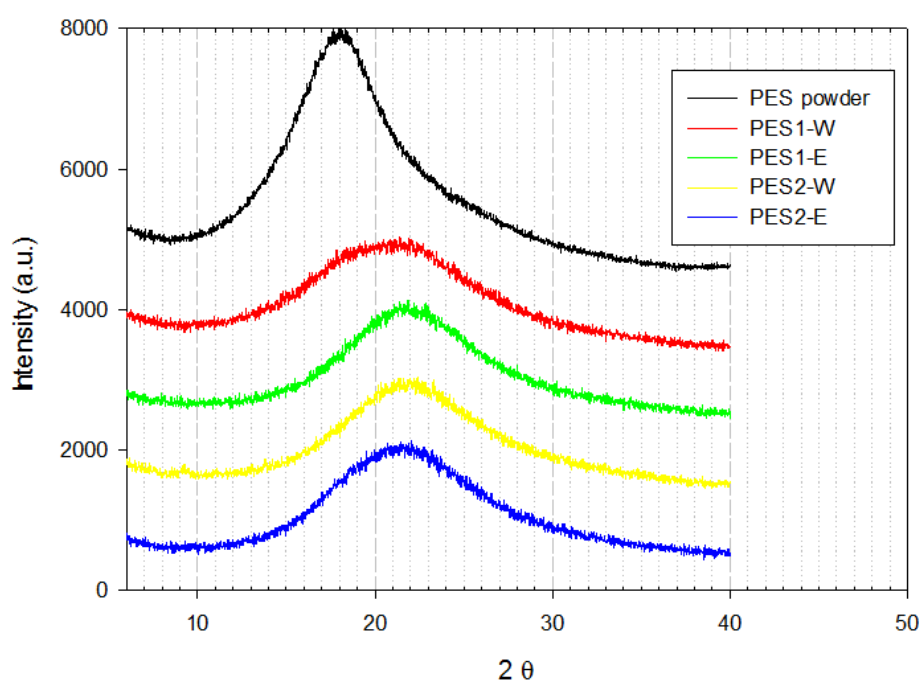


Figure A 1 - XRD Pattern of PES Powder and PES Membranes

Even though, PES is known to be amorphous polymer, XRD measurements are also done for PES pellets and membranes. As expected, no crystallinity is detected for those samples.

APPENDIX B

Solution Viscosities

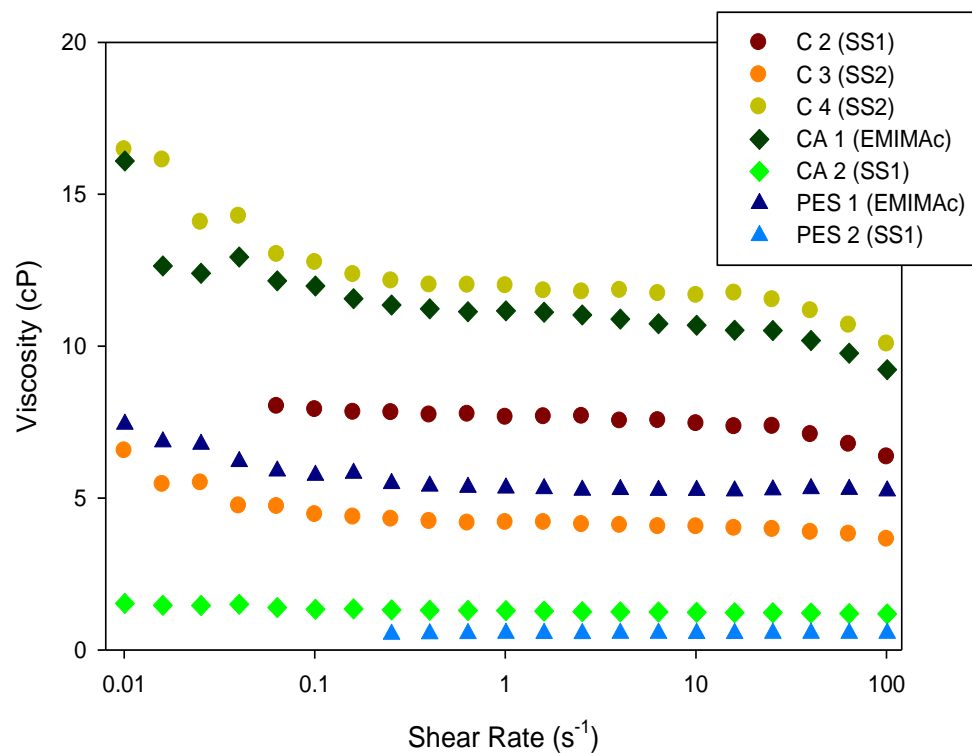


Figure B 1 - Solution Viscosities at Different Shear Rates

APPENDIX C

Solubility Parameters

Table C - 1 Solubility Parameters of Ternary System Components

	Chemical	δD (MPa) ^½	δP (MPa) ^½	δH (MPa) ^½	δT (MPa) ^½
<i>Co-Solvent</i>	<i>Dimethyl Sulfoxide</i>	18.4	16.4	10.2	26.7
<i>Non-Solvent</i>	<i>Ethanol</i>	15.8	8.8	19.4	26.5
<i>Non-Solvent</i>	<i>Water</i>	15.5	16.0	42.3	47.8
<i>Polymer</i>	<i>Cellulose</i>	25.4	18.6	24.8	40.1
<i>Polymer</i>	<i>Cellulose Acetate</i>	18.6	12.7	11.0	25.1
<i>Polymer</i>	<i>Polyether Sulfone</i>	19.6	10.8	9.2	24.2
<i>Solvent</i>	<i>EMIMAc</i>	22.20	15.90	16.90	32.11
<i>Solvent</i>	<i>NMP</i>	18.00	12.30	7.20	
<i>Solvent System 1</i>	<i>EMIMAc/DMSO (1:1)</i>	20.36	16.14	13.66	29.36
<i>Solvent System 2</i>	<i>EMIMAc/DMSO (1:2)</i>	19.72	16.23	12.53	28.45

Table C - 2 Ra and RED Values of Interactions between Two Species

<u>Distance btw</u>				distance	
				Ra	RED (poly)
Cellulose-Water	9.9	2.6	-17.5	26.55	1.224
Cellulose-Ethanol	9.6	9.8	5.4	22.22	1.024
Cellulose Acetate-Water	3.1	-3.3	-31.3	32.08	3.645
Cellulose Acetate-Ethanol	2.8	3.9	-8.4	10.82	1.230
PES-Water	4.1	-5.2	-33.1	34.49	5.564
PES-Ethanol	3.8	2.0	-10.2	12.88	2.077
EMIMAc-Water	6.70	-0.10	-25.40	28.72	
EMIMAc-Ethanol	6.40	7.10	-2.50	14.85	
SS1-Water	4.86	0.14	-28.64	30.24	
SS1-Ethanol	4.56	7.34	-5.74	13.04	
SS2-Water	4.22	0.23	-29.77	30.94	
SS2-Ethanol	3.92	7.43	-6.87	12.80	
Cellulose-EMIMAc	3.20	2.70	7.90	10.52	0.485
Cellulose-SS1	5.04	2.46	11.14	15.21	0.701
Cellulose-SS2	5.68	2.37	12.27	16.88	0.778
Cellulose Acetate-EMIMAc	-3.6	-3.2	-5.9	9.84	1.119
Cellulose Acetate-SS1	-1.76	-3.44	-2.66	5.60	0.637
Cellulose Acetate-DMSO	0.20	-3.70	0.80	3.81	0.614
PES-EMIMAc	-2.60	-5.10	-7.70	10.60	1.710
PES-SS1	-0.76	-5.34	-4.46	7.13	1.150
PES-DMSO	1.20	-5.60	-1.00	6.17	0.996
PES-NMP	1.6	-1.5	2.0	4.06	0.655

APPENDIX D

DLS Measurements

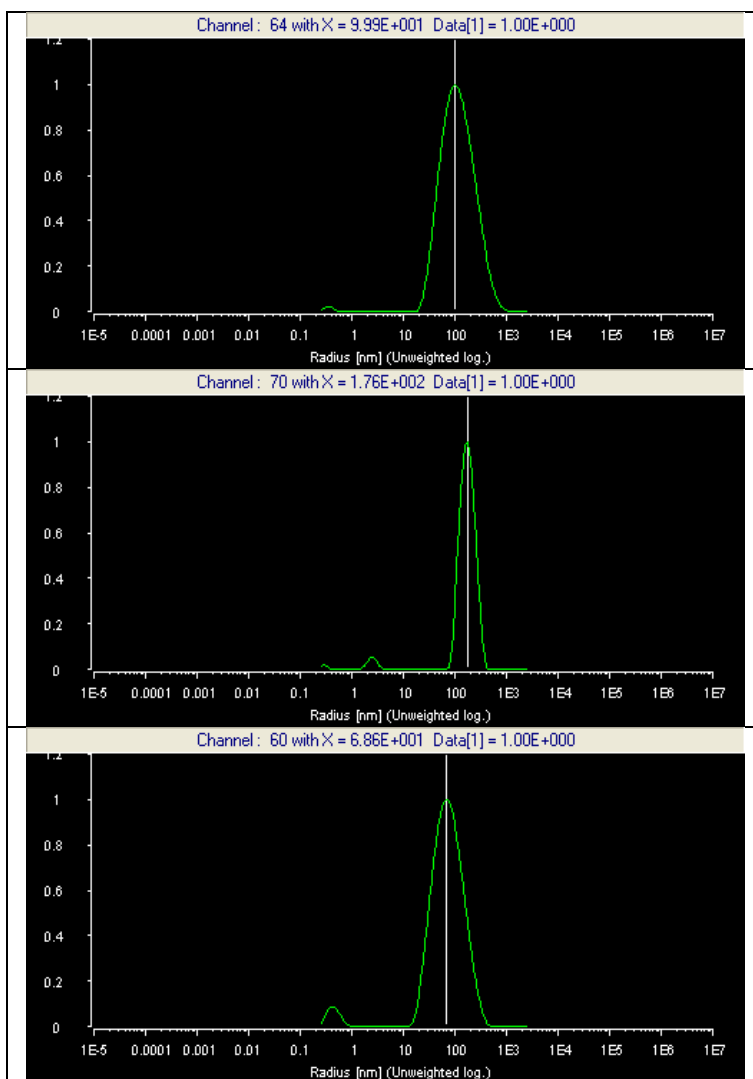


Figure D 1 DLS Results of Cellulose-EMIMAc Solutions (Z-average)

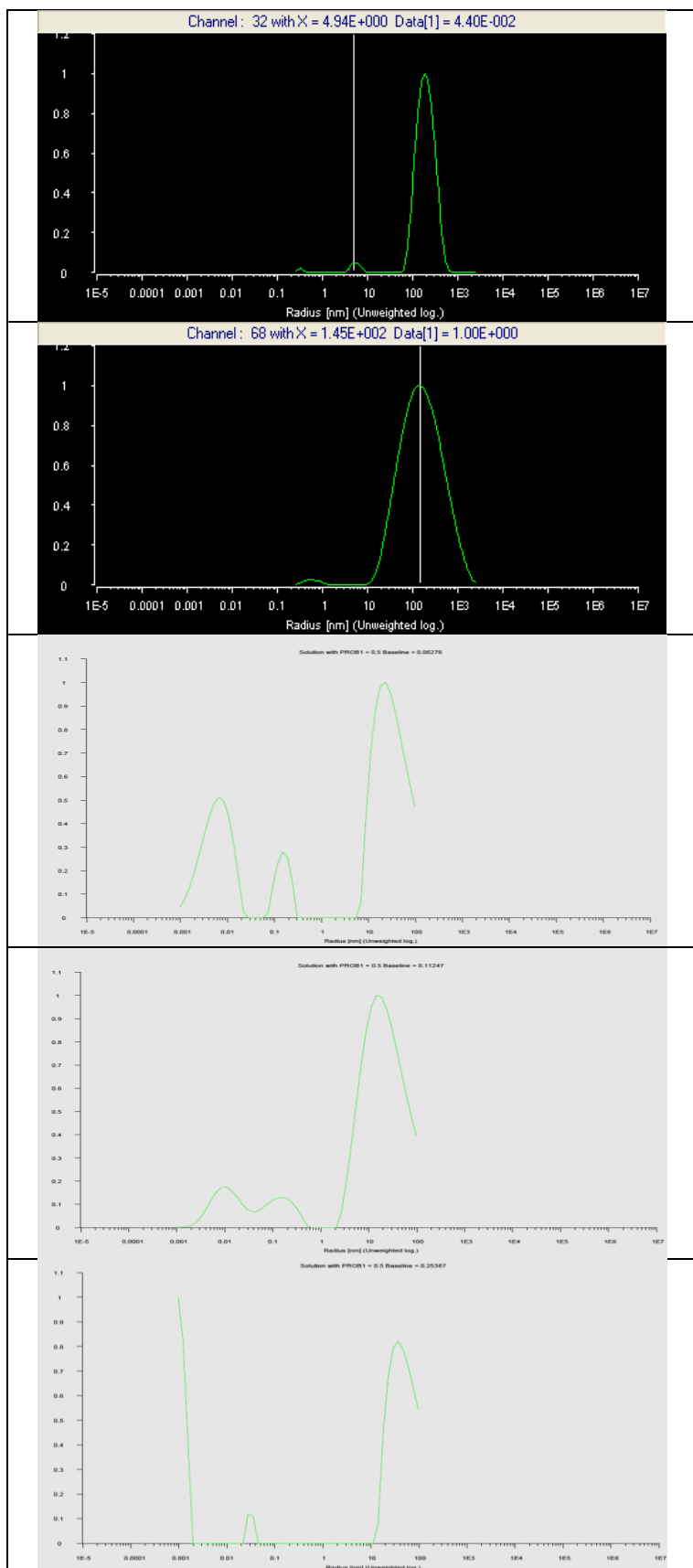


Figure D 2 DLS Results of Cellulose-EMIMAc Solutions (Z-average)

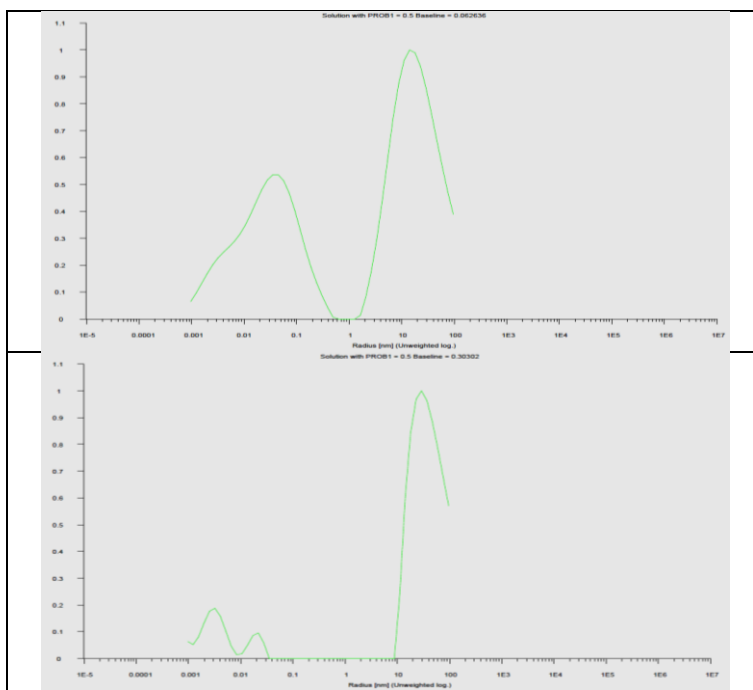


Figure D 3 DLS Results of Cellulose-EMIMAc Solutions (Z-average)

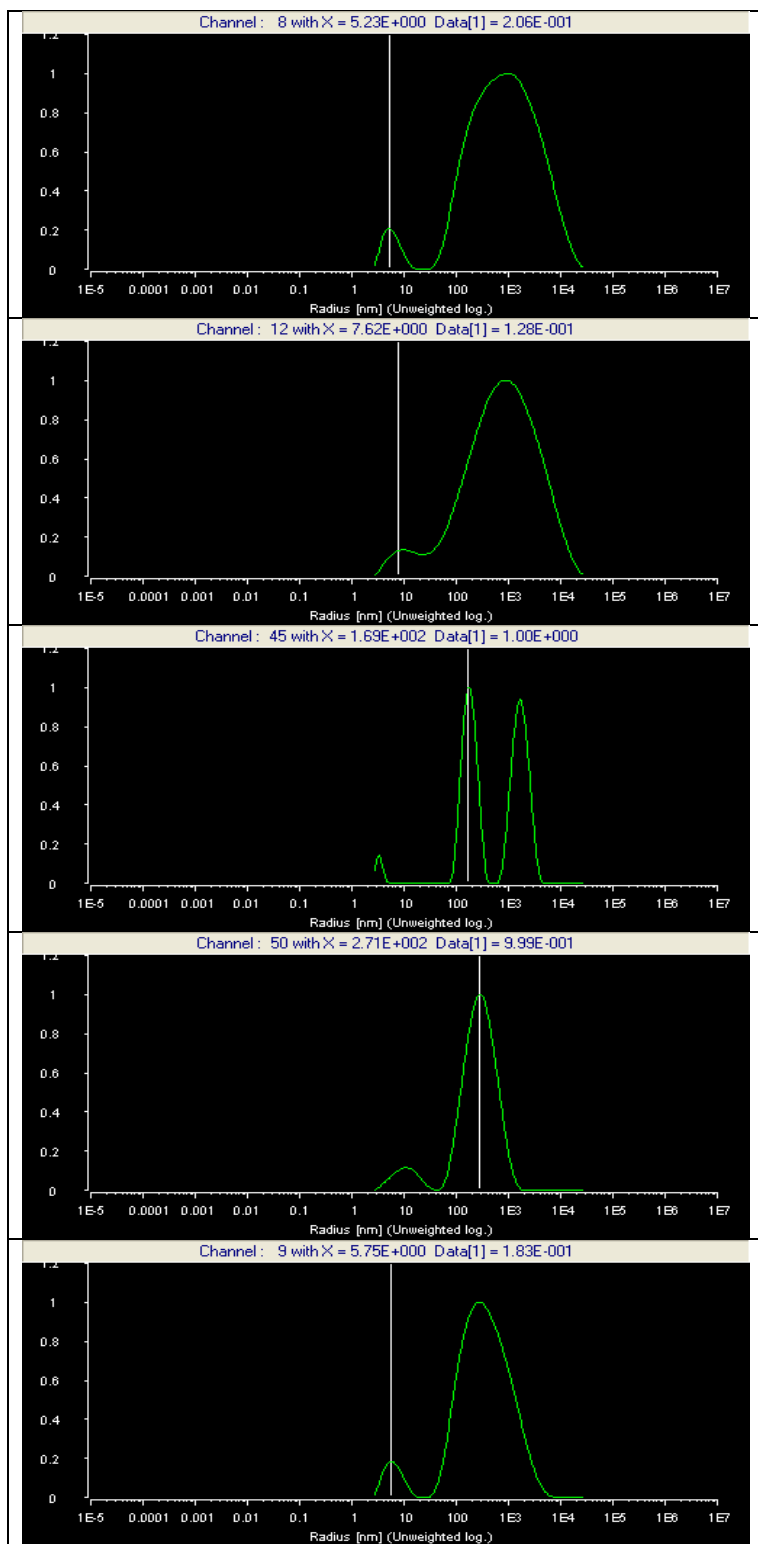


Figure D 4 DLS Results of Cellulose-SS1 Solutions (Z-average)

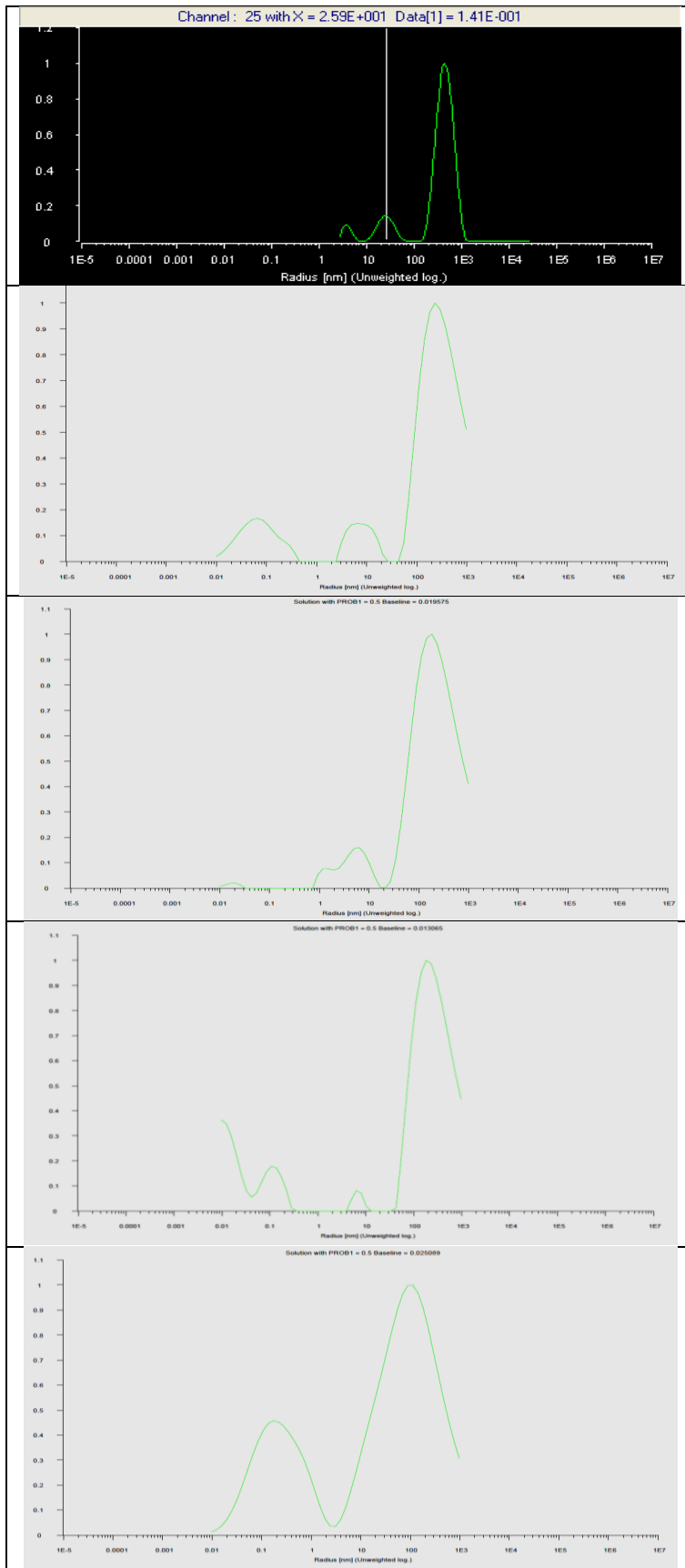


Figure D 5 DLS Results of Cellulose-SS1 Solutions (Z-average)

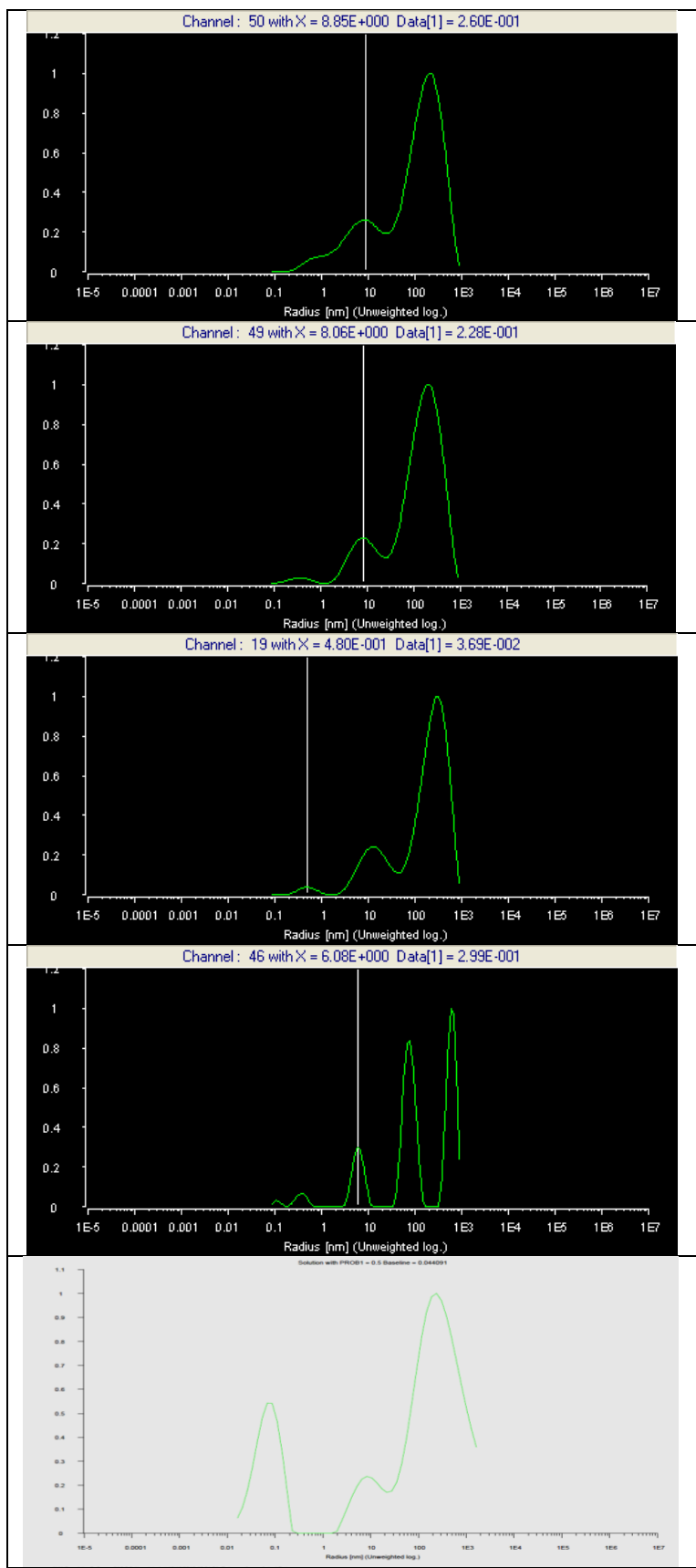


Figure D 6 DLS Results of Cellulose-SS2 Solutions (Z-average)

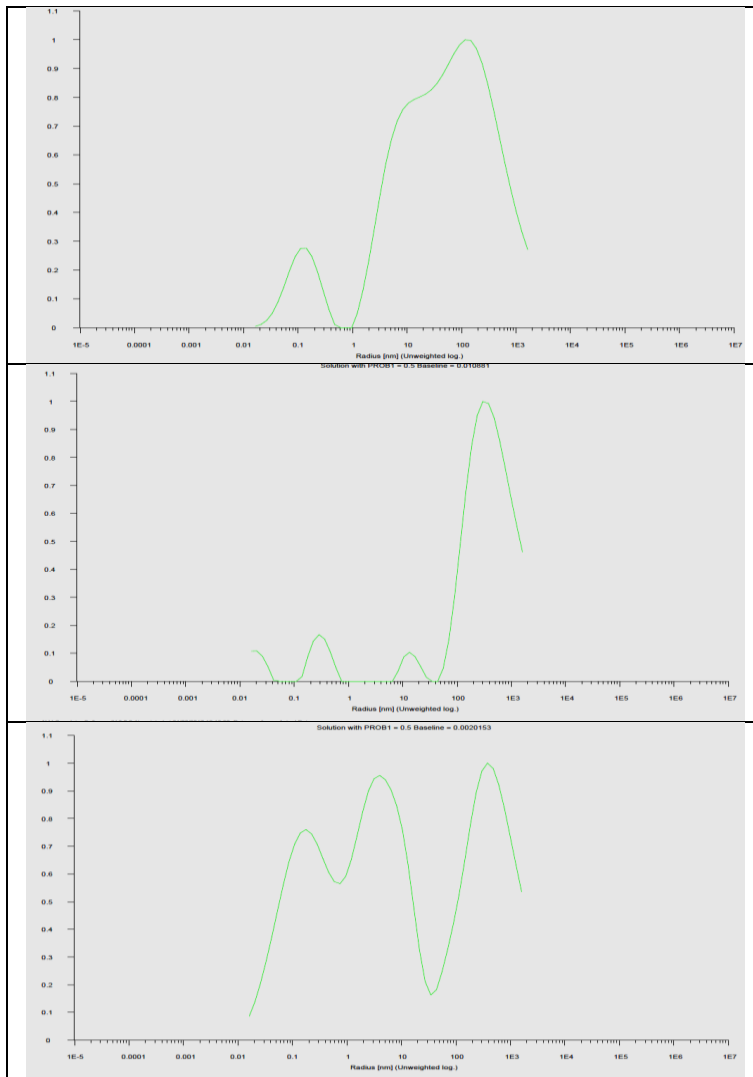


Figure D 7 DLS Results of Cellulose-SS2 Solutions (Z-average)

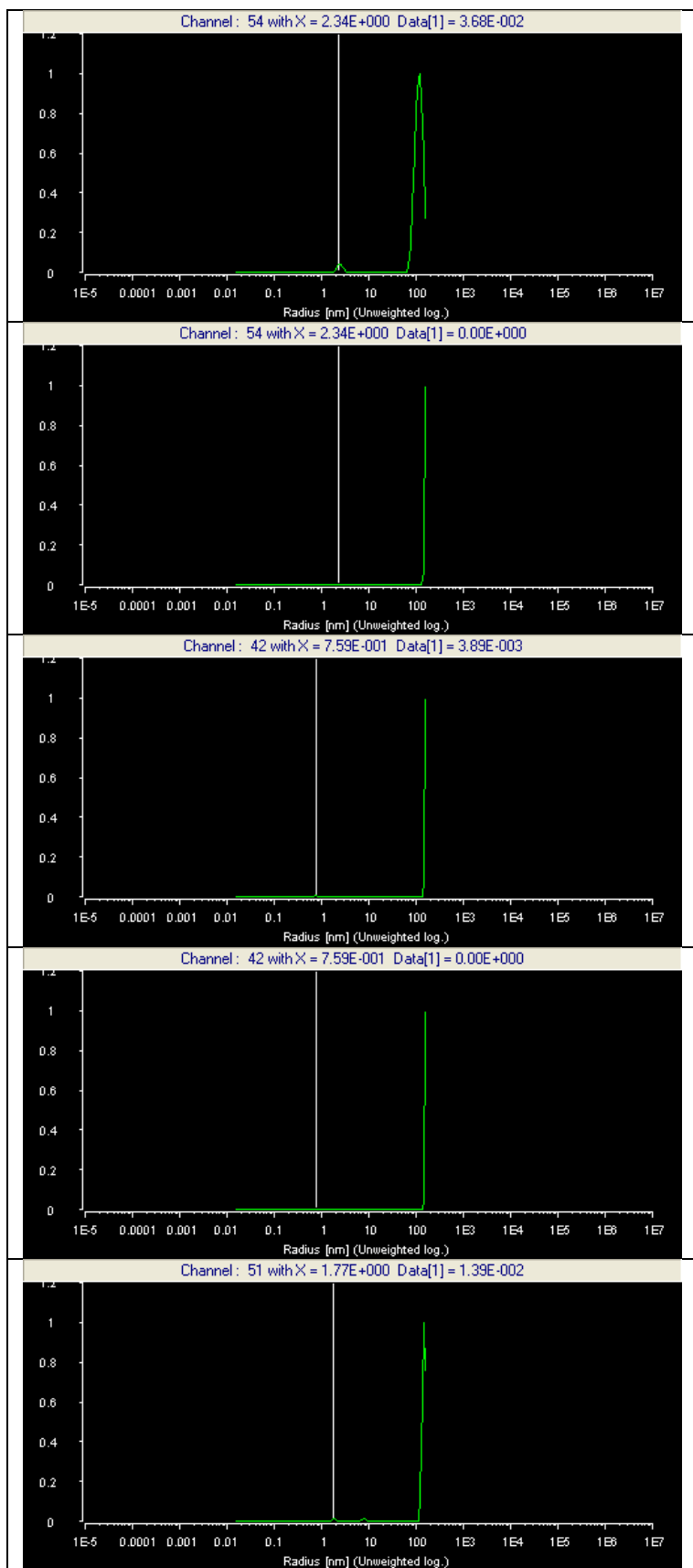


Figure D 8 Results of Cellulose Acetate – EMIMAc Solutions (Z-average)

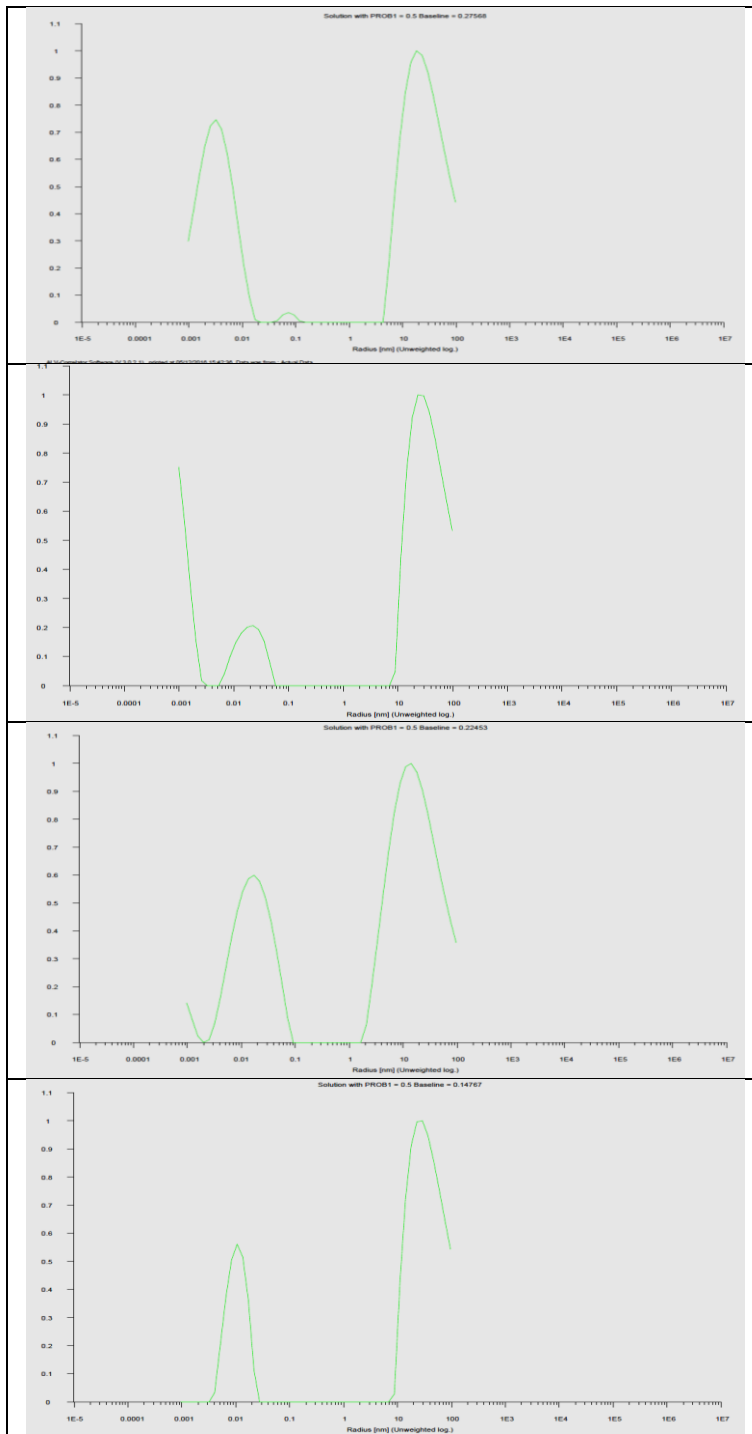


Figure D 9 Results of Cellulose Acetate – EMIMAc Solutions (Z-average)

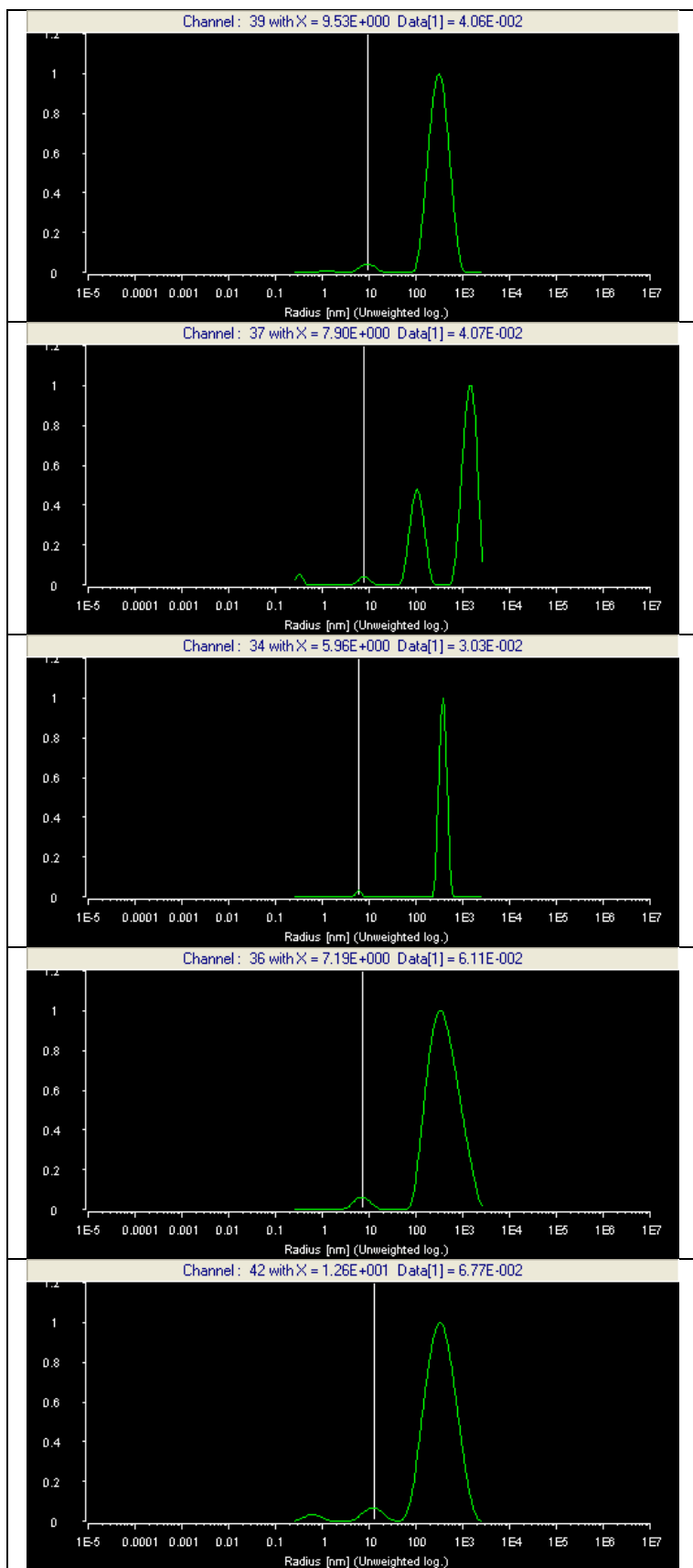


Figure D 10 Results of Cellulose Acetate – SS1 Solutions (Z-average)

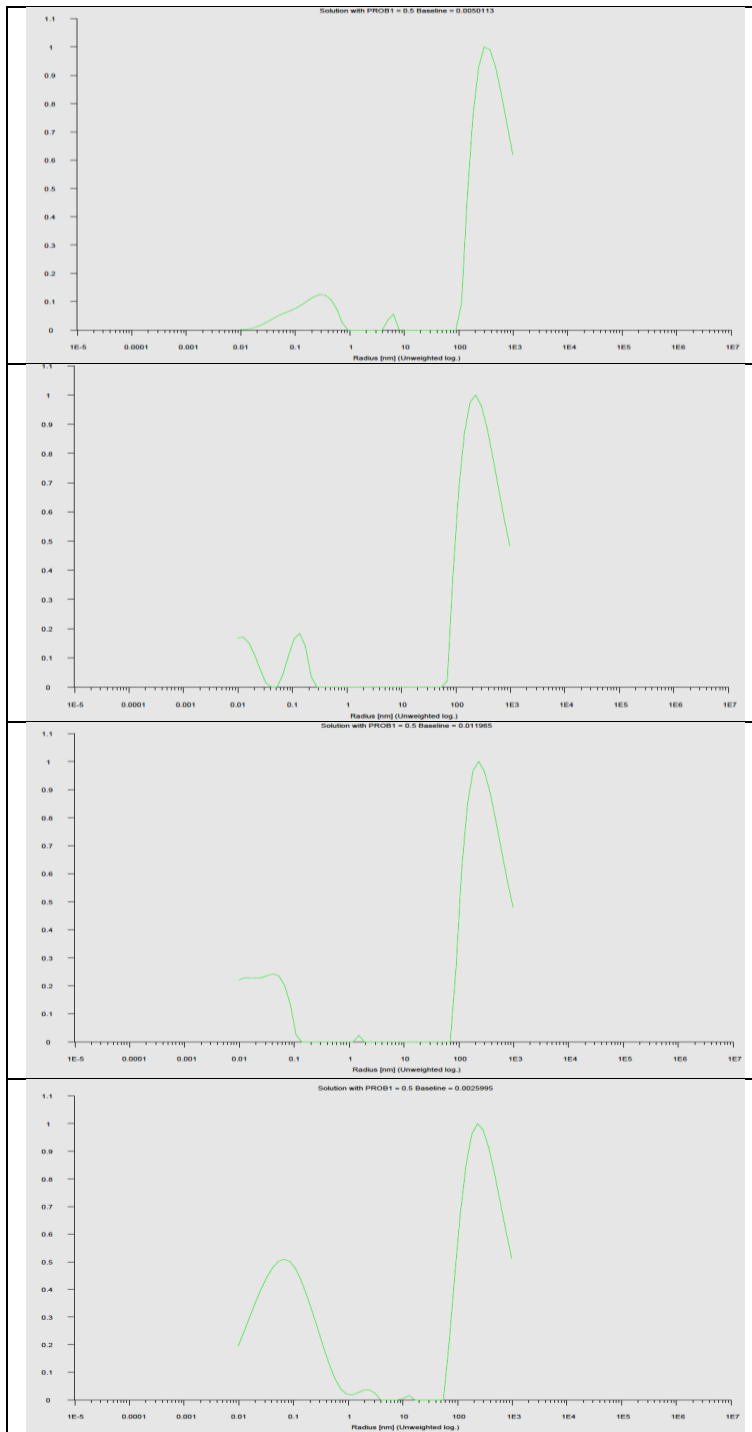


Figure D 11 Results of Cellulose Acetate – SS1 Solutions (Z-average)

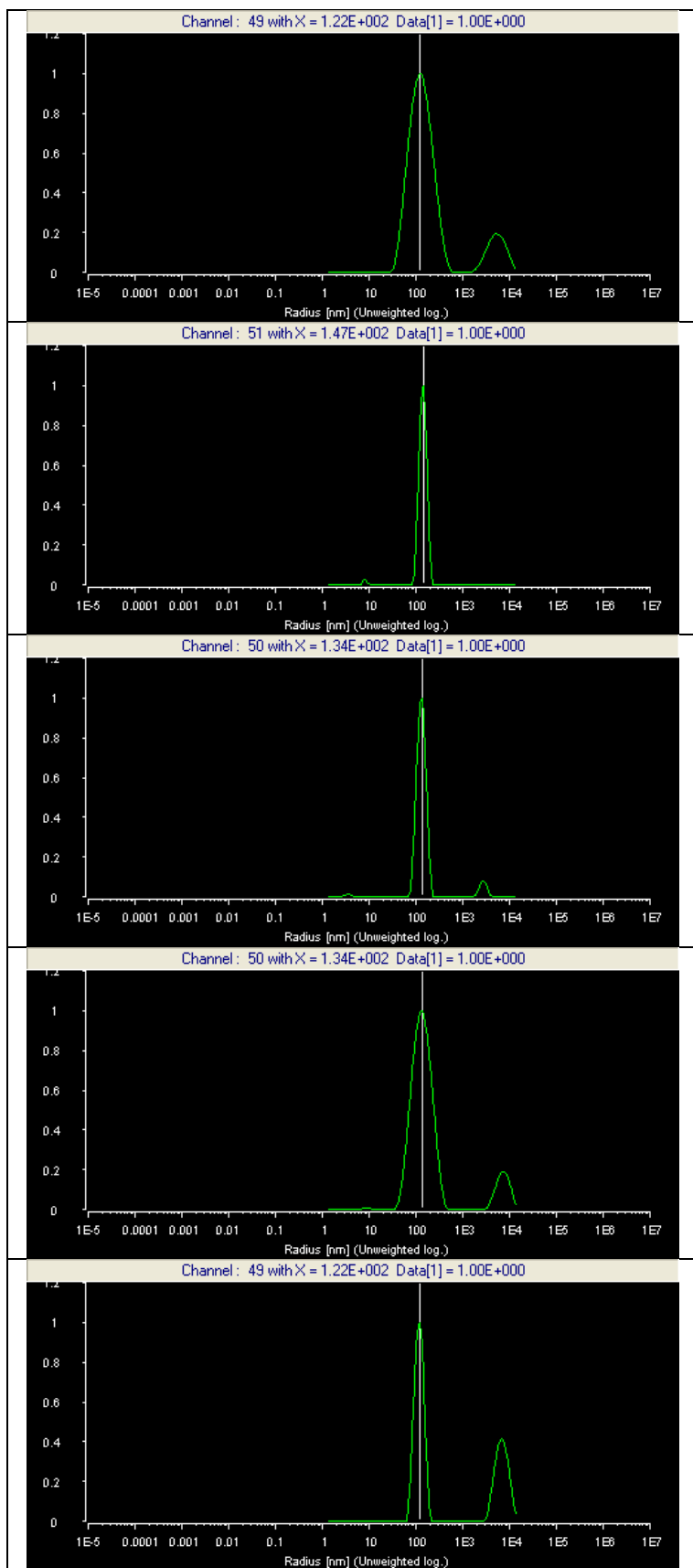


Figure D 12 DLS Results of Cellulose Acetate - DMSO Solutions (Z-Average)

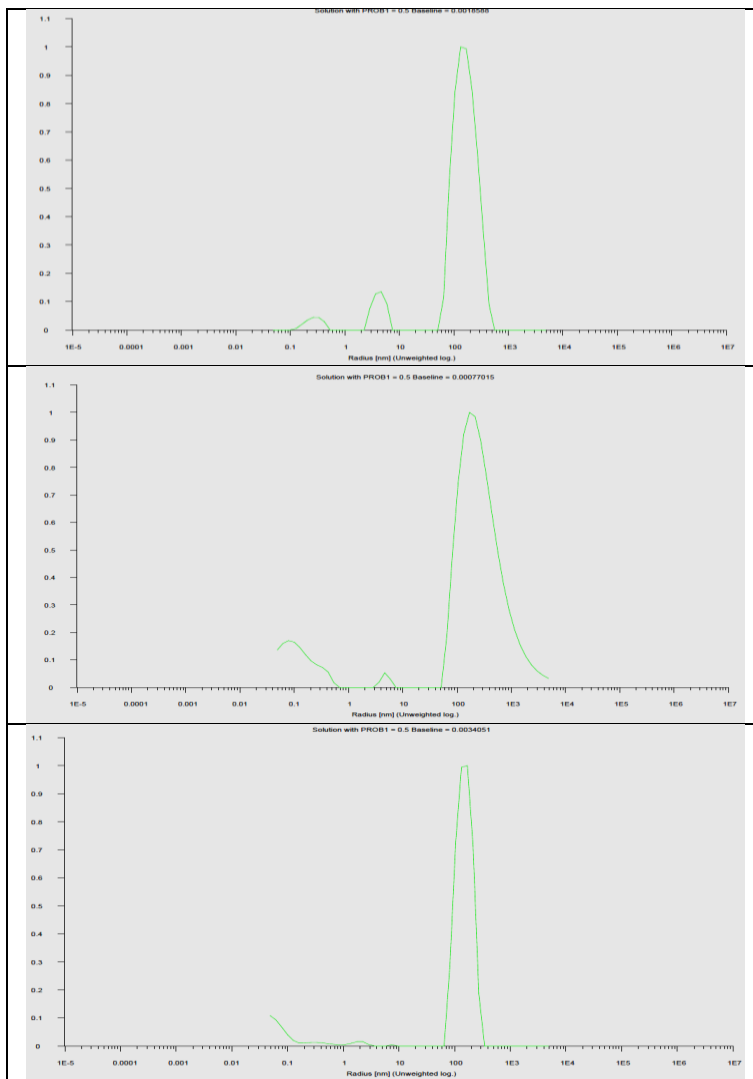


Figure D 13 DLS Results of Cellulose Acetate - DMSO Solutions (Z-Average)

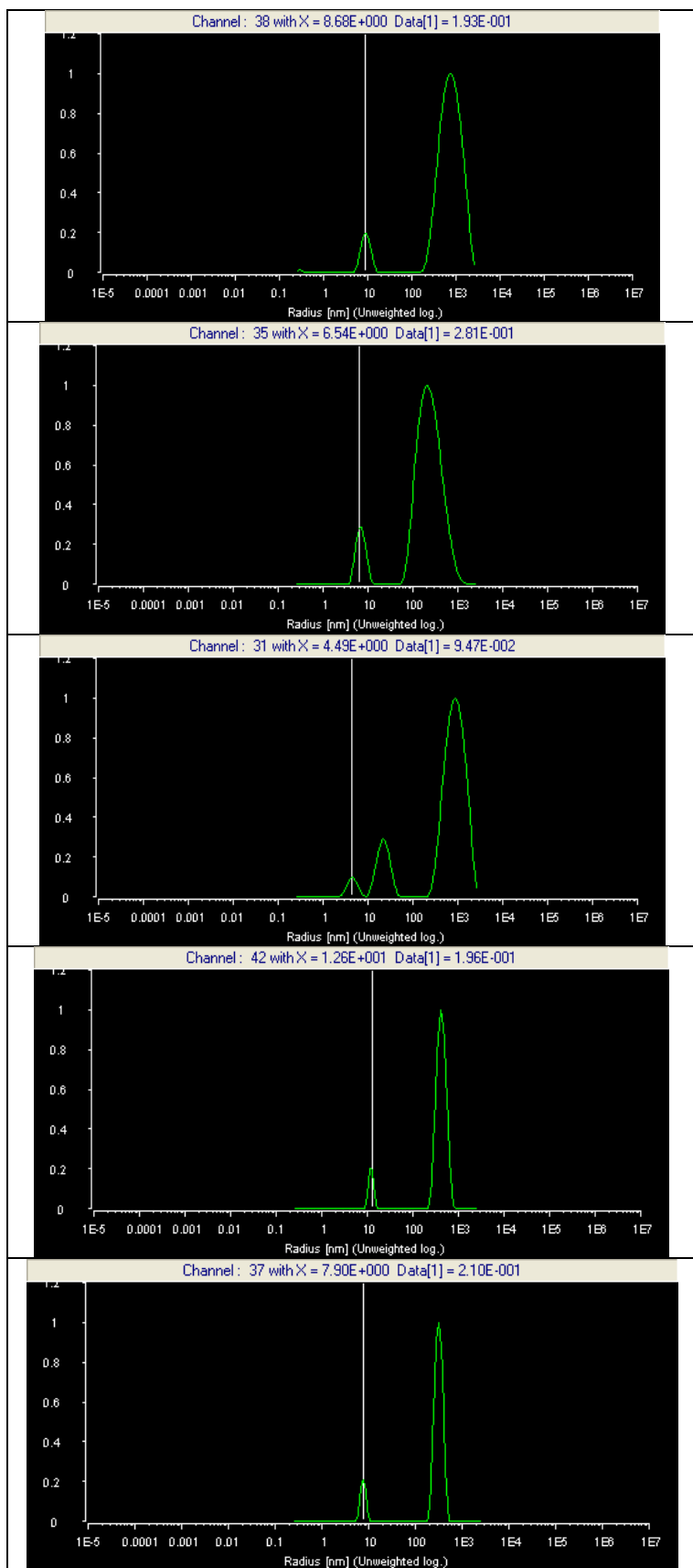


Figure D 14 Results of PES-EMIMAc Solutions (Z-Average)

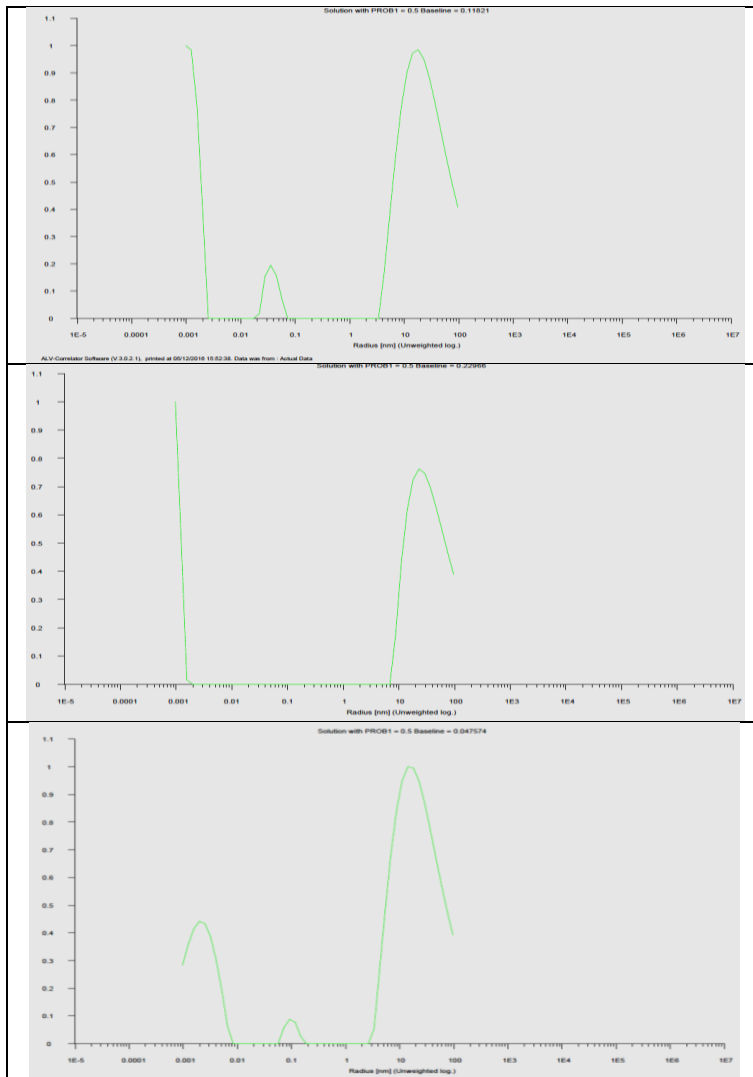


Figure D 15 Results of PES-EMIMAc Solutions (Z-Average)

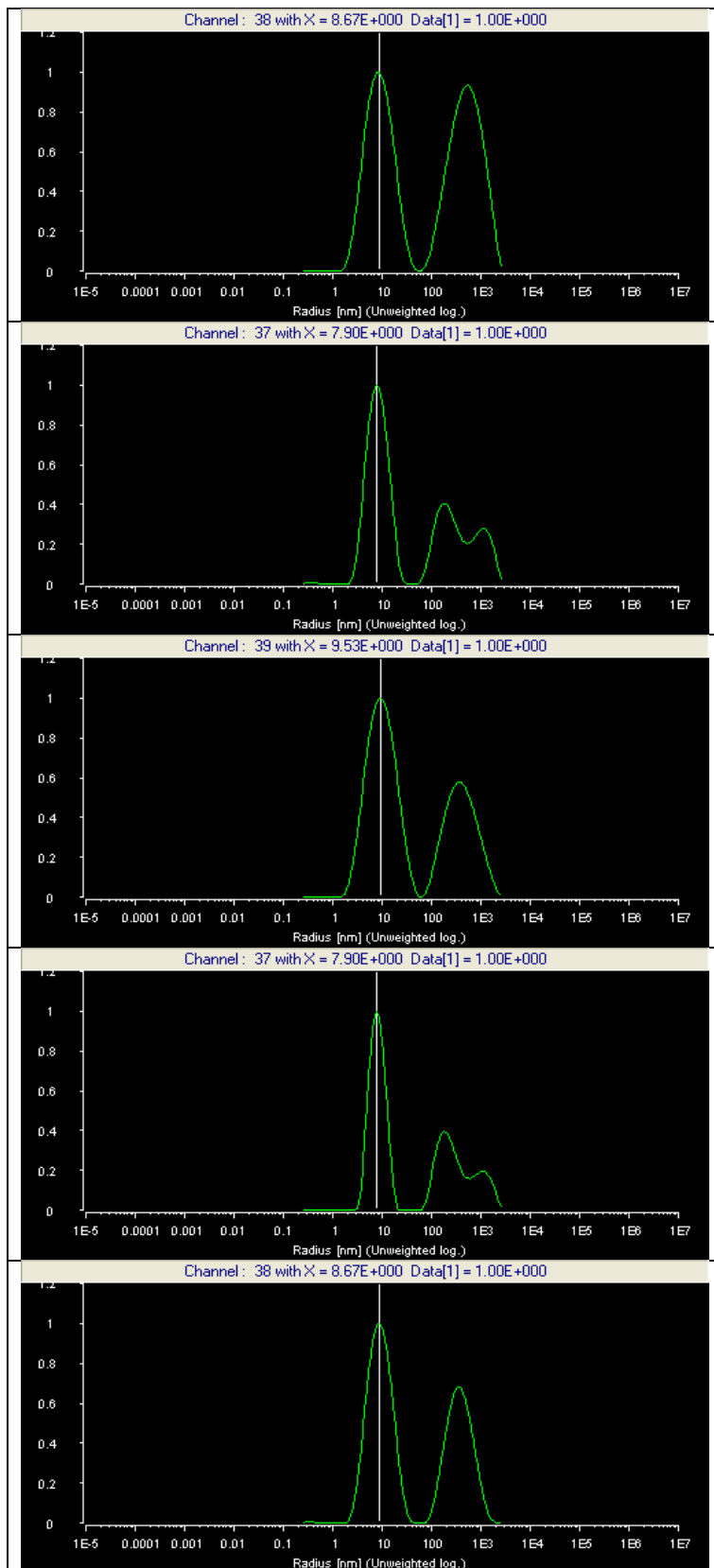


Figure D 16 Results of PES-SS1 Solutions (Z-Average)

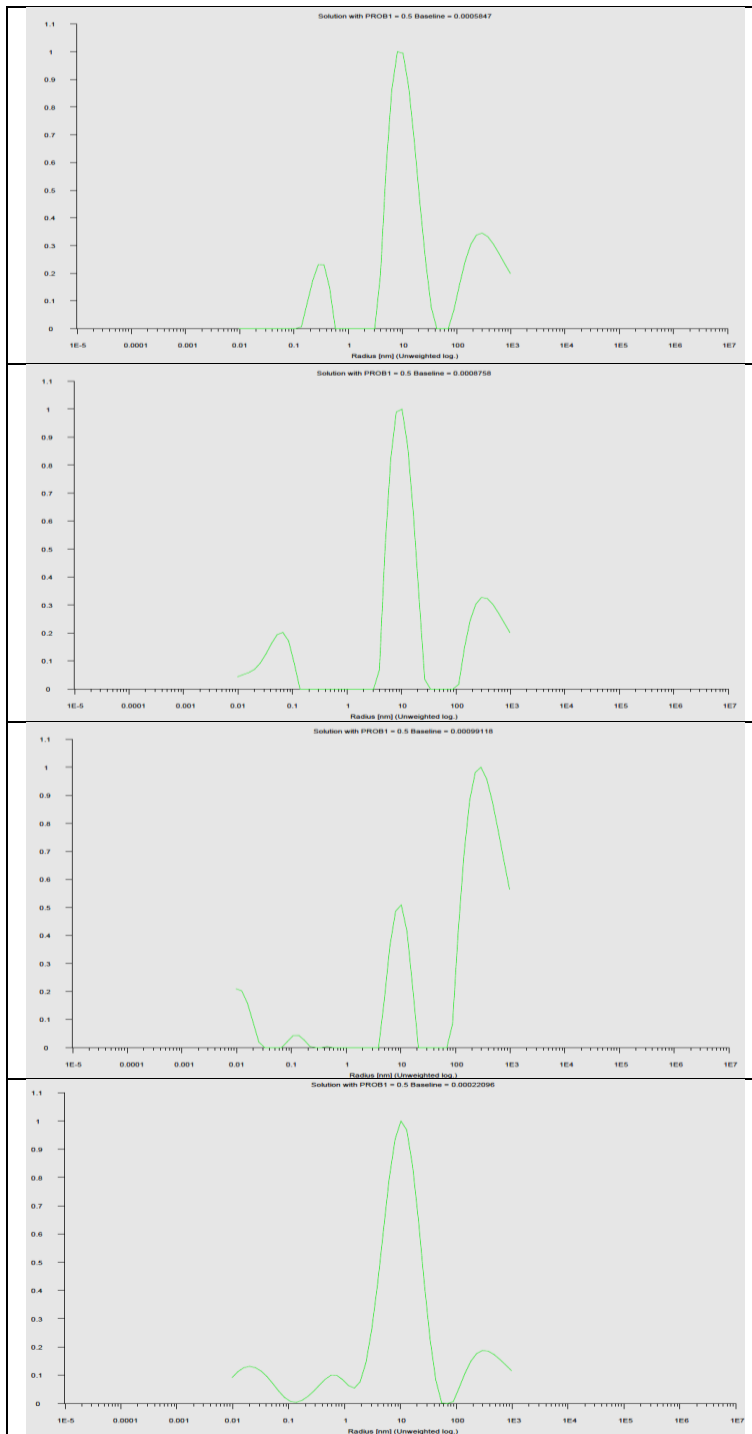


Figure D 17 Results of PES-SS1 Solutions (Z-Average)

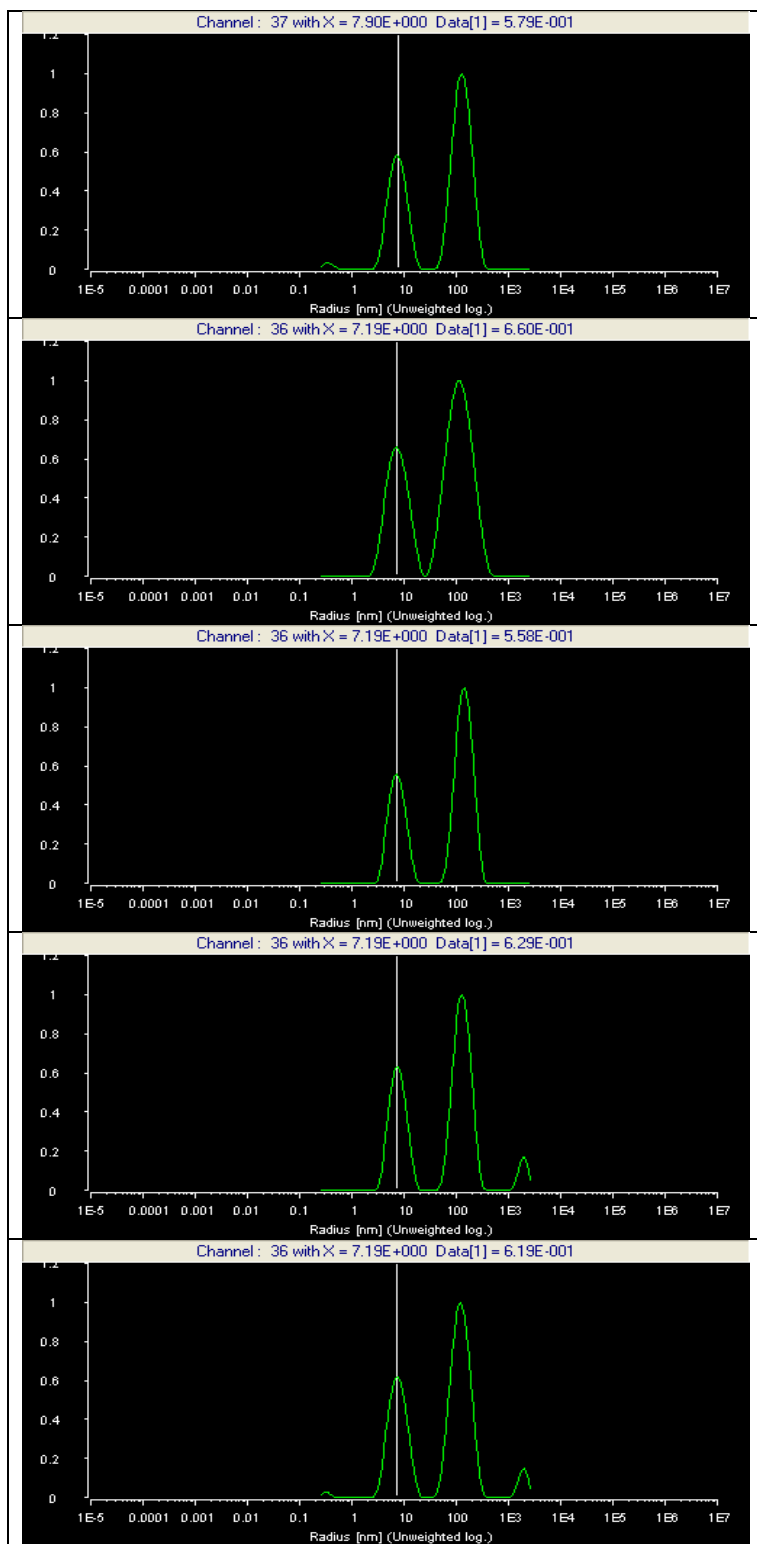


Figure D 18 Results of PES-DMSO Solutions (Z-Average)

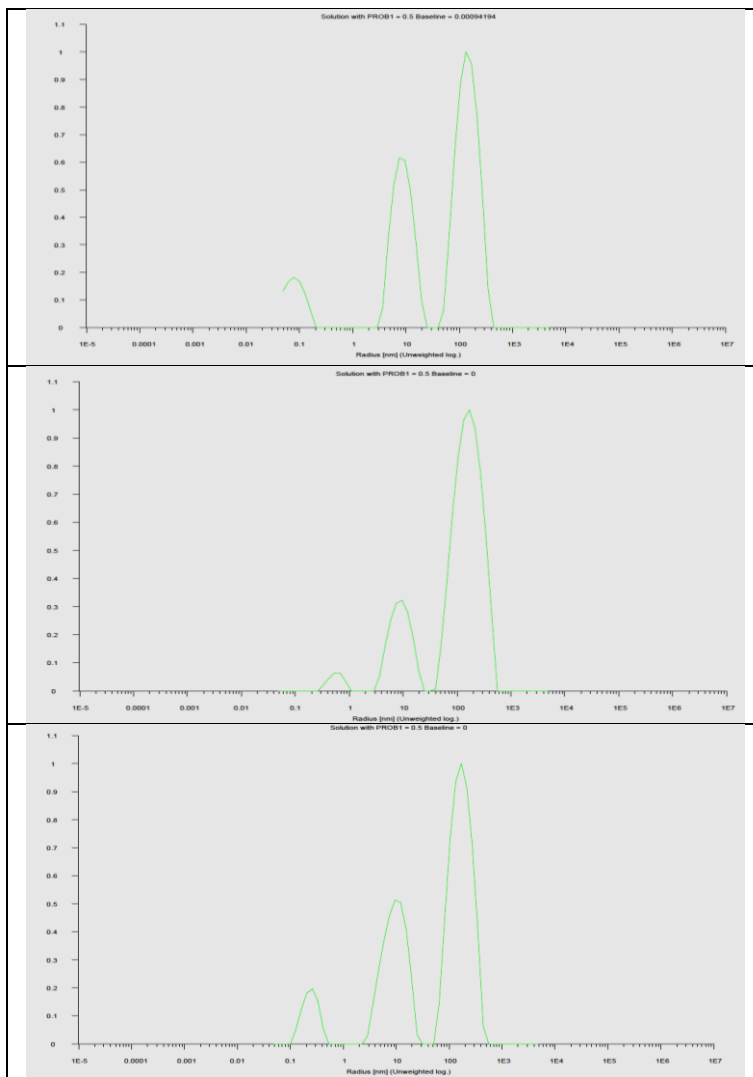


Figure D 19 Results of PES-DMSO Solutions (Z-Average)